Master's thesis
Master's degree program in Environmental Engineering
Specialization: Climate Change

Fluvial Vegetation Dynamics: An Innovative Approach to Modeling Root Biomass in Riparian Environments

Supervisors
Prof. Carlo Camporeale
Prof. Annunziato Siviglia

Author
Lorenzo Frisone *s319653*

DIATI dipartimento di Ingegneria dell'Ambiente del Territorio e delle Infrastrutture

Politecnico di Torino

October 2025

Contents

Abstract

The aim of this thesis work is to investigate on the variety of the most common modeling approaches used to describe vegetation dynamics in river systems and to propose improvements to some of their key aspects. According to a large body of literatures the multitude of external factors that influences vegetation evolution - both positively and negatively - makes it difficult to construct a complete and realistic mathematical model.

For this reason, most studies focus only on the most significant factors, such as groundwater level, which has been widely shown to strongly affect vegetation behavior. A significant portion of the thesis is dedicated to a critical review of some of the most well-known vegetation modeling approaches. This analysis aimed to identify which aspects are consistently addressed and which are still treated with insufficient detail. Among these, root biomass emerged as a crucial yet oversimplified component despite its role in the interaction between vegetation and hydrological conditions,

Therefore ,this works focuses mostly on the role that the root system plays in the modelling approach and how it is influenced by groundwater level variability, in order to prioritize root biomass as the main characterizing variable of the dynamic computation. Starting from a pre-existing root biomass model that describes dynamics of phreatophytic species, typically found in riparian environment, a new implementation is proposed in the form of a 2D time depending computation.

This model simulates local variation of the biomass in the subsoil and of the rooting depth, based on groundwater level, distance from the riverbed and vegetation characteristics. The model has been tested under different conditions in order to assess its validity and potential. Different geometries were considered – both linear and irregular – and the input hydrological regime was implemented in both statistical (sinusoidal) and stochastic form. In the latter case, a water level generator was used to reproduce the natural variability of river flow, by imposing different conditions such as varying coefficients of variation and integral time scales.

Ultimately, statistical analysis over the results of the simulation has been conducted to identify the most influential factors governing the system, with the aim of improving the predictive capabilities of vegetation dynamics models in riparian environments.

List of Figures

List of Tables

Chapter 1

Introduction

1.1 River hydro-morphodynamics: Basics concepts

The core concept behind the research proposed in this thesis involves *"river hydro-morphodynamic modeling"*, which simulates both hydraulic processes and sediment transport in natural riverbeds. It combines free-surface flow in fluid dynamics with mobile-bed processes in morphodynamics. Over time, it predicts discharge evolution, water levels, and river morphology.
This field is based on solid physical principles: fundamental equations of fluid mechanics (Navier–Stokes equations) describe water movement, while empirical-physical laws of solid transport, and together with sedimentary mass conservation principles (Exner equation) they govern riverbed evolution.

The key concepts of these fundamentals are presented below:

– Navier–Stokes Equations and Saint-Venant Approximations: The Navier–Stokes equations describe how mass and momentum are conserved for an incompressible viscous fluid, and they also explain how water moves in an open channel. These equations, in their full 3D form, are a system of partial differential equations.
The De Saint-Venant equations (de Saint-Venant 1871), also called the *shallow-water equations*, are derived by assuming a weakly compressible Newtonian, 1D flow regime with a hydrostatic pressure gradient (i.e., ignoring vertical acceleration) and integrating along the depth.

Continuity Equations:

$$\frac{\partial A}{\partial t} + \frac{\partial Q}{\partial x} = 0 \tag{1.1}$$

$$\frac{\partial Q}{\partial t} + \frac{\partial}{\partial x}\left(\alpha \frac{Q^2}{A}\right) + gA\frac{\partial h}{\partial x} + gA\left(S_f - S_0\right) = 0 \tag{1.2}$$

Where:

Q = discharge (flow rate),
A = wetted area,
h = flow depth (hydraulic depth),
S_f = friction slope (energy losses),
S_0 = channel bed slope,
α = Coriolis coefficient (velocity distribution correction).

The de Saint-Venant equations form the basis of numerical hydrodynamic models used to simulate flood propagation.

– Reynolds number and flow regime: A fundamental dimensionless parameter in river hydraulics is the Reynolds number Re, defined as the ratio between inertial forces and viscous forces (where V is the average velocity, L is the characteristic dimension—e.g., hydraulic diameter—and ν is the kinematic viscosity of water) and distinguishes between laminar and turbulent flow regimes in fluid dynamics.

$$Re = \frac{VL}{\nu} \tag{1.3}$$

In the river context, given the typical scales (velocities of the order of 1 m/s and metric dimensions), the Reynolds numbers are very high (typically $Re > 10^5$), well above the transition threshold (2000 for closed conduits); therefore, the current in rivers is almost always turbulent on rough bottoms.

– Engelund's equation, Manning's formula, and hydraulic resistance: A key component of river hydrodynamic models is the representation of motion resistance brought on by the riverbed's roughness, which establishes frictional energy losses. Manning's formula (Manning 1891), which is represented in SI units as follows, is the traditional method for estimating the current velocity under conditions of uniform motion and turbulent flow:

$$V = \frac{1}{n} R^{2/3} S^{1/2} \tag{1.4}$$

Where:

V = average flow velocity (m/s),
R = hydraulic radius (m),
S = energy slope (dimensionless, approximated by the slope of the uniform bed),
n = Manning's coefficient.

Engelund's model (Engelund 1966) also addresses the complexity caused by the contribution of grain size roughness and the presence of macro-irregularities (dunes and other bottom features).

– Shields criterion and triggering of bedload transport: To establish the critical condition beyond which sediment particles begin to move, the Shields criterion (Shields 1936) is traditionally used. Through systematic experiments in rivers, a dimensionless parameter was introduced —the Shields number j defined as the ratio between the shear stress exerted by the fluid on the bottom (t_0) and the submerged weight per unit area of sediment:

$$\theta = \frac{\tau_0}{(\rho_s - \rho)\, gD} \tag{1.5}$$

Where:

ρ_s = sediment density,
ρ = water density,
g = gravitational acceleration,
D = representative grain diameter (typically D_{50}).

The Shields criterion therefore provides an objective criterion for assessing the onset of erosion at the bottom: if the stress exerted by the current exceeds the critical value, the bottom begins to mobilize and sediment transport takes place.

– Exner equation (Exner 1925) and coupling with continuity equations: the interaction between the flow and the mobile bed is formalized by the Exner equation, which expresses the conservation of sediment mass in the bed over time. In one-dimensional differential form (abscissa x along the riverbed), the Exner equation is written as:

$$(1 - p)\, \frac{\partial \eta}{\partial t} + \frac{\partial q_s}{\partial x} = 0 \tag{1.6}$$

Where:

$\eta(x, t)$ = bed elevation (sediment bed level with respect to a reference plane),
$q_s(x, t)$ = sediment transport rate per unit width (m^2/s),
p = bed sediment porosity,
$(1 - p)$ = solid fraction of the bed deposit (relative density of the solid matrix).

A variation in solid load along the space causes a variation in the depth of the bottom over time: if q_s decreases along the direction of flow (i.e., $\partial q_s/\partial x < 0$), it means that material accumulates (sedimentation) and therefore $\partial \eta/\partial t$ is positive (the bottom rises, aggradation); conversely, if q_s increases forward (i.e., there is transport divergence, $\partial q_s/\partial x > 0$), the bottom loses material (erosion) and $\partial \eta/\partial t$ is negative (the bottom lowers, degradation).
In a hydro-morphodynamic model, therefore, the following are solved simultaneously: the Saint-Venant equations for flow (from which the bottom stress and sediment transport rate q_s are obtained using an appropriate transport formula) and the Exner equation to update the morphology.

The joint study of morphodynamic and hydrodynamic changes is of fundamental importance for understanding the mutual dependence between hydrodynamic phenomena and morphodynamic changes (and vice versa) and for predicting and managing the consequences of certain phenomena from the point of view of civil protection and the management and protection of river ecosystems.
For example, from the point of view of civil protection, numerical hydromorphodynamic models make it possible to predict and manage the impact of exceptional floods on the riverbed and surrounding area, simulating, for example, bank erosion, the formation of new branches, or the occlusion of the riverbed due to sedimentation, which can significantly alter the river's flow capacity and thus the propagation of flood waves and flood-prone areas.
As far as environmental protection is concerned, understanding and maintaining the natural hydromorphodynamic variability of river environments is of fundamental importance, since the biodiversity of these ecosystems is based on the physical heterogeneity of erosion and deposition processes that follow one another and allow their structure to be continuously created and renewed.
Similarly, the alteration of morphological processes, the simplification of habitats, and the ecological degradation of the river. Hydromorphodynamic studies provide tools for assessing these impacts and planning river restoration interventions: for example, the removal of transverse structures to restore sediment continuity, or the reactivation of river diversions in the plains, can be simulated to estimate their beneficial effects on habitats before being implemented in the field.

1.2 The role of riparian vegetation

Adding to the already complex dynamics governing the hydrodynamic and morphodynamic phenomena of riverbeds is a component of great importance whose dynamics are not easily determined by physical laws as they were in previous cases: riparian vegetation.
The literature has long acknowledged that riparian vegetation has a close relationship with river dynamics, impacting both hydraulic parameters and the morphological development of watercourses (Naiman and Décamps 1997)(Angela M. Gurnell 2014).
Its function in regulating hydro-morphodynamic phenomena manifests itself in a number of ways, primarily influencing sediment dynamics, flow resistance, and bank stability.
The presence of vegetation cover along banks, bars, and floodplains tends to increase the roughness of the channel, offering resistance to flow. This results in a reduction in water velocity in vegetated areas and an increase in water level for a given flood discharge. (Angela M. Gurnell 2016)
In particular, during flood events, the presence of vegetation can attenuate flow velocity and promote sediment deposition, contributing to the formation of diverse habitats by influencing nutrient transformation processes and also contributing to the protection of surrounding areas.
Optimal management of riparian vegetation is therefore a key element of river restoration projects in order to promote the morphological stability of watercourses (Palmer and Ruhi 2019).

For example, Anderson et al. (2006) showed through one-dimensional modeling that a higher roughness coefficient (due to dense riparian vegetation) slows down the speed of the flood wave and attenuates its peak, with more pronounced effects for moderate floods than for extreme events. Similarly, vegetation in riverbeds or floodplains increases flow resistance and can dampen flood propagation, locally reducing the risk of sudden flooding downstream (Anderson et al. 2006).
Riparian vegetation acts as a factor of hydraulic stability, reducing the energy available for bed erosion. However, it should be noted that these local benefits may be offset by effects at the edges of vegetated patches: differences in velocity between vegetated and non-vegetated areas can generate edge turbulence and scour the sediments at the perimeter of the vegetated patches (Nepf 2012).

The study of the effect of vegetation on flow often also uses experimental techniques involving laboratory simulation using artificial channels.
Among the various examples of studies of this type, one that stands out is that of (Tal and Paola 2007), which, starting from a configuration with a mobile bed and intertwined morphology, demonstrated through the progressive introduction of artificial vegetation (represented by plastic plants) that vegetation not only slows down the flow and promotes local sediment deposition, but above all triggers positive morphogenetic feedback: vegetated bars tend to reduce the active riverbed, decreasing the river's tendency to braid by limiting its lateral mobility. Conversely, in the ab-

sence of vegetation, river forms tend to be more mobile and less consolidated: a bed without vegetation cover is free to remodel itself with each flood, favoring multiple channel configurations and large unstable bars.

From a more strictly mathematical point of view, however, the experimental analysis proposed by (Vargas-Luna et al. 2014) is noteworthy, which proposes an assessment of how various types of vegetation (submerged, rigid or flexible emergent) influence river dynamics, showing a significant increase in hydraulic roughness and a consequent reduction in shear stress applied to the bottom, with a decrease in both suspended and bottom sediment transport.
Just as vegetation has a decisive effect on flow and solid transport, it can also be strongly affected by hydro-morphodynamic pressure in exceptional flood conditions, causing vegetation mortality, which in turn causes significant changes in the characteristics of the flow itself. For example, strong current stress during a flood event can uproot trees and shrubs from the riparian zone if the force exerted exceeds the mechanical resistance of the roots in the soil, eliminating the additional resistance component of the flow and also introducing an additional load of plant debris and sediments previously immobilized by the roots into the watercourse. Episodes of vegetation removal are therefore often associated with increased erosion and mobility of the river channel (Edmaier et al. 2011).

In summary, riparian vegetation strongly modulates the hydraulic and morphological behavior of rivers during floods: when present, it tends to increase flow resistance and promote deposition and stability, while its absence (or removal) is associated with faster flows, greater sediment transport, and more unstable morphologies.

The role of vegetation in fluvial dynamics can therefore be summarized and schematized into two main aspects:

- The description of how vegetation interacts with and influences the hydromorphodynamic characteristics of the riverbed;

- The dynamics of proliferation, growth, decline, and death of vegetation within the channel and, consequently, the influence that the flow exerts on the vegetation.

With regard to this last point, the description of the biological mechanisms and hydromorphological interaction of riparian species can be organized into five main phases:
- Dispersal
- Recruitment
- Growth
- Reproduction and Succession
- Mortality

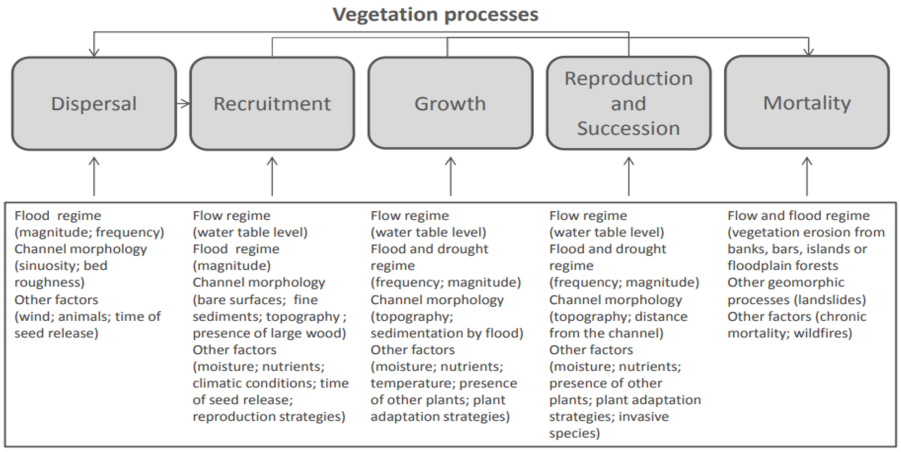

Figure 1.1: Description of the phenological phases of vegetation

Dispersal: The vegetative cycle begins with the dispersion of propagules. Riparian vegetation has evolved to take advantage of the river's energy as a means of transportation: Many species (like Salix and Populus) spread light seeds that are carried by "hydrochory" along the current, in particularly during spring floods. (van Splunder et al. 1995). The duration of the flood and the amount of time it takes for the water to recede—both of which affect the window of time during which wet substrates are exposed and available for germination—are also important factors in the success of dispersal. Furthermore, deposition sites are influenced by local topography and river micro-morphology (banks, depressions, and bars), resulting in spatial heterogeneity that is essential for riparian biodiversity (Solari et al. 2015).

Recruitment: When seeds successfully sprout and seedlings make it through the first few weeks of dynamic conditions, the recruitment phase starts. It is essential that the top few centimeters of soil be free from competition, subject to moderate disturbance, and have moist soil (as measured by infiltration, water retention, and capillary rise) (Mahoney and Rood 1998). According to empirical research, in order for the roots of young plants to follow the downward slope, the rate of water level decline following a flood must stay below critical thresholds (e.g., ¡ 3 cm/day) (Karrenberg et al. 2002). This stage, which marks a turning point in the dynamics of riparian communities, also depends critically on the texture, nutrient content, and lack of competition of the soil (Angela M. Gurnell 2014).

Growth: Once the initial phase is over, seedlings enter a period of structural and functional development. Pioneer species show characteristic adaptive traits: high morphological plasticity, rapid growth, biomechanical flexibility, and regrowth capacity (Karrenberg et al. 2002) (Dov Corenblit et al. 2015). Constant access to water is essential during growth. In areas close to the canal, plants must follow the seasonal lowering of the water table with their root system, while on higher surfaces, success depends on the residual moisture in the soil and its water retention capacity. Interaction with sediments is also ambivalent: a moderate supply of fine material can promote nutrition and topographic elevation, but excessive burial can damage the plant or inhibit photosynthesis (Camporeale and Ridolfi 2010).

Reproduction and Succession: After reaching maturity, asexual (suckers, rhizomes) or sexual (seeds) reproduction is possible. Particularly after disturbances, this process guarantees population persistence and the colonization of new areas (Angela M. Gurnell 2014). Ecological succession can occur over time, with pioneer species giving way to more resilient and competitive species, resulting in the formation of shrublands or even riparian forests. The frequency of disturbances, the site's morphological stability, and hydrological dynamics all affect the direction and rate of succession (D. Corenblit, Tabacchi, et al. 2007). The composition of the plant community is regulated by eco-hydrological processes (groundwater fluctuations, seasonal water balance) in higher environments farther from the canal, where disturbance is less frequent .

Mortality: A key component of vegetation dynamics, mortality can be caused by mechanical (erosion, burial), biological (competition, senescence), climatic (frost, drought), or physical (submersion, desiccation, uprooting) stresses (Stella et al. 2013). Additionally, mortality serves as a mechanism for renewal: upsetting occurrences that result in the removal of significant vegetation leave room for new colonization, preserving a dynamic succession mosaic (D. Corenblit, Baas, et al. 2011). The majority of stress or mortality phenomena are strongly influenced by the hydraulic or morphodynamic pressures of the surrounding environment. For instance, they are influenced by the water table's position and the degree of solid transport, especially during flood events.

1.3 Approaches to Eco-Hydro-morphodynamic modelling

The complexity of the biological and physiological mechanisms governing the evolution of vegetation in sheltered environments in response to atmospheric and hydrological conditions does not allow for the derivation of unambiguous mathematical solutions and forces us to adopt models that reproduce their behavior as faithfully as possible.
For this reason, when attempting to produce such models, not all the variables that are significant in reality are always taken into account, but there is a tendency to select the phenological or hydro-morphological aspects that are considered most relevant and to focus on them.
To date, a large number of software programs have been developed that attempt to combine the more classic and established hydro-morphodynamic modeling with the more insidious ecological modeling, and the problems in agreeing on a single solution are evident in the diversity of the approaches adopted. In fact, sometimes the solutions follow a similar logical basis but are implemented differently, or sometimes the theoretical bases on which the design of a model is founded are widely different and consider different aspects of the theoretical foundations a priori.

The following section analyzes some of the main eco-hydro-morphodynamic modeling approaches, distinguishing between:

- Modeling the dynamics of vegetation growth, decline, and evolution;
- Modeling the hydro-morphodynamic contribution that vegetation provides to the river.

1.3.1 Delft 3D (Flexible Mesh)

The Delft3D Flexible Mesh (DFM) (Deltares 2025) system is an advanced numerical platform for multidimensional simulation of hydraulic, sedimentological, and more recently, ecological processes in river and coastal systems, through coupling with the D-vegetation Python module. It is one of the most widely used systems worldwide, both in academia and in professional settings, thanks to its modularity and reliability.
The modeling environment is illustrated by a conceptual schematization in Figure and demonstrates the link between the vegetative module and the idromorphodynamic module that interact for every timestep.

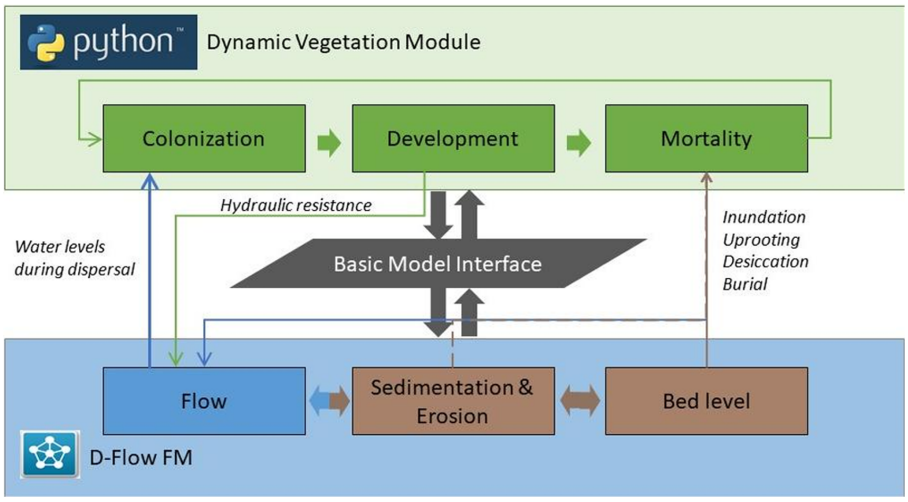

Figure 1.2: Delft 3D Flexible Mesh flow chart

The software in question is capable of simulating, through its vegetation development module, a large number of different biota depending on the case study. In particular, it provides descriptions, using different modeling approaches, of the following plant types: generic vegetation (generally refers to seagrass), salt marshes, mangroves, and riparian vegetation.
The latter, based on Van Oorschot's PhD study (2017), is the most relevant case for the subject of this study. It has been applied to various studies on different river systems (Maartje M. P. Van Oorschot 2017)(Kleinhans et al. 2018) and estuaries (Brückner et al. 2019) and is perfectly suited to describing some of the most common riverine plant species such as willows and poplars, expressing the characteristics of the plant in terms of stem density, stem height, stem diameter, and root depth.

Model description

Colonization: Colonization of vegetation takes place during the seed user-defined dispersal period, and requires that colonization occur if the cell is considered "dry" and was previously in "wet" conditions.
According to the following relationships:

$$t - 1 > \varepsilon_{hu} \quad \cap \quad h_w < \varepsilon_{hu} \quad \text{(water depth)} \tag{1.7}$$

based on the input conditions from D-Flow FM in order to simulate a hydrochory process.
When cells are already completely filled with older vegetation, new vegetation cannot settle. Vegetation is added to a cell with a maximum fraction. Each cell can contain a series of different types of vegetation, each characterized by its own age.

Growth: the model provides for two distinct approaches to plant growth, one for seedlings and one for mature vegetation. Seedling growth tends to be faster and is calculated at each timestep. Mature growth follows a different model and is updated annually.

Seedling growth is determined by shoot length and root length, which are represented respectively by a sigmoid curve in the case of the shoot

$$s(t) = \frac{c}{1 + e^{(a+b\cdot t)}} + d \tag{1.8}$$

and a logarithmic curve in the case of root length.

$$r(t) = (c - d) \cdot \left(1 - e^{-k\cdot t}\right) + d \tag{1.9}$$

Where:

$$\begin{aligned} a, b &= \text{parameters of the sigmoid curve,} \\ c &= \text{maximum shoot or root attainable,} \\ d &= \text{shoot or root value after colonization.} \end{aligned}$$

Once they reach adulthood, plants follow a law of annual logarithmic growth of the type

$$s(a) = g \cdot \log_{10}(a) \tag{1.10}$$

Where:

$$g = \text{growth parameter adjusted according to the characteristics of the plant.}$$

In conclusion, the Delft 3D model predicts that growth always occurs outside of conditions in which external pressures cause mortality or decline in the cell.

Mortality: Vegetation mortality can be caused by uprooting, burial, flooding or desiccation and is age dependent.
Uprooting occurs if the erosion is greater than the length of the vegetation root times an uproot factor. The $uproot_factor$ is the fraction of the root that has to be exposed to be uprooted.

$$Uprooting = erosion > (r \cdot ur) \tag{1.11}$$

Mortality by burial takes place when a shoot is completely covered with sediment.

$$Burial = Sedimentation > (s) \tag{1.12}$$

Where:

$$s = \text{shoot height.}$$

Mortality by flooding starts to take place if the consecutive flooding in a grid-cell (so when water level has a height superior to the cell height) exceeds a threshold. The threshold and rate at which mortality takes place is dependent on vegetation age and vegetation type. This is calculated in several steps. First, the current survival is calculated with the threshold value, a slope determining the rate of mortality, and the consecutive flooding days of the grid-cell (equation).
Because the survival rate is calculated incrementally, the ratio between the previous

and the current survived fraction determines the amount of mortality. The previous survival is calculated with Equation:

$$\begin{aligned} sr(t) &= 100 - (fd - ft) \cdot fs \\ sr(t-1) &= 100 - \big((fd - ts) - ts\big) \cdot fs \end{aligned} \tag{1.13}$$

Where:

sr = percentage of surviving vegetation,
fd = number of consecutive days the cell is submerged,
ft = mortality threshold for flooding (`flood_thrshld`),
fs = mortality rate (`flood_slp`).

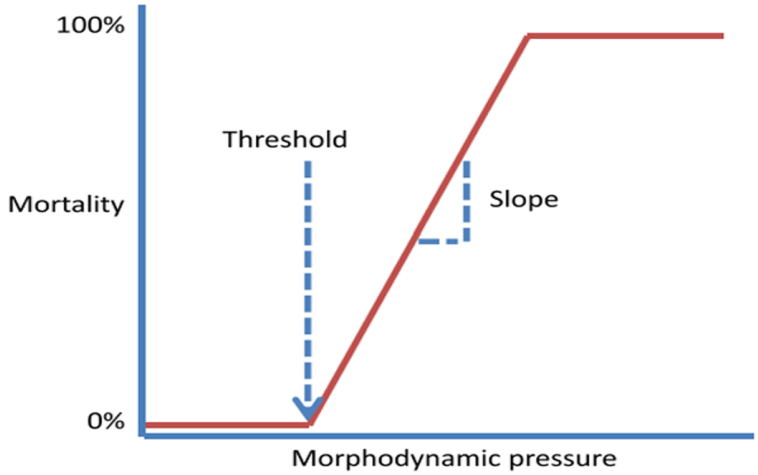

Figure 1.3: Mortality by flooding

The final fraction of vegetation that persists in a cell is calculated by

$$f = f_{t-1} \frac{sr(t)}{sr(t-1)} \tag{1.14}$$

Where:

f = the fraction of vegetation that is left after mortality is calculated.

Desiccation-induced mortality is estimated in a similar way to flood-related mortality, but takes into account the number of consecutive days that a grid cell remains dry, as well as the groundwater level, root depth and the capillary fringe (see Equation (1.15). Plants only experience drought stress when their roots are unable to reach groundwater (see Figure 1.4). The groundwater level (gwl) in a floodplain cell is determined by averaging the distances to the three nearest grid cells containing water.

$$gwl + cf < r \tag{1.15}$$

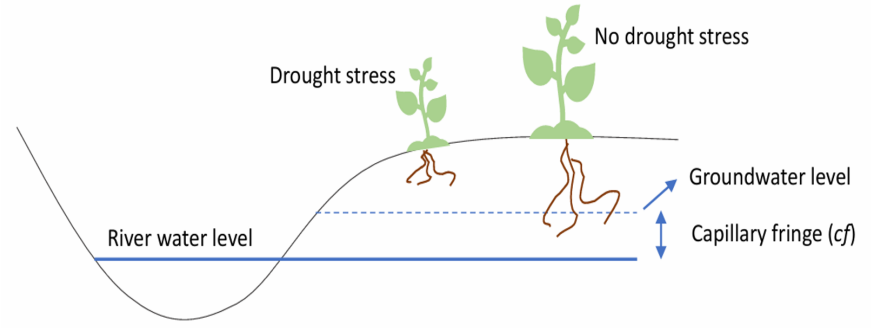

Figure 1.4: Scheme of water stress and dependence from gwl

In Figure 1.5 it is possible to appreciate the input that the the user has to insert in order to perform the simulation

Parameter	Description	Life stage dependent
years_lifestage	The amount of years a species is in a certain life stage	yes
nr_stems	the amount of stems per (stems/m2)	yes
drag_cf	vegetation drag coefficient	yes
dry_thrshld	threshold for desiccation mortality process	yes
dry_slp	slope for desiccation mortality process	yes
flood_thrshld	threshold for flooding mortality process	yes
flood_slp	slope for flooding mortality process	yes
vel_thrshld	threshold for uprooting mortality process	yes
vel_slp	slope for uprooting mortality process	yes
root_depth_min	minimum rooting depth [m]	yes
root_depth_max	maximum rooting depth [m]	yes
uproot_factor	factor determines which fraction of the roots should be exposed before uprooting	yes
ini_fraction	initial fraction of vegetation in grid-cell after colonization	no
factor_shoot	growth factor shoot	no
factor_diameter	growth factor stem diameter	no
factor_root	growth factor root	no
ini_shoot	initial size of shoot [m]	no
ini_diameter	initial size of stem diameter [m]	no
ini_root	initial size of root [m]	no
dispersal_period	[day no. start dispersal, month no. start dispersal, day no.end dispersal, month no. end dispersal]	no
shifting_month	month where colonization and aging of vegetation takes place	no
capillary_fringe	capillary fringe, i.e. water available above groundwater level [m]	no
seedling_sigmoid_fit	parameters to calculate sigmoid growth function for seedlings	no
seedling_root	parameters to calculate the root growth for seedlings	no

Figure 1.5: Inputs of the model

With regard to modelling the impact of vegetation on the hydrodynamic and morphodynamic characteristics of the river, the model uses a relationship extrapolated from (Baptist et al. 2007). This relationship updates the riverbed's roughness characteristics by modifying the Chezy coefficient according to stem density and plant height.

$$C = \frac{1}{\sqrt{\frac{1}{C_b^2} + \frac{C_d n h_v}{2 \cdot g}}} + \frac{\sqrt{g}}{\kappa} \ln\left(\frac{h}{h_v}\right) \tag{1.16}$$

Where:

C = vegetation roughness according to the Chézy formulation [$m^{0.5}/s$],
C_b = natural bed roughness in the Chézy formulation [$m^{0.5}/s$],
c_d = drag coefficient depending on vegetation type,
n = vegetation density [stems/m],
h_v = vegetation height [m],
κ = von Kármán constant, equal to 0.41,
h = flow depth [m].

In his study, Maartje M. P. Van Oorschot (2017) demonstrates that the assumption of dynamic vegetation, i.e., vegetation that undergoes continuous evolution according to the model described above, which also includes differentiation according to life stage, reproduces, based on a study carried out on a section of the Allier River (France), a behavior that is decidedly faithful both from a morphodynamic point of view and in consistently reproducing (based on comparisons made using aerial photographs) the evolution of vegetation, in the forms and distribution of the vegetation cover observed and the age of the plants reproduced. However, the amount of simulated vegetation is slightly underestimated compared to the actual amount observed in the aerial photographs (10% compared to the actual 16%).
The software is therefore particularly suitable for predictive models of river and floodplain evolution.

1.3.2 HEC-RAS RVSM

The RSVM module integrates with the renowned HEC-RAS hydro-morphodynamic simulation software and offers an alternative solution for simulating the dynamics of riparian vegetation together with hydraulic processes, based mainly on the inclusion of user-defined variables that can be adapted to each specific case.

It is designed to predict the spatial and temporal evolution of vegetation along river areas (banks and floodplains) in response to runoff patterns, groundwater variations, and the morphodynamic processes of the river. It has been tested on a wide variety of riparian species, and riparian vegetation can represent not only a single species but also an aggregate of different species. Vegetation is represented by six main characteristics: plant height, canopy height, canopy width, stem diameter, number of stems, and root depth.

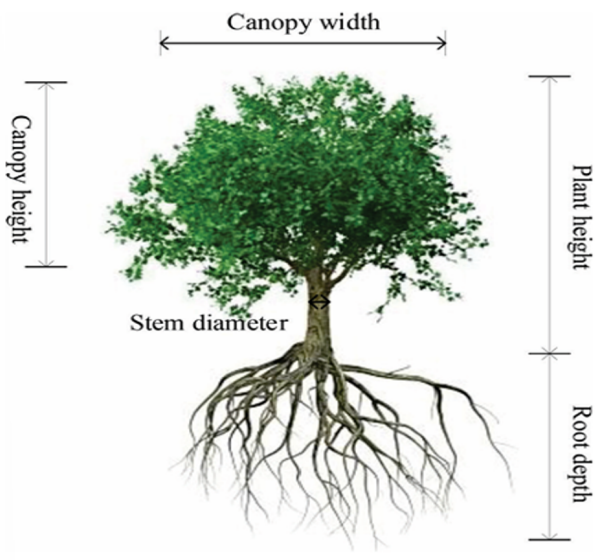

Figure 1.6: Single element of vegetation characteristics

HEC-RAS provides RVSM with the necessary physical conditions at each time interval: free surface elevation, water depth, average velocity, and energy slopes along each section of the river.
These informations are supplemented by a simple sub-model that estimates the groundwater level in the plain and the height of the capillary fringe above the water table. The height of the water table (h) is therefore a function of the free surface of the river and also depends on the distance from the free surface itself and on time.

$$\frac{\partial h}{\partial t} = \frac{\partial}{\partial y}\left(h_c \frac{\partial h}{\partial y}\right) \tag{1.17}$$

The model consists of four main phases that define its structure:

- Definition of the geometry of the study area;
- Vegetation establishment;
- Vegetation simulation;
- Mortality simulation.

Vegetation Computation Mesh

The floodplain is spatially discretized into polygons (vegetation calculation cells) distributed along the river banks, typically as a grid of "slices" parallel to the riverbed. Each polygon represents a homogeneous unit of land (in terms of soil, groundwater, and vegetation cover) on which plant growth or death processes will be evaluated. Starting from satellite images, the matrix is also initialized by entering initial vegetation values.

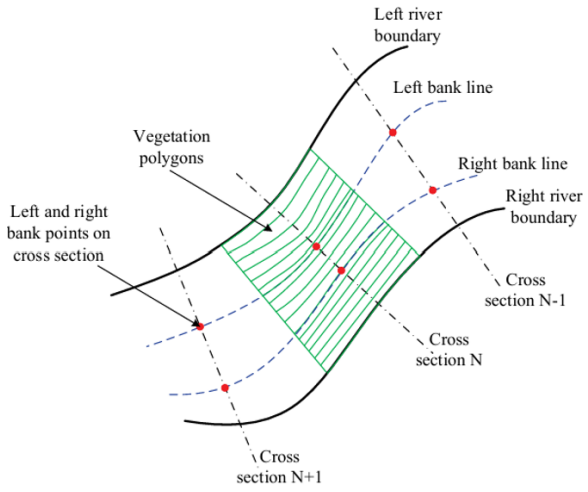

Figure 1.7: Computation mesh

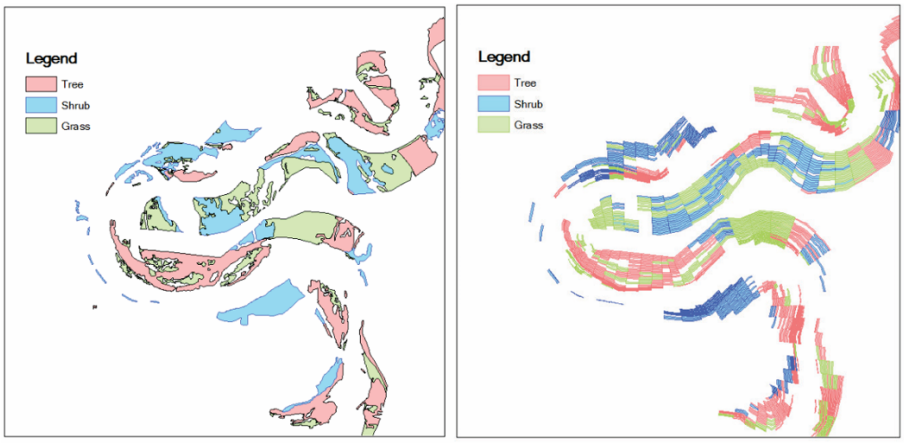

Figure 1.8: Mesh initial conditions

After initializing the initial conditions through the computational mesh, the simulation proceeds for each time step. At every time step, the simulator performs the following operations in sequence:

1. Hydraulic simulation with HEC-RAS under unsteady flow conditions to update flow dynamics (optionally coupled with sediment transport if included);

2. Update of the groundwater model to estimate the piezometric head in the soil of each polygon;

3. Ecological simulation of vegetation on a polygon-by-polygon basis, including the sub-processes of new colonization, growth, and mortality;

4. Update of hydraulic parameters according to the new vegetation state.

Vegetation development
Establishment: During the seed dispersal season—defined for each species based

on the natural seed release period—the model makes seeds available in suitable polygons. Seed germination occurs within predefined time windows (germination seasons) and only if physical suitability criteria are met in the polygon: in particular, the soil must be sufficiently moist (a condition often represented by the rise of the capillary fringe to the surface following a flood) and there must be no competing vegetation cover in the polygon that would prevent rooting. This logic is based on the well-known concept of the 'recruitment box model' (Mahoney and Rood 1998), which identifies the altitude range and time period within which a receding flood allows survival.

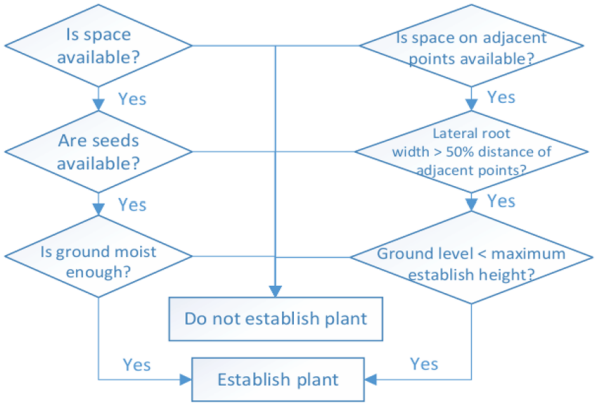

Figure 1.9: Establishment Flow chart

Plant Growth: Plant growth simulation is performed based on monthly growth values input differentiated by plant age group (e.g., faster growth in the early years and then a gradual slowdown as the plant matures) to track three main parameters calculated: root depth, stem, and canopy, which vary from species to species. The remaining three characteristics are calculated using three allometric relationships that link them uniquely to the calculated variables.

$$H_p = aD^b, \quad H_c = \alpha H_p, \quad W_c = \beta H_p \tag{1.18}$$

The model can track multiple individuals belonging to different species within each polygon. However, once a certain vegetation becomes established in a polygon, it generally tends to exclude the colonisation of other species (unless subsequent disturbances occur). The daily time step enables the cumulative effects of short-lived events (e.g. floods lasting a few days) and rapid changes in the water table to be captured.

Mortality: Mortality is calculated at each time step for every cell and occurs through seven different processes:

1. *Desiccation* (death by drought), due to an excessive lowering of the groundwater table with respect to the root system. It can be calculated with two alternative methods: one based on the number of days during which the root

tips remain above the capillary fringe (beyond a certain limit the plant withers), and another based on a cumulative water stress index that integrates the rate of groundwater decline;

2. *Drowning*, due to prolonged submergence of plants during a flood, when the water level exceeds the plant top for more consecutive days than the species-specific tolerance;

3. *Mechanical erosion or uprooting (scour)*, caused by current action during floods, when flow velocity exceeds the threshold resistance of plants against detachment;

4. *Burial*, occurring during a high-flow event, when the deposited sediment exceeds the plant height by a pre-defined percentage, leading to death;

5. *Interspecific competition*, when different species coexist within the same polygon and some (e.g., invasive species) prevail over others until outcompeting them;

6. *Natural senescence*, i.e., when plants exceed their maximum biological age.

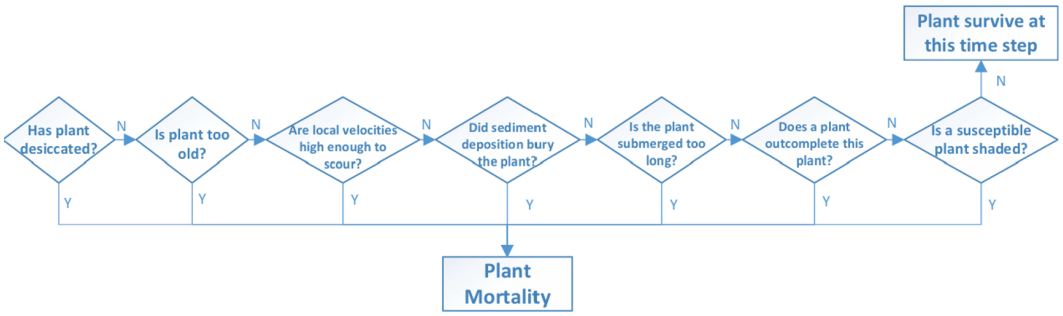

Figure 1.10: Mortality Flow chart

The proposed model is both versatile and comprehensive, but it requires a large amount of input data in order to operate. Each plant type is associated with relevant biological parameters, such as the growth rate of roots and stems (by age class and month), maximum root depth, thresholds for flooding tolerance (the number of days of flooding tolerated), critical uprooting speed and maximum longevity.

Considering instead the modeling of the influence that vegetation exerts on hydraulic and morphodynamic characteristics, this is achieved through the dynamic updating of flow resistance parameters. The model incorporates various methods for updating the Manning's coefficient n in order to describe the alteration of the roughness of the bottom. RVSM allows the user to choose between 11 different methods depending on the characteristics of the vegetation that are considered relevant and the type of vegetation. Some of the available formulations are, for example, the n–UR curves, the Kouwen and R.-M. Li (1980) method for flexible grasses, the formula by Huthoff et al. (2007), Baptist et al. (2007), Järvelä (2004) for woody shrubs.

The model has been tested in multiple situations to verify its effectiveness, the most relevant of which is represented by the simulations on the Sacramento River in California by Wang et al. (2018), in which the evolution of riparian vegetation under different hydrological conditions was simulated.

In this case study, 20 vegetation types were simulated, including pioneer tree species, mature forest species, and invasive species. The model results were validated by comparison with GIS maps and field surveys, demonstrating high spatial consistency in the prediction of post-flood colonization areas.

1.3.3 CASiMir

CASiMiR Vegetation is a dynamic riparian vegetation simulation software module developed as part of the CASiMiR (Computer Aided Simulation Model for Instream Flow Requirements) platform. It is designed to assess the impact of human interventions (dams, embankments, flow alterations) or climate scenarios on the dynamics of riparian vegetation succession and regression (Benjankar, Yager, Tonina, Egger, and Plank 2014).

Succession and regression are two key concepts in the growth and development of plant species, especially when it comes to riparian species, as flooding and hydrological pressure often force the areas closest to the river course to find themselves in bare soil conditions, subject to the proliferation of pioneer species.

Succession is a series of phases (successional stages), starting with pioneer communities that settle on bare or disturbed soils and ending with more stable and complex communities that don't have any disturbances. In a river setting, the usual order of things begins with annual grasses and pioneer shrubs (like willows and young poplars) on sandy-gravel bars that appear after floods. It then moves on to mature riparian forests (like poplar and broadleaf galleries). Some of the things that affect this process are how much moisture is available, how stable the substrate is, how deep the groundwater is, and how often the river is disturbed.

Regression is the opposite of succession: it occurs when vegetation regresses to younger stages or is completely eliminated due to intense environmental disturbances (e.g., very strong floods, prolonged flooding, mechanical erosion, or excessive submersion).

The structure of the model is organized into three main modules, each representing a physical–ecological process governing the evolution of riparian vegetation:

- **START MODULE**: based on the "height medium level," the topography, and the reference zone, it predicts the PNV (Potential Natural Vegetation) as initial condition;
- **DYNAMIC MODULE**: simulates and reproduces vegetation changes driven by morphodynamic and flood disturbances;

- **VISUALIZATION MODULE**: allows the visualization of the simulation results.

Each module operates according to Boolean logic (true/false), using predefined critical thresholds derived from experimental data.
In practice, the model assesses whether the physical conditions in each cell exceed certain thresholds each year. Depending on the outcome, the vegetation in that cell either progresses through the succession stages, regresses to pioneer stages, or is eliminated.

A fundamental aspect of the model is its approach to modeling based not on specific species, but on "successional stages". Vegetation is categorized into types or successional stages (e.g., herbaceous pioneer stage, young riparian forest, mature forest, etc.), each defined by a specific age range and comparable ecological requirements, independently of the particular species involved. This method makes the model more general and easier to use in different places around the world. The approach is therefore much less specific and less focused on a detailed description of the spatial distribution of vegetation, and is therefore less suitable for engineering applications, but more suitable for biological analyses.
This methodological choice, proposed by A. García-Arias et al. (2013), allows for the definition of 13 succession phases grouped into 4 stages and 3 major succession series, representing the entire evolutionary spectrum of riparian communities from pioneer to mature climatic communities.

Its conceptual development is based on the work of Benjankar, Yager, Tonina, Egger, Plank, and Segura (2011), integrating existing ecological theories with empirical field data. The model uses a two-dimensional grid (raster cells) representing the floodplain as its basis for calculation; each cell is assigned a vegetation status (successional type and, internally, the approximate age within that phase).

The evolution of vegetation in each cell depends on rules and functional relationships between physical river processes, hydrological conditions, and the requirements of plant communities.

At each time step (annual), the model evaluates for each cell:

a) whether new plants can establish (recruitment) on bare soil,

b) whether the intensity of physical disturbances in that year (e.g., a flood) is sufficient to damage or remove the existing vegetation, and

c) in the absence of strong disturbances, whether the existing plant community can increase in age and progress to the next successional stage.

The "Dynamic module" was introduced previously. It contains the main processes involving the life and evolutionary processes of vegetation. The module is composed of three submodules.

1. Recruitment Module: determines where and when new seedlings (pioneer vegetation) can establish themselves on vegetation-free surfaces. Recruitment typically occurs on recent sediment deposits (sand-gravel bars) or on bare soils created by the disturbance of the last flood. CASiMiR defines potential recruitment areas, often distinguishing between AZ (bank area, closest to the active channel, e.g., between the average spring water level and a minor flood reference level) and FZ (higher plain area). In each 'free' cell in these areas, the establishment of new shoots is subject to two main conditions: the availability of seeds/substrate and adequate water conditions. In practice, the model requires that the groundwater level or soil moisture be within an optimal range (neither too deep to cause drought nor too shallow to create anoxia). The timing of floodwater withdrawal must coincide with the period of pioneer species dispersal (hydrochory). These conditions are simplified in the model through threshold parameters: for example, a minimum and maximum groundwater level during the growing season to allow recruitment, and a range of suitable altitudes HBFL (height above base flow level) and HML (height above mean water level).

2. Morphodynamic Disturbance Module: This module represents the effects of physical river forces (mainly shear stress caused by the current and sediment flow pressure). The parameter adopted is shear stress. In CASiMiR, the maximum annual flood shear stress (derived from hydraulic modeling) is compared with critical thresholds associated with various types of vegetation cover. If the annual shear stress in a given cell exceeds the threshold for the vegetation present, the model considers that a destructive disturbance has occurred: the vegetation is largely removed or regressed to a previous stage. If, on the other hand, the flood does not exceed the threshold, the morphodynamic disturbance is insufficient to cause significant changes and the existing vegetation can persist undisturbed.

3. In addition to mechanical stress, riparian plants can suffer physiological stress due to the duration of flooding and the resulting conditions of anoxia. CASiMiR assesses the annual duration of flooding by identifying intensity classes (very low, low, medium, high, very high). Pioneer species and young riparian communities tend to be more tolerant of frequent submersion, while later stages are less tolerant of prolonged standing water. If the annual flooding in a cell exceeds the tolerance of the vegetation present, the physiological disturbance module results in the mortality or regression of the community.

Just as the presence of disturbance factors defines and leads to processes of elimination or regression of plant species, in the same way, implicitly, the absence of these disturbance factors for one year creates the conditions for the aging of the plant niche and subsequently for succession phenomena. For example, if an area has been colonized by annual herbs for three years without disturbance, the transition to pioneer shrubs may begin; after several more years without disturbance, the area will transition to young trees (willow groves) and so on until it reaches a mature forest stage. These transitions occur according to predefined age intervals for each

phase.

The processes of settlement, succession, and regression are therefore rigidly established by well-defined rules that determine their evolution depending on disturbance factors. Figure 1.11 and 1.12 show some examples of these rules depending on the sources of disturbance, in this case defined by the height of the flow and expressed in terms of HBFL (Height above base flow level) and HML (height above medium level), by the boundary conditions previously introduced (AZ, BZ) and by time-dependent threshold values that must be respected in order to trigger succession.

Rules	Existing vegetation types	Zones	If Condition	Outcome
R1	Gravel and sand bar (GS)	BZ	HBFL $<$ 0.65 m	GS
R2	Gravel and sand bar (GS)	BZ	HBFL $\geq$ 0.65 m	PV
R3	Gravel and sand bar (GS)	FZ	HBFL $\leq$ 0.60 m	DM
R4	Pioneer vegetation (PV)	BZ	HBFL $<$ 0.65 m	GS
R5	Pioneer vegetation (PV)	BZ	HBFL = 0.65–0.70 m	RF
R6	Pioneer vegetation (PV)	FZ	HBFL $\leq$ 0.60 m	DM
R7	Deep marsh (DM)	FZ	HBFL $>$ 0.65 m	PV
R8	Pioneer vegetation (PV)	BZ	HBFL $>$ 3.2 m	RF
R9	Pioneer vegetation (PV)	BZ	HBFL = 0.70–3.20 m	CWS
R10	Pioneer vegetation (PV)	FZ	HBFL $>$ 0.6 m	RF

Figure 1.11: Establishment rules

Rules	Existing vegetation types	HML (m)	Age range	SS_c (N/m^2)	if Condition	Outcome	FD_c (d)	If Condition	Outcome
R11	Gravel and sand bar (GS)	<-0.15	0–1	4	SS>SS_c	GS	H	FD=H	GS
R12	Pioneervegetation (PV)	-0.15–0.55	2–3	5	SS>SS_c	GS	H	FD=H	GS
R13	Reed and forbs (RF)	>1	4–25	5–10	SS>SS_c	GS	H	FD=H	GS
R14	Cottonwood and willow shrub (CWS)	0.55–1	4–15	5–9	SS>SS_c	GS	H	FD=H	GS
R15	Deep marsh (DM)	<0.3	0–3	6–7	SS>SS_c	DM	M	FD=M	DM
R16	Shallow marsh and wet meadow (SMM)	0.3–1.35	4–25	7–18	SS>SS_c	DM	H	FD=H	DM
RI7	Wet forbs and shrubs (WFS)		26–110	21–30	SS>SS_c	DM	H	FD=H	DM
R18	Reed, forbs and shrub (RFS)	1.72–2	26–110	11–22	SS>SS_c	GS	H	FD=H	PV
							M	FD=M	RP
RI9	Young cottonwood forest (YCF)	1.35–1.72	16–55	9–21	***SS>SS_c***	***GS***	***H***	***FD=H***	***PV***
							M	***FD=M***	***CWS***
R20	Old cottonwood forest (OCF)	2.0–5.7	56–110	21–25	SS>SS_c	GS	H	FD=H	PV
							M	FD=M	CWS
R21	Mature mixed forest (MMF)	>5.7	111–300	25–31	SS>SS_c	GS	H	FD=H	PV
							L	FD=L	CWS

Figure 1.12: Succession and retrogression rules

CASiMir has been used in numerous applications to validate its effectiveness, proving to be a highly flexible and reliable tool for simulating the evolution of riparian vegetation based not only on hydraulic and morphological dynamics but also on climatic factors.

In the work of Benjankar, Yager, Tonina, Egger, Plank, and Segura (2011), the model was implemented along the Boise River (Idaho, USA) to simulate vegetation succession from 1990 to 2005, integrating flow, groundwater, and geomorphology data, and validating it with a 2005 reference map. In this case, the simulation showed high consistency, producing excellent model accuracy rates: the simulated vegetation classes showed a spatial overlap rate of 76% with those observed in the 2005 map. The greatest discrepancy was found in herbaceous vegetation and in

areas with high morphological dynamics.

The model was extended to incorporate long-term dynamics (1952–2007) in the follow-up study by Benjankar, Yager, Tonina, Egger, and Plank (2014), taking into account different anthropogenic regulation-induced changes in the river regime. 1952, 1992, and 2007 historical maps were used to calibrate and compare the model. Depending on the vegetation type and reference year, the simulation's spatial accuracy ranged from 67% to 81%. Casimir also correctly reproduced the transition from mature forest to pioneer species following flood events and changes in runoff management. The analysis also found further evidence that groundwater depth and the hydraulic disturbance index are the main factors determining vegetation distribution.

Egger et al. (2011) applied an adapted version of the model along the Nakdong River (South Korea), a large river subject to artificial regulation. The model successfully reproduced the colonization of bare areas following the construction of dams, simulating succession trajectories and the expansion of plant communities in a very realistic manner. The years 1970–2010 are included in the simulated period. The results show that regions that were formerly subject to dynamic flows have now been colonized by invasive species and secondary forests, and the distribution of plant communities along the length and altitudinal axes was in agreement with data from independent monitoring.

Finally, the study by Egger et al. (2013) tested an updated version of the model on several European rivers (Austria, Portugal, Spain), exploring scenarios with different hydrological and climatic characteristics. The results were consistent with actual observations in all three cases. In particular, it was effectively found that in scenarios of reduced runoff, the simulation predicted a decrease in pioneer species and an increase in mature forest cover, consistent with the lower frequency of hydraulic disturbances. The results were validated by comparative analyses between simulated maps and observed GIS maps, with results in agreement for over 70%.

1.3.4 RVDM (riparian vegetation dynamic model)

The Riparian Vegetation Dynamic Model (RVDM), developed by Alicia García-Arias and Francés (2015), was designed with the aim of assessing the effects of changes in the hydrological regime on plant succession, taking into account the temporal variability of flow and the interaction between soil, water, and plants, with a strong biological approach and with the intention of describing in detail the phenological dynamics of vegetation. The evolutionary dynamics of vegetation are described by distinguishing the following phases: recruitment, plant growth, succession/retrogression, impacts (flooding or drought), competition. The model integrates within the same framework:

– a classification of vegetation not by species but into "successional classes" called SPFT (Successional Plant Functional Types);

– modules that simulate hydrological impacts (flood and drought damage), recruitment and growth processes, succession and retrogression processes, and intraspecific competition;

– a soil water balance coupled with groundwater dynamics and plant evapotranspiration capacity.

As already mentioned, the fundamental unit of ecological modeling is the SPFT, i.e., a series of classes that combine taxonomic and ecological characteristics, ordered according to ecological succession lines. RVDM distinguishes three main succession lines, corresponding to three types of vegetation with different characteristics (and interactions with the river).
These range from those closest to the river and most subject to hydromorphodynamic pressures (riparian seed), to those present in intermediate areas (riparian cottonwood), and finally those belonging to the area outside the frequent flood zone (terrestrial cottonwood).

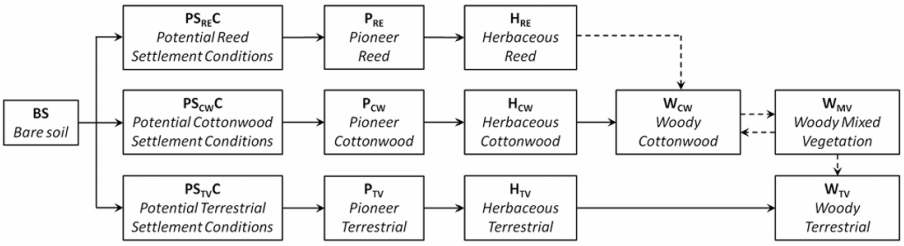

Figure 1.13: Succession lines

RVDM is structured in four modules that interact daily to update the vegetation status in each cell of a two-dimensional grid.

At each time step, the model performs:

1. Impacts module (hydrological disturbances): calculates the reduction in biomass or plant mortality due to flooding events (shear force of water), periods of root asphyxia due to soil saturation, and water stress due to prolonged drought.

2. Evolution Module (recruitment, growth, succession): updates the status of vegetation by simulating the birth and establishment of new individuals (seed recruitment), the growth in biomass of existing vegetation, and the succession transition (stage advancement or possible regression) within each succession line.

3. Competition Module: resolves both intra-line competition (between riparian plants of different lines) and inter-line competition (between riparian communities and surrounding terrestrial communities), determining changes in vegetation type in transition zones based on the ability of plants to exploit available water resources.

4. Water Balance Module: calculates soil moisture and local groundwater levels based on precipitation, evapotranspiration, runoff, and soil characteristics, taking into account rain interception by vegetation and evaporation from bare soil. These updated environmental variables directly influence the ecological modules in the subsequent steps (e.g., determining water availability for transpiration or possible root anoxia).

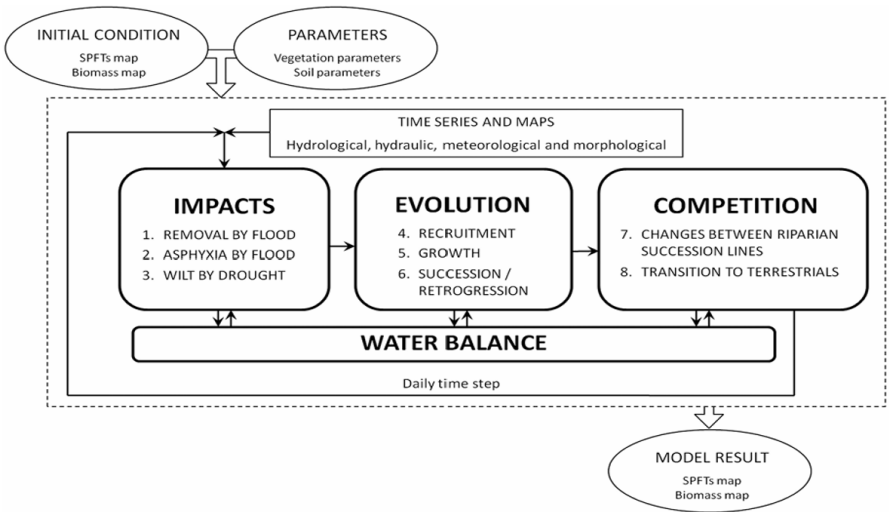

Figure 1.14: RVDM Flow chart

Thanks to this structure, RVDM is able to represent in detail the daily eco-hydrological cycle that links water flow (surface and groundwater) to the response of riparian vegetation.

However, the model is based on a fixed-bottom geometry and therefore does not include any type of morphodynamic modeling, nor (consequently) any link between the presence of vegetation and morphodynamic and hydrodynamic characteristics (shear stress). The only modification allowed is the updating of the topography using DTM.

Water balance module

An essential component of the RVDM model is the Water Balance Module, in which a water balance is performed for each soil unit (for each cell) to determine the groundwater level (a key characteristic) and certain evapotranspiration characteristics, which are useful for establishing certain plant growth dynamics specific to this model.

For each cell and each year of simulation, the module calculates the depth of the water table (zw) using a simplified approach based on the calculation of the total amount of water in the soil and transpiration.

The simplified equation can be represented as:

$$\Delta S = I - ET - P \pm L \tag{1.19}$$

The balance of the amount of water in the unsaturated zone of the soil at the end of the day is given by:

$$H(t) = H(t-1) + I(t) - T_u(t) - E(t) \tag{1.20}$$

Where:

I = daily water input into the soil [mm],
T_u = plant transpiration [mm],
E = soil evaporation [mm],
ET_0 = maximum potential evapotranspiration of the system.

$$E_i(t) + T(t) + E(t) \leq ET_0(t) \tag{1.21}$$

Interaction with the aquifer is also defined by two inflows from the saturated zone:

– U (hydraulic lift) interpreted as root water uptake that occurs only if the root is in contact with the water table

$$U(t) = -Cr\, h_n \left(\psi_{fc} - \psi(t)\right) r_s \frac{1}{1 + \left(\dfrac{\psi(t)}{\psi_{50}}\right)^{3.22}} \tag{1.22}$$

– Cwf (upward capillary water flow) is the capillary rise from the aquifer to the unsaturated layer, which is defined by
If the roots reach the water table ($Zwt \geq Ze$)

$$Cwf(t) = H_{fc} - H(t-1) - U(t) \tag{1.23}$$

If the roots reach the water table but are outside the effective root connectivity ($Ze > Zwt > Zr$)

$$Cwf(t) = \left[\frac{-0.102 \cdot \psi(t)}{Z_{wt}(t) - Z_e} - 1\right] \cdot 24K(t) \tag{1.24}$$

At this point, transpiration T is calculated.

$$T(t) = T_u(t) + T_s(t) \tag{1.25}$$

Where Tu is transpiration due to the unsaturated zone (under conditions NOT of asphyxia):

– In the presence of connectivity between the root zone and the saturated zone $Ze < Zwt$:

$$T_u(t) = r_u \cdot Cv \cdot \big(ET_0(t) - E_i(t)\big) \cdot \left(1 - \frac{Z_{wt} - Z_e}{Z_a - Z_e}\right) \tag{1.26}$$

– In the absence of connectivity between the root zone and the saturated zone $Ze > Zwt$ Tu is calculated based on the relative amount of capillary water H_rel in the soil:

$$H_{rel}(t) = \min\left(\frac{H(t-1) - H_{wp}}{H^* - H_{wp}}\,;\,1\right) \implies T_u(t) = r_u\, cv\, \big(E_0(t) - E_i(t)\big)\, H_{rel}(t) \tag{1.27}$$

And Ts is transpiration due to the saturated zone, referring only to cases where the roots are connected to the water table ($Ze > Zwt$).

$$T_s(t) = \min\Big(cv\,(E_0(t) - E_i(t)) - T_u(t)\;;\; r_s\, cv\,(E_0(t) - E_i(t))\, Z_{rel}(t)\Big) \tag{1.28}$$

Impacts module

The Impacts module assesses three types of hydrological stress that can cause biomass reduction or vegetation death in each cell:

1. REMOVAL BY FLOOD
   if a flood occurs on a given day, the model estimates the shear stress exerted by the water on the soil in each cell (without calculating the contribution of vegetation), interpolating the peak instantaneous flow value for the day on the pre-calculated reference fields for shear stress, and then compares it with two threshold values tm (minimum) and tc (critical) typical of each SPFT.

$$\tau(t) = \tau_{j-1} + \left(\frac{Q_i(t) - Q_{i\,j-1}}{Q_{i\,j} - Q_{i\,j-1}}\right) \cdot (\tau_j - \tau_{j-1}) \tag{1.29}$$

   – If $\tau > \tau_c$, the biomass is completely removed and the SPTF becomes BS;
   – If $\tau < \tau_m$, the biomass remains intact;
   – If $\tau_m < \tau < \tau_c$, the biomass undergoes a linear decrease.

   The decrease will be represented by a law that reports the final biomass value.

$$B(t) = B(t-1) \cdot \xi_\tau(t) \tag{1.30}$$

   where:

$$\xi_\tau(t) = \frac{\tau(t) - \tau_c}{\tau_m - \tau_c} \tag{1.31}$$

2. ANOXIA
   The model estimates the daily water table height. If the water table rises to saturate the root zone of a plant for a prolonged period, the roots may suffer from anoxia due to lack of oxygen.

$$Z_{wt}(t) = Z_{wt\,j-1} + \left(\frac{Q(t) - Q_{j-1}}{Q_j - Q_{j-1}}\right) \cdot (Z_{wt\,j} - Z_{wt\,j-1}) \tag{1.32}$$

- If $Z_{wt} < Z_a$, the biomass remains intact;
- If $Z_{wt} > Z_a$, the biomass suffers from asphyxia.

Each SPFT has parameters that define a tolerance range: for example, am (number of consecutive days of saturation beyond which stress begins) and ac (critical number of days beyond which the plant dies of asphyxia). In the model, if the duration of continuous saturation exceeds the critical threshold ac for a given plant, the cell is considered dead due to anoxia (transition to bare soil). For moderate periods of saturation (between am and ac consecutive days), the residual biomass is partially reduced in a similar way to the case of flooding (with a reduction factor xt or similar for asphyxia).

- If $a(t) < a_m$, growth is limited;
- If $a_m < a(t) < a_c$, the biomass decreases.

$$\xi_a(t) = \frac{a(t) + u_a\left(a_m - a(t)\right) + a_c}{a_m - a_c} \implies B_a(t) = B_\tau(t) \cdot \xi_a(t), \quad (1.33)$$

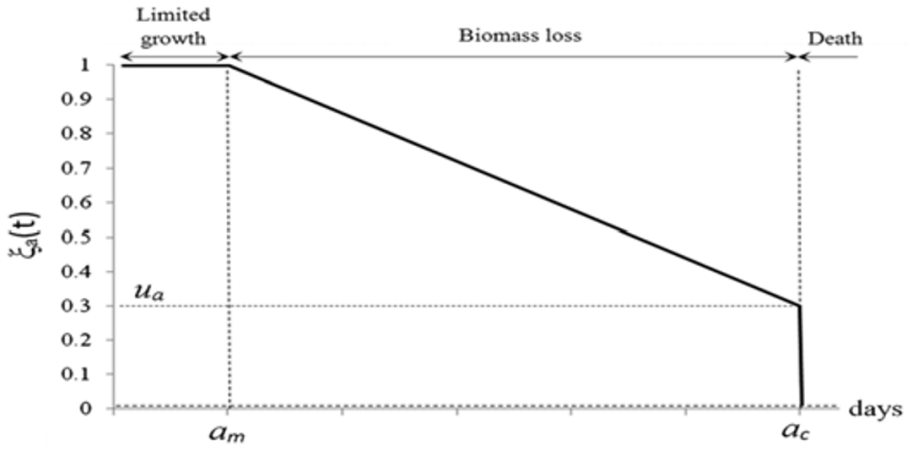

Figure 1.15: Anoxia Mortality mechanism

- If $a(t) > a_c$, the biomass dies, SPTF = BS.

3. WILTING RVDM identifies water stress conditions when soil moisture is insufficient to allow transpiration (plant in stomatal closure) -> zero transpiration T(t)=0.
   In this case too, a minimum wm and critical wc number of consecutive days of desiccation are defined for each SPFT, beyond which reversible stress or lethal damage occurs, respectively. If a cell remains below the wilting point for more than wc consecutive days, the plant is considered dead due to drought. For intermediate stress (wm < days < wc), the model gradually reduces the available biomass according to a linear function with respect to the duration of the stress, similar to the case of asphyxia.

   - If $d < w_m$, the biomass remains intact;

- If $d > w_c$, the biomass is removed and the SPTF becomes BS;
- If $w_m < d < w_c$, the biomass decreases.

$$\xi_w(t) = \frac{w(t) + u_w \left(w_m - w(t)\right) + w_c}{w_m - w_c} \implies B_w(t) = B_a(t) \cdot \xi_w(t), \tag{1.34}$$

The module is applied at the beginning of each time step, updating the status of each cell based on the hydrological characteristics input.
It should be noted that RVDM, unlike other models, does not assume fixed losses of biomass under stress but calculates gradual reductions based on the intensity of the stress and the specific thresholds of each vegetation class.

Evolution module

The Evolution module is activated once the daily impacts have been applied. It regulates the biological processes that lead to the establishment and growth of new and existing vegetation, as well as progress along the expected succession trajectories.

Is made of:

1. Recruitment
   Recruitment determines where and when new plants can establish themselves from existing seeds. For recruitment to be successful, the RVDM model checks three key conditions in a BS cell (i.e., without vegetation):

   - *Presence of seeds:* assumed possible only after spring flooding when $Q > Q_{isr}$ (hydrochory hypothesis);
   - *Germination:* possible only if the daily temperature range remains within the reference range $T_{g,\min} < T_{\min}(t) \cup T_{\min}(t) > T_{g,\max}$, the groundwater level $Z_w(t)$ remains below the anoxia threshold Z_s, and the soil moisture is above $H_{g,\min}$;
   - *Establishment:* depends on TSG (number of days since germination) and NDE (number of days required for establishment). When $TSG > NDE$, the SPTF that has accumulated a higher transpiration value $\sum T$ prevails.

   In addition, the model accounts for light availability: many pioneer riparian species (such as willows and poplars) require high sunlight to germinate. RVDM uses the photosynthetically active radiation (PAR) estimated for the cell as a discriminant: if light is limiting, the germination success of heliophilous species is reduced, possibly favoring more shade-tolerant species.

2. Growth
   In cells already covered with vegetation, the growth sub-module updates the plant biomass, simulating the increase due to primary production. Growth is calculated on a daily basis, considering ecophysiological parameters such as

the Leaf Area Index (LAI), Light Use Efficiency (LUE), and the fraction of Absorbed Photosynthetically Active Radiation (APAR) for each community.

A logistic growth function is applied, accounting for the progressive attainment of a maximum biomass ceiling based on available resources and vegetation coverage (vegetation coverage factor, Cv).

$$\frac{dB}{dt} = \big(LUE \cdot ET_{idx}(t) \cdot APAR(t) - Re(t)\big) \cdot \varphi_l(t-1) - k_a \cdot B(t-1) \quad (1.35)$$

For each vegetated cell, the model increases plant biomass according to the available light (derived from incident solar radiation, reduced by shading and LAI) and the water available in the soil: if there is sufficient moisture to allow transpiration, the plant grows; otherwise, growth is slowed or stopped.

3. Succession/Retrogression
   Within each riparian succession line (reed bed, riparian forest) and in the terrestrial line, the model evaluates whether the vegetation present in a cell can advance to the next stage (succession) or must regress to a previous stage (retrogression) based on age and accumulated biomass. Each SPFT is characterized by a minimum age $A_{\min}$ and a minimum biomass $B_{\min}$ required to transition to the next stage.
   If the thresholds A_s and $B_{\min}$ are reached, the plant (SPFT) undergoes succession to the next stage. Conversely, regression occurs if the vegetation reaches the predefined maximum age ($SPTF = BS$) or if A_{max} is attained while biomass remains below $B_{\min}$.

Competition module
The Competition module acts on cells where several different vegetation types coexist or are possible, examining two cases of spatial competition: (1) competition between different riparian lines, and (2) natural transition from riparian vegetation to terrestrial vegetation under conditions of reduced disturbance. This module therefore determines which plant community prevails in border or mixed areas, taking into account the fact that riparian species thrive in unstable hydrological conditions, while terrestrial species tend to invade riverbanks when river disturbances decrease.

In summary, the model defines a succession path for each type of riparian and terrestrial vegetation and applies rules based on age, biomass, and disturbances to move along these paths. This representation allows us to capture important aspects of river communities, such as the fact that water-demanding species (e.g., reeds) will never colonize areas far from the river.

The model was then validated in the case of the Jucar River basin (Spain), as reported by Alicia García-Arias and Francés (2015), a semi-arid Mediterranean basin. The location has characteristics that are suitable for highlighting the potential and main features of the model, as it has well-developed riparian vegetation connected to the surrounding terrestrial vegetation, conditions that are suitable for highlighting the potential for describing the succession variability of vegetation. In fact, all three succession lines considered by the model are present. Two validation periods were

considered: the first from August 31, 2006, to December 31, 2009, and the second covering the entire decade from July 1, 2000, to December 31, 2009. The results were compared with aerial photographs collected on July 7, 2009, indicating a good spatial correspondence between simulated and observed vegetation. Furthermore, if more general categories are adopted (for example, grouping the classes into only pioneer/herbaceous/woody phases, or only reed/riparian/terrestrial lines), the model's performance is even higher, reaching 70-80%.

1.3.5 Camporeale & Ridolfi (2006)

Camporeale and Ridolfi (2006) developed a stochastic mathematical model to describe the dynamics of riparian vegetation subject to the variability of the river's hydrological regime. The objective was to capture the key processes of interaction between hydraulic flow and vegetation based on the representation of ecological and physical processes using a probabilistic approach.

The model considers "phreatophyte" vegetation and has a simpler structure than the previous cases, in which morphodynamic changes are not considered and hydrodynamic characteristics have no direct effect on vegetation. However, the model is of particular interest as it reduces the complex and varied description of the different dynamics of growth, proliferation, and mortality of some other models to a more essential structure that unifies the representation of various phenomena that influence them.

A fundamental driving force behind dynamic plant processes is the water table level, which is calculated assuming zero time delay in the oscillations between the water level and the water table.

The model is defined by two fundamental equations, one describing the dynamics of growth when the water table is below the vegetation level, while the other defines the dynamics of decline when the water table exceeds the vegetation level, ultimately providing a long-term description of the distribution of plant biomass.

– In flood conditions (when the water level in the river h exceeds the local ground level, i.e., the site is submerged), vegetation undergoes decay due to submersion stress and hydromorphodynamic pressure.

$$\frac{dv}{dt^*} = -\alpha_1 v^n, \qquad h \geq \eta \tag{1.36}$$

Where:

α_1 = decay coefficient during flooding,
n = exponent (often assumed to be equal to 1, implying pure exponential decay).

In practice, during a flood, plant biomass decreases rapidly; the case $n = 1$ indicates that the rate of biomass loss is proportional to the amount of biomass present.

– In non-flood conditions (emerged site, not covered by river water), vegetation can regrow thanks to the availability of light and the presence of water in the soil/aquifer. The model uses a generalized logistic growth equation to describe the increase in biomass towards a maximum carrying capacity V_c of the site.

$$\frac{dv}{dt^*} = \alpha_2 v^m (V_c - v)^p, \qquad h < \eta \tag{1.37}$$

Where:

α_2 = growth coefficient during exposed phases,
m, p = exponents that can adjust the shape of the growth curve,
V_c = maximum attainable biomass (carrying capacity) at that location.

A fundamental aspect of the model is precisely the entity of the carrying capacity V_c, which is not constant but varies according to long-term water conditions, in particular based on the average depth of the aquifer. Riparian phreatophytic species have an optimal aquifer depth range for maximum growth, while they suffer if the aquifer is too low (too deep, causing water stress) or too high (saturation and root anoxia). The negative impact on vegetation of an aquifer that is too deep is therefore not described by a law that directly penalizes the amount of vegetation, but is represented by a smaller carrying capacity and, consequently, slower or no plant growth. In the model, this mechanism is represented by the following equations.

$$V_c = V_c(\delta) = \begin{cases} 1 - a\,(\delta - \delta_{opt})^2, & \delta_1 \le \delta \le \delta_2, \\ 0, & \delta < \delta_1 \text{ or } \delta > \delta_2. \end{cases} \tag{1.38}$$

Where:

δ_{opt} = optimal groundwater depth, i.e., the depth at which the carrying capacity is max
$[\delta_1, \delta_2]$ = groundwater depth range compatible with vegetation survival.

The analysis of previous models, which are a sample of just some of the best-known mathematical models that describe ecological dynamics in rivers, provides important information on the operational approach to be implemented with a view to refining the modeling approach in this regard. As previously stated, the mathematical description and prediction of ecological dynamics involving vegetation (especially riparian vegetation) is neither a straightforward nor a simple process. The complexity of the biological factors and processes involved in the growth and decline of a plant go far beyond the physical description of morphodynamic and hydrodynamic processes (for example), and attempting to describe its behavior through an extremely detailed representation would most likely prove extremely difficult, if not almost impossible.

For this reason, most of these models approach the problem with equations that attempt to approximate as best as possible the multitude of phenomena and processes involved, sometimes accepting not to take into account certain factors that

we know to be biologically or physically fundamental to plant development. This is in order to obtain a model with simpler and faster computational capabilities that can be easily applied to a wider range of case studies with a certain ease (therefore without the need for preliminary data collection and analysis, which would be too burdensome).

For this reason, it is clear that not all models use the same approach and take the same factors into account when describing phenomena. For example, Alicia García-Arias and Francés (2015) include two elements in their model that are not usually taken into account, but which we know to be two key elements in the biological processes of a plant's life: the plant's transpiration capacity T , which is included in the water balance per unit of soil, and the influence that exposure to the sun has on the plant itself, represented as PAR, which we know to be the basis of chlorophyll photosynthesis processes. However, in most other models, these fundamental phenological aspects are not taken into account, or at least are "omitted" due to the modeling difficulties and data research they would entail.

Another concrete example of this phenomenon is the DRIPVEM model (Mechanism of Riparian Vegetation Growth and Sediment Transport Interaction in Floodplain) in which, as reported by Baniya et al. (2020) and Asaeda, Md Harun Rashid, et al. (2020), a descriptive model of plant dynamics and interaction with hydrodynamics and morphodynamics is developed, starting from a series of commonly used factors, such as groundwater characteristics, hydro-morphodynamic pressures, the simulation of dispersal processes, but also an aspect that is known to have a strong impact on vegetation, namely the nutritional characteristics of the soil (such as the presence of phosphorus and nitrogen). In this case, these factors are taken into account through a dedicated module of the system called the "nutritious module," which describes the nutritional characteristics of the soil based on the cyclical processes of plant mortality (which enrich the soil with nutrients) or the oscillation and variability of flooded soil areas, characteristics that clearly demonstrate the importance of river variability in the diffusion of nutrients (Asaeda, Rajapakse, et al. 2000) (Asaeda and Md. H. Rashid 2014), (Asaeda, Md. H. Rashid, and Abu Bakar 2015).

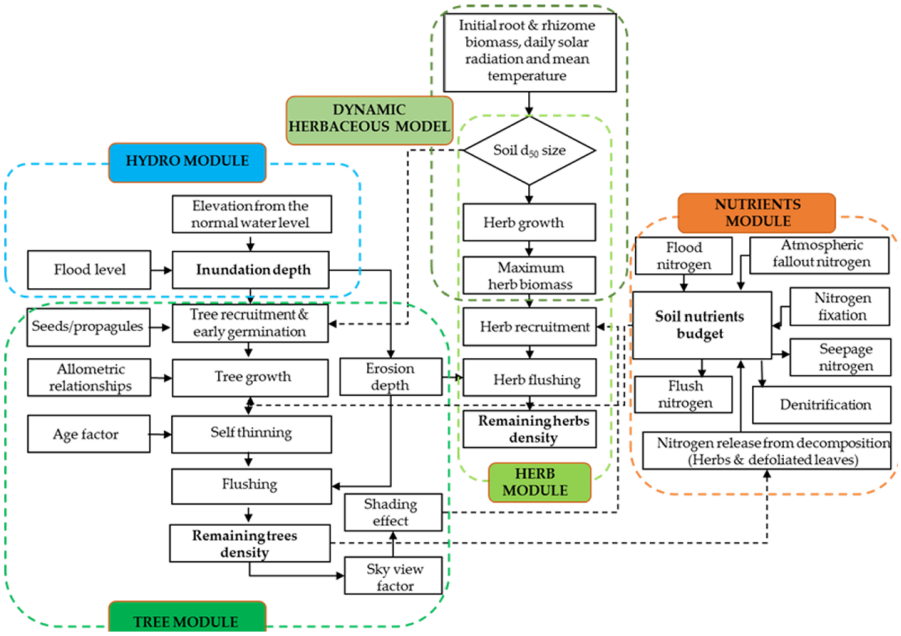

Figure 1.16: DRIPVEM modules flow chart

This information can have a significant impact on ecological dynamics in river environments, particularly with regard to human interaction with rivers (such as the effect of dams on reducing flow variability in river courses).

However, the implementation of these characteristics is still imprecise and ineffective at present and can sometimes even lead to conflicting results. Consequently, the most common approach is to avoid overloading the already complex description of river dynamics by taking into account the aspects that are most commonly and effectively recognized as relevant in influencing dynamics. . These factors are:

- The relative position between the aquifer and the plant, which determines both optimal growing conditions and conditions of anoxia or low water availability that hinder growth.
- Hydromorphodynamic pressures that tend to physically damage plants during flooding events

Although reducing biological complexity to these factors alone may seem simplistic, considering the case studies provided above, it is clear that the models are still able to reproduce the distribution of vegetation detected by satellite images fairly accurately.

For example, it has previously been shown that models such as HECRAS-RVSM or DELFT3D are able, after calibration of specific characteristics of the local vegetation, to reproduce the actual distribution with remarkably high and encouraging percentages.

Chapter 2

BASEMENT and the module BASE-VEG

Following the analysis of the previous models, the discussion now focuses on a more in-depth analysis of another highly accredited dynamic ecological model, BASE-VEG, based on the more popular hydro-morphodynamic computation model BASEMENT, whose theoretical foundations will be used as the main premises for the further model modifications that will be proposed below.

2.1 Design process and role of optimization

As previously mentioned, the reference model is BASEMENT, which is open-source software developed at the Hydraulics Laboratory of ETH Zurich. It is designed for one- or two-dimensional numerical simulations of hydraulic and morphodynamic river processes (Vanzo et al. 2021).

It is effectively applied to a wide range of river processes on different spatial and temporal scales. For instance, it can handle flood propagation at the river basin level and study local morphodynamic processes in detail, such as the formation and evolution of river bars.

BASEMENT is also compatible with models of very high spatial resolution, even down to centimetres, making it suitable for eco-hydraulic modelling and the assessment of river habitats on an ecological scale. Another notable feature is its ability to handle highly non-stationary and transient flows in the presence of complex hydraulic conditions, such as subcritical and supercritical conditions. This capability is particularly useful for simulating events such as rapid flooding or flow variations due to hydroelectric operations ('hydropeaking').

The software also allows for realistic simulation of water front propagation, making it suitable for analyzing extreme events (such as dam failure) and ecologically relevant phenomena such as flooding and cyclical drying of riparian areas.

Basement operates on an unstructured triangular mesh on which it is possible

to apply a multi-core approach or use GPU parallelization in order to significantly speed up computation times when working on very large domains.

On each cell of the mesh, the systems of differential equations that govern hydrodynamic and morphodynamic phenomena are solved using a modular approach. Each physical process is implemented in an independent module, which interacts with the others through a data flow that occurs at each temporal interaction. The modular approach also allows the various river processes involved in the simulation to be activated or deactivated individually.

There are 3 main modules, with the option to add other "secondary" modules as desired:

1. Hydrodynamic Module (HYD): The model is represented by the two-dimensional de Saint-Venant equations expressed in particular as:

$$\begin{cases} \partial_t H + \partial_x q_x + \partial_y q_y = S_h, \\ \partial_t q_x + \partial_x \left(\dfrac{q_x^2}{h} + \frac{1}{2} g H^2 - g H z_B \right) + \partial_y \left(\dfrac{q_x q_y}{h} \right) = -gH \partial_x z_B - gh S_{fx}, \\ \partial_t q_y + \partial_x \left(\dfrac{q_x q_y}{h} \right) + \partial_y \left(\dfrac{q_y^2}{h} + \frac{1}{2} g H^2 - g H z_B \right) = -gH \partial_y z_B - gh S_{fy}. \end{cases} \tag{2.1}$$

Where:

$q = (q_x, q_y)$ [m^2/s],	flow discharge per unit width,
$z_B =$ [m],	bottom elevation,
$h = (H - z_B)$ [m],	water depth,
$g =$ [m/s^2],	acceleration due to gravity.
S_{fx}, $S_{fy} = [-]$,	dimensionless friction terms in the x and y directions,
$S_h =$ [m/s],	potential external contribution/subtraction of flow discharge.

The depth-averaged velocity vector can be expressed as:

$$\mathbf{u} = (u, v) = \left(\frac{q_x}{h}, \frac{q_y}{h} \right) \text{ [m/s]}.$$

The solution of equations can be represented in vector form as:

$$\frac{\partial \mathbf{U}}{\partial t} + \nabla \cdot \mathbf{F}(\mathbf{U}) = \mathbf{S}(\mathbf{U}) \tag{2.2}$$

Where:

- $\mathbf{U} = \begin{bmatrix} h \\ hu \\ hv \end{bmatrix}$, vector of conservative variables,
  with h = water depth, u, v = velocity components;

- $\mathbf{F}(\mathbf{U})$, convective flux;
- $\mathbf{S}(\mathbf{U})$, source terms (bed slope, friction, etc.).

2. Morphodynamic module (MORPH): obtained by solving Exner's equation:

$$\frac{\partial z_b}{\partial t} + \frac{1}{1-\lambda_p}\left(\frac{\partial q_{sx}}{\partial x} + \frac{\partial q_{sy}}{\partial y}\right) = 0 \tag{2.3}$$

Where:

- z_b is the bed elevation,
- λ_p is the sediment porosity,
- q_{sx}, q_{sy} are the components of the sediment flux (bedload) in the two directions.

In which solid transport is described by a submodule (SED) and represented by empirical formulas such as "Meyer-Peter & Muller."

$$q_s = \alpha\left(\tau^* - \tau_c^*\right)^{1.5} \tag{2.4}$$

Where:

- q_s is the sediment transport rate per unit width,
- τ^* is the Shields stress,
- τ_c^* is the critical Shields stress,
- α is an empirical coefficient.

The shear stress at the bottom is therefore calculated as:

$$\tau_b = \rho g h S_f \tag{2.5}$$

Where:

- ρ is the water density,
- g is the gravitational acceleration,
- h is the water depth,
- S_f is the hydraulic slope.

3. Advection-diffusion module (SCALAR): used to simulate the transport of scalar quantities, such as non-reactive pollutants, temperature, or nutrient concentrations, within the hydraulic flow, and is described by the following advection diffusion equation:

$$\frac{\partial(hC)}{\partial t} + \frac{\partial(huC)}{\partial x} + \frac{\partial(hvC)}{\partial y} = \frac{\partial}{\partial x}\left(hD_x\frac{\partial C}{\partial x}\right) + \frac{\partial}{\partial y}\left(hD_y\frac{\partial C}{\partial y}\right) + hS_C \tag{2.6}$$

The equation represents the conservative form of the scalar transport law, where the first term on the left represents the temporal variation of the solute mass, the second and third terms represent advection in the two axes, and the terms on the right represent horizontal turbulent diffusion plus any external contributions.

Simulation flow

The workflow in BASEMENT is divided into three main phases:

1. Pre-processing: definition of the domain geometry (2DM mesh), assignment of physical parameters, boundary conditions, and forcing functions (time series of flow rates, levels, rainfall inputs, etc.). All input data are described in structured JSON files.

2. Numerical simulation: execution of the core solver according to the modular architecture, with time resolution controlled by the Courant stability condition. Each module can have a different update frequency set by the user, enabling temporal decoupling between morphodynamics and hydrodynamics, for instance. Because each module has the same amount of memory, information that is updated by one module (like depth or flow velocity) is instantly accessible to the others, eliminating the need for pointless recalculations.

3. Post-processing: visualization and analysis of results, which are saved in HDF5 binary format and made compatible with external tools (such as ParaView via XDMF files). It is possible to extract time series, spatial distribution maps, longitudinal profiles, and cross sections.

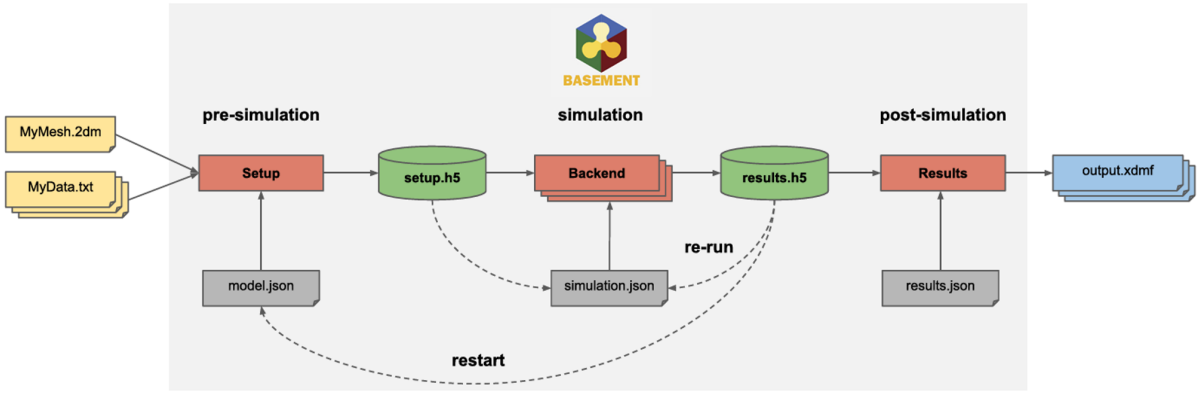

Figure 2.1: BASEMENT Flow chart

2.2 The module BASEveg

Following the examination of the various models describing the dynamics of riparian vegetation in Chapter 1, we will now analyze one of the multiple modules that can be coupled with the BASEMENT software and integrated into its workflow: BASEVeg.

BASEveg is, in fact, the module dedicated to the implementation of vegetation as a dynamic element that influences the characteristics of flow and bed. Its structure is particularly interesting because, in addition to being particularly effective and structured, it presents a unique approach to describing some fundamental dynamics of growth and decay, based on a more detailed description of phenological phenomena and focused on the dynamics of growth and decay of the root system. While it is true that the height of the water table is now unanimously considered to be of fundamental importance and is well implemented in all relevant models, the importance of the development and characteristics of the root system is something that is much less established and detailed. Base-veg is therefore particularly interesting because, in addition to introducing a certain descriptive variety of phenomena adverse to vegetation proliferation, the evolution of the root system is a fundamental element in describing vegetation, as it establishes a direct dependence between surface vegetation and root vegetation. (Caponi, Vetsch, and Vanzo 2023)

BASEveg is a Python module that works closely with BASEMENT and, as already mentioned, represents the complex eco-morphodynamic feedback between water flows, sediment transport, and riparian vegetation.

BASEveg adopts a hypothesis of separation of the time scales between plant growth and flood events, inspired by the characteristics of the hydrological regime. In terms of modeling, it is considered that on sub-annual time scales (days-seasons) the morphology of the river remains virtually stable during low water periods, allowing vegetation to colonize the emerged areas of the riverbed, while significant morphological changes occur mainly during floods, when erosion and sediment deposition can uproot or bury vegetation. Consequently, the distinction between these two types of behavior translates into a multi-stage modeling approach, in which longer phases of fixed-bottom hydro-morphodynamic simulations (where vegetation growth dynamics occur) alternate with shorter phases under dynamic morphodynamic conditions, in which the description of vegetation degradation and mortality phenomena is implemented.

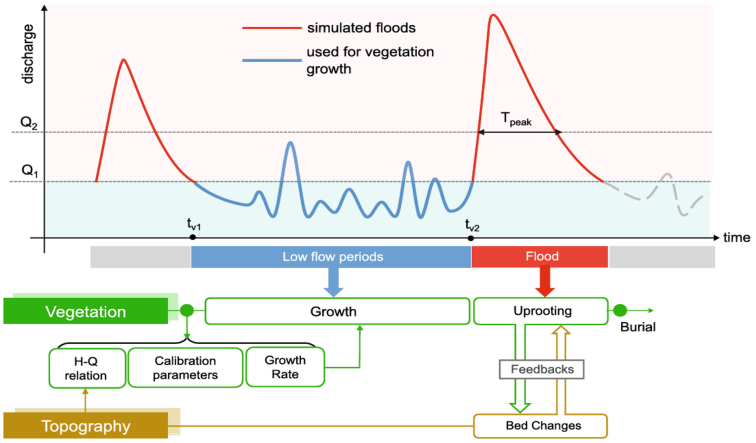

Figure 2.2: Alternation of computational phases based on flow characteristics

The alternation of these two phases is determined based on the input of hydrological regimes and the characteristics used to distinguish the two periods, i.e., a threshold flow rate Q_{morpho}.

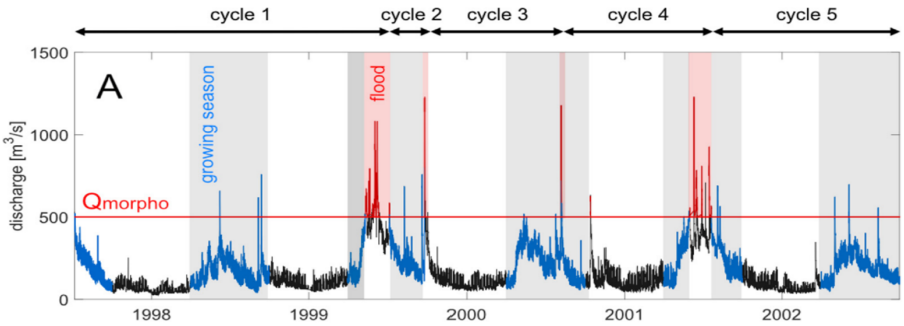

Figure 2.3: Discrimination between high flows and low flows

During periods of low water, BASEveg calculates plant growth based on fluctuations in groundwater levels. Conversely, during periods of high water, the model takes into account how the acquired plant properties influence the resistance of the riverbed to flow and solid transport, thus modulating the morphological evolution of the riverbed.

The workflow consists of five main stages:

1. Pre-processing: an initial script analyzes the time series of flow rates provided by the user and divides it into hydrological cycles, distinguishing between periods of low flow and periods of high flow. Based on this classification, the files needed for subsequent simulations are generated.

2. Low water hydrodynamic simulation: BASEveg launches a steady-state 2D hydrodynamic simulation with a fixed bottom using BASEMENT, corresponding to the vegetative growth period. The purpose of this simulation is to calculate the distribution of the water level in the river domain at low flow rates, which

is necessary information for estimating the position of the water table in the emerged areas in the subsequent steps.

3. Vegetation Growth Module: BASEveg's Vegetation Growth module comes into play, updating the vegetation status cell by cell based on local hydrological conditions, distinguishing between favorable and unfavorable conditions for growth, It does this by reading the output data from previous simulations, together with the parameters defined by the user in a JSON file, calculating the groundwater level in each cell by interpolating the water elevation in wet cells using a distance-weighted interpolation algorithm (IDW) for each simulated flow value. At this point, the vegetation status is updated according to the previously defined models.

4. Pre-flood hydraulic simulation: Before launching the simulation with solid transport, BASEveg performs a brief hydrodynamic simulation with a fixed bed settlement. This step serves to stabilize the initial flood conditions by performing a fixed-flow simulation at a base value close to the start of the flood hydrograph. During this simulation, the constant flow rate Q_1 is applied until steady-state conditions are reached.

5. Hydro-morphodynamic simulation: The actual simulation is conducted within BASEMENT, which updates the characteristic values of the simulation, taking into account the presence of vegetation and its effects on flow and sediment transport. In each computational cell, vegetation is represented in terms of above-ground biomass, below-ground biomass, and root system depth. These parameters directly influence river dynamics, modifying hydraulic resistance, shear stress on the bottom, and the susceptibility of plants to mortality processes such as burial or uprooting.

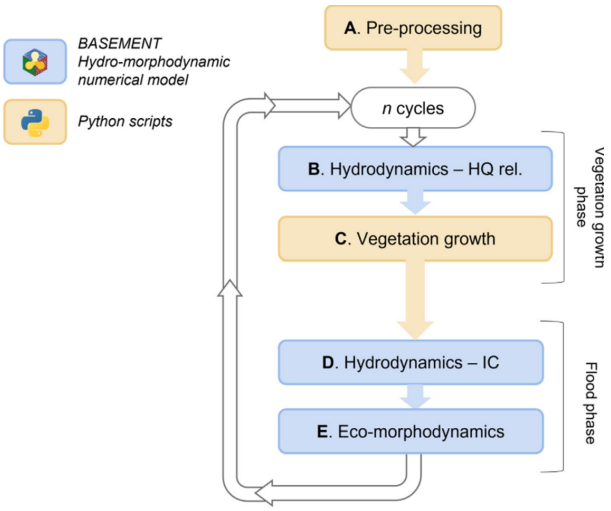

Figure 2.4: Coupling of BASEMENT and BASE-veg

Vegetation is therefore represented by three main characteristics:

- Above-ground biomass,
- Below-ground biomass,
- Root depth.

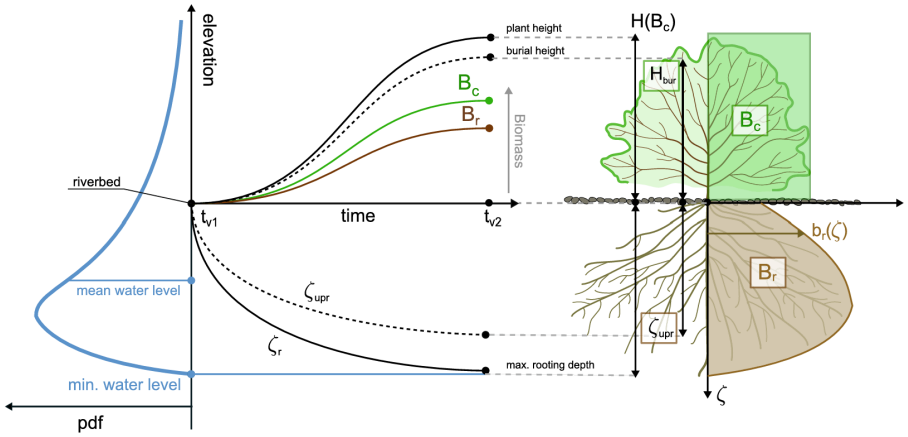

Figure 2.5: Single element of vegetation characteristics

These are the main characteristics useful for describing the pressures to which plants are subjected by hydromorphodynamic conditions and for describing the influence of eco-hydromorphodynamic feedback that vegetation exerts on the river.

The other dimensions of the plant are calculated using allometric laws that link the AG biomass value to its spatial dimensions as a function of species.

Biomass Growth
Biomass growth is described by the equations defined by Caponi, Vetsch, and Siviglia (2020) and, as mentioned above, occurs during pre-identified growth periods and is represented by a logistic dynamic with finite carrying capacity. In the absence of water stress, the dimensionless equation adopted is:

$$\frac{dB}{dt} = \sigma_B B \left(1 - \frac{B}{B_{\max}}\right) \tag{2.7}$$

Where:

- $B_{\max}$ is the maximum achievable biomass density (carrying capacity),
- σ_B is the specific growth rate.

The latter is not constant, but depends on local water conditions during the growth period: BASEveg links σ_B to fluctuations in the water table, assuming that the availability of water in the soil regulates the growth rate of plants and is defined by:

$$\sigma_B = \phi_B \int_0^1 b_r(z)\, dz \tag{2.8}$$

Where:

- $b_r(z)$ is the root biomass distribution,
- ϕ_B is a coefficient related to growth efficiency.

The biomass of the root system is in turn described by the root model of Tron et al. (2014), which provides a definition of favorable growth conditions for certain water table levels (considered optimal) and unfavorable conditions when the water table is too far or too close, to represent conditions of anoxia (roots completely submerged by water) or lack of moisture.

Another fundamental characteristic is root depth, which also grows over time according to the following differential law, causing root depth to tend exponentially toward a limit value.

$$\frac{d\zeta_r}{dt} = \sigma_r \left(\zeta_{r,\max} - \zeta_r\right) \tag{2.9}$$

Where:

- σ_r is the root elongation coefficient (fixed depending on the species, e.g., in m/day),
- $\zeta_{r,\max}$ is the maximum potential root depth achievable under given environmental conditions. In the BASEveg model, $\zeta_{r,\max}$ is chosen as the distance between the riverbed and the minimum groundwater level recorded during the growth period. This assumption reflects the ecological idea that phreatophytic plants tend to extend their roots downward as the water table drops, up to a limit dictated by the minimum depth of water in the subsoil.
- ζ_r is the actual root depth.

The equation implies that roots grow faster the further they are from the water table (i.e., drier soil stimulates the root to grow deeper) and slow down as they approach the boundary.

Hydro-morphodynamic pressures and mortality

Mortality processes occur during periods of flooding and are divided into two main phenomena, directly linked to two contrasting morphodynamic processes of erosion and sedimentation.

- UPROOTING: during floods, progressive erosion of the soil can lead to the uprooting of plants. BASEveg implements a criterion based on root biomass,

whereby once the erosion height corresponding to a critical value of root biomass Br_{cr} is exceeded, the plant is uprooted.

$$B_{r,cr} = \int_0^{\hat{\zeta}_{upr}} b_r(z)\, dz = \beta_{upr} \int_0^1 b_r(z)\, dz \tag{2.10}$$

When this value is exceeded, the root biomass and depth values are set to 0.

– BURIAL: similarly, sediment accumulation can affect the plant by burying it. At the end of each flood event, the model checks for each cell whether the rise in the bed (Δz deposited) has buried the plants beyond their survival capacity. A critical burial height H_{bur} proportional to the height of the plant is defined.

$$\Delta z_b > H_{\text{bur}} \qquad \text{where} \qquad H_{\text{bur}} = \beta_{\text{bur}} \cdot H, \quad \beta_{\text{bur}} \in [0, 1] \tag{2.11}$$

If the height of the solid deposited at full capacity is greater than H_{bur}, the plant dies and the biomass goes to 0.

HYDRAULIC AND MORPHODYNAMIC FEEDBACK: as already mentioned , BASEveg associates vegetation and computed variables with changes in the hydraulic and morphodynamic parameters of the flow, in order to describe the influence that vegetation itself has on the flow.

Unlike previously analyzed models in which the influence of vegetation was reflected in the Manning coefficient n through different formulations depending on the specific case, Caponi and Siviglia (2018) and Caponi, Vetsch, and Siviglia (2020) associate the presence of vegetation with a direct variation in the Strickler coefficient K_s. At each time step of the hydro-morphodynamic simulation in BASEMENT, the variations in K_s are updated according to changes in vegetation, following the following law:

$$K_s = K_{s,g} + (K_{s,v} - K_{s,g})\, \frac{B_c(t)}{B_{c,\max}} \tag{2.12}$$

Where:

$K_{s,g}$ = Strickler coefficient of the bare bed (depending on grain size),
$K_{s,v}$ = (lower) Strickler value for a fully vegetated bed (when B_c reaches $B_{c,\max}$),
$B_c(t)$ = above-ground biomass at time t,
$B_{c,\max}$ = maximum above-ground biomass.

The contribution of vegetation therefore has a positive effect on soil cohesion. The impact of root-enhanced riverbed cohesion on the evolution of gravel-bed rivers is took in consideration by implementing an increase of the critical Shields parameter when roots are present:

$$\theta_{cr} = \theta_{cr,g} + (\theta_{cr,v} - \theta_{cr,g})\, \frac{Br(t)}{Br_{\max}} \tag{2.13}$$

where:

- $\theta_{cr,g}$ and $\theta_{cr,v}$ ($\theta_{cr,v} > \theta_{cr,g}$) represent the threshold values for incipient sediment motion on bare and vegetated riverbeds, respectively;

- $Br_{\max}$, as $Bc_{\max}$, represents the biomass density that can be achieved when $B = B_{\max}$, which is defined as $Br_{\max} = rB_{\max}$.

Validation

To verify the predictive capacity of the BASEveg module, Caponi, Vetsch, and Siviglia (2020) applied the model to a section of the Isar River in southern Germany, known to have undergone river restoration work. The section analyzed, approximately one kilometer long, is characterized by dynamic morphologies, seasonal fluctuations in flow, and a heterogeneous presence of riparian vegetation.

The simulation, conducted over a three-year period, calculated the spatiotemporal evolution of biomass, root depth, and Ks (updated according to vegetation). The results obtained were compared with data from field surveys and existing literature on the same river section. Although the work does not explicitly report numerical accuracy indicators (such as R^2 or RMSE), the qualitative analysis conducted shows a strong consistency between the simulated vegetation distributions and the observed configurations; in fact, the vegetation is concentrated in areas subject to less morphodynamic disturbance.

2.3 Tron's root model

As mentioned above, a fundamental and particularly interesting aspect of the BASEveg model is the method used to incorporate and describe the plant root system within the model. Compared to other models, the role of roots is implemented in much greater detail in terms of root biomass and plays a much more central role in the modelling process itself.

Root size is now expressed in terms of root biomass and depth, each of which is determined by independent systems of equations. Furthermore, the direct dependence of above-ground biomass on root biomass is an entirely novel concept, but one that is fully justified given the importance of roots in intercepting moisture from the aquifer and understanding riparian biomass dynamics.

The fundamentals of modelling these characteristics can be traced back to the theories formulated by Tron et al. (2014), who developed a probabilistic model to reproduce biomass growth and decay processes, as well as biomass distribution along root depth.

This model is based on the assumption that phreatophytic species have developed adaptive strategies to cope with water shortages and tend to colonise the soil

according to water availability. Consequently, the groundwater level profoundly influences the distribution of roots in the soil as they seek the optimal humidity zone favourable to root growth, which tends to be located at the capillary rise zone.

The rationale behind the model lies in the need to quantitatively understand the interaction between stochastic hydrological processes and the biological response of plants, with the aim of integrating previous ecological concepts into an engineering implementation.

The approach taken by Tron et al. (2014) is probabilistic and attempts to describe the irregularity of groundwater fluctuations using 3 parameters:

- λ: frequency of groundwater rise events,
- α: average amplitude of rises (mean groundwater rise per event),
- η: decay rate of the groundwater level.

and then introduces the probabilistic equation that defines the oscillations of the aquifer:

$$p(z_w) = \frac{\alpha^{-\lambda/\eta}}{\Gamma\left(\frac{\lambda}{\eta}\right)} \exp\left(\tfrac{z_w-1}{\alpha}\right) (1 - z_w)^{\lambda/\eta-1}, \tag{2.14}$$

Consequently, the probability that the water table will fall within or outside the optimal zone that favors plant growth is calculated based on average hydrological characteristics and determining factors such as the extent of the capillary rise zone L.

$$k(z) = \begin{cases} \dfrac{\Gamma\left(\frac{\lambda}{\eta}, \frac{h_1-z-L}{\alpha}\right) - \Gamma\left(\frac{\lambda}{\eta}, \frac{h_1-z}{\alpha}\right)}{\Gamma\left(\frac{\lambda}{\eta}\right)}, & \text{if } -\infty < z < h_1 - L, \\ \dfrac{\Gamma\left(\frac{\lambda}{\eta}, \frac{h_1-z}{\alpha}\right)}{\Gamma\left(\frac{\lambda}{\eta}\right)}, & \text{if } h_1 - L < z < h_1, \end{cases} \tag{2.15}$$

After a detailed probabilistic description of groundwater fluctuations, we now turn to the most interesting factor, which is consistent with the modeling approach pursued in this research. Tron et al. (2014) propose a pair of equations that define and distinguish the evolution of root biomass depending on the conditions in which the portion of soil in which the biomass itself is located.

The proposed pair of equations is as follows:

$$\frac{dr(z)}{d\tilde{t}} = \begin{cases} \tilde{f}_1(r(z)) = \beta(z)\big(1 - r(z)\big), & \text{if } z_i - L < z < z_i, \\ \tilde{f}_2(r(z)) = -\gamma r(z), & \text{if } z < z_i - L \quad \vee \quad z > z_i, \end{cases} \tag{2.16}$$

And it provides for:

1. A logistic-like root biomass GROWTH equation based on the assumption of a term $\beta(z)$, which represents the growth factor (assumed to vary depending on the distance of the root depth from the bottom profile), and which corresponds to that portion of soil between the water table and the maximum height reached by moisture through the phenomenon of capillary rise (directly dependent on the porosity characteristics of the soil), where moisture conditions are ideal for root growth and proliferation

2. An exponential root biomass DECREASE equation based on γ, which represents the decrease factor and is valid for two different conditions considered unfavorable for root biomass. If the considered quota is greater than the quota reached by capillary rise, the biomass within it will be under stress due to lack of moisture (drought), while if the considered quota is lower than the water table quota, the biomass at that quota will be under anoxic conditions.

In order to simplify the formulation, the equations are normalized and made dimensionless (in temporal terms) on the basis of the decay factor γ, thus obtaining two equations scaled by a single factor θ ($= \beta/\gamma$).

$$\frac{dr(z)}{dt} = \begin{cases} \theta(z)\,(1 - r(z)), & \text{if } z_i - L < z < z_i, \\ -r(z), & \text{if } z < z_i - L \ \vee \ z > z_i, \end{cases} \tag{2.17}$$

In light of these relationships and the probabilistic structure of optimal water table heights, the dynamic behavior of root growth and decay is then extrapolated through a mechanistic use of dichotomous noise, leading to the probabilistic distribution of root biomass along its depth, represented by the following formula.

$$p(r(z)) = C\left(\frac{1}{f_1(r(z))} - \frac{1}{f_2(r(z))}\right) \times \exp\left[-\int_{r(z)}\left(\frac{k_1}{f_1(r'(z))} + \frac{k_2}{f_2(r'(z))}\right) dr'(z)\right] \tag{2.18}$$

By applying the equations $f_1(r(z))$ and $f_2(r(z))$ and solving the integral with respect to dr, it is possible to obtain the mean value of the distribution along the depth.

$$\overline{r}(z) = \int_0^1 r(z) \cdot p(r(z))\, dr = \frac{2\theta(z)k(z)}{\theta(z) + \theta(z)k(z) + 1 - k(z)}. \tag{2.19}$$

The distribution obtained, which depends directly on θ and k, is therefore also indirectly dependent on all those factors typical of the variability of the aquifer previously introduced, which constitute $k(z)$ and on which Tron et al. (2014) carry out statistical investigations in order to ascertain their influence on the distribution profile obtained.

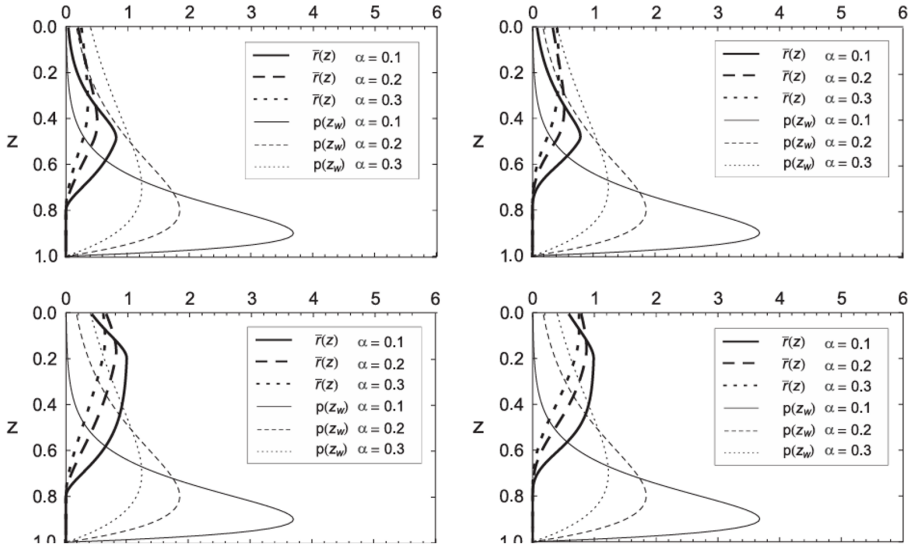

Figure 2.6: Variation of root distribution based on different regime characteristics

For example, in Fig. 2.6 it is possible to observe how the average probability distributions of biomass $r(z)$ vary as a function of the water table pdf $p(z_w)$, distinguishing between different cases of capillary rise height ($L = 0.3$ for the upper plots and $L = 0.6$ for the lower ones) and different growth factors θ ($\theta = 1$ constant for the plots on the left and $\theta = 2 - 2.5z$ for the plots on the right).

Tron et al. (2014) further note that although the variation of some fundamental values, such as θ, is not very significant, the variation of other characteristics, such as the variability of water table fluctuations (expressed through the parameter α), can lead to much more significant differences in the distribution values.

It is precisely the final formulation developed Tron et al. (2014), expressed in equationx, that is used by the BASEveg module to describe the distribution of below-ground biomass in the model along the calculated root depth. Distribution is, in fact, a fundamental element in establishing certain characteristic values of the model, such as the uprooting depth of a plant.

Chapter 3

Methodological proposal: Implementation of the Tron model

3.1 Working assumptions and specific objectives of the proposal

As mentioned above, BASEveg's methodological approach is of particular interest because it constitutes a complete eco-hydro-morphodynamic interaction model that includes plant life cycle dynamics. It is also distinguished by its in-depth functional description of the root system as the driving force behind ecological processes, implying a direct dependence of above-ground vegetation on below-ground vegetation.

However, the current implementation uses the final equation (2.18) to calculate the probability of root biomass distribution for each plant specimen in the model. This equation is applied based on the root depth value, ζ_r, which is established according to the equation (2.14).

Although this approach is much simpler computationally, it can be limiting for several reasons.
In fact, the distribution of roots does not always take on that characteristic form. The form obtained from the study by Tal and Paola (2007) is given by the average biomass values on the reference timescale. This timescale depends heavily on certain aquifer characteristics (e.g. the average height of the water table and its fluctuations). Using a non-statistical approach based on point resolution of the reference equations (2.16) at time t yields very different distributions. This is because, as the root growth factor q increases, differences in biomass values and distributions at two time instants t, even if close together, can be significant, implying profound differences from the statistical distribution referring to the same time series.

In light of this, the following section proposes a non-statistical but precise approach to solving the equations that govern the dynamics of root development as theorised by Tron et al. (2014).

3.2 Extensive description of the model

The following model therefore implements the root biomass evolution module based strictly on its dependence on the groundwater table height values h_i along a 2D river section, including both the entire cross-section and a portion of the underlying soil (sufficient to fully describe the spatial evolution of the roots).

The computation of the characteristic values is then carried out on 2D matrices, whose dimensions are defined according to the spatial characteristics of the profile and certain typical input parameters. The matrix will have a number of columns equal to the horizontal extension of the profile (difference between the minimum and maximum coordinates) and a number of rows equal to the vertical extension of the profile (difference between the minimum and maximum coordinates) plus the maximum root depth $\xi_{r,\max}$.

The "water table height" is the only forcing factor that shapes the behavior of root biomass, and its position defines and regulates the evolution of biomass by influencing its two main dimensions:

1. Root biomass $B_r(z)$: the local biomass value at a given vertical distance from the bed surface;

2. Root depth ξ_r: the depth reached by the roots, i.e., the vertical portion of soil starting from the bed where the root biomass $B_r(z)$ can develop.

For the moment, the water table level h_i is approximated as being constant throughout the length of the section and equivalent to the hydraulic head of the river. This approximation therefore does not provide for any type of latency between the moment when the free surface reaches a certain height and the moment when the groundwater reaches it. Consequently, there are no modeling techniques capable of emulating the conductivity characteristics of the aquifer, resulting in a groundwater pulse flow (Barenblatt 1996), as has been done for some models, such as HEC-RAS RVSM (eq (1.17)). In this case, similar to what was done in BASEveg, the conductivity of the porous medium is considered high enough to make the latency time approximately equal to 0. This is justified by the conductivity characteristics typical of gravel-bed rivers.

Considering initial Bare Soil conditions (absence of vegetation), the following values are assumed: $B_{r,0}(z) = 0$ and $\xi_{r,0} = 0$.

Starting from the initial conditions, equations are applied that regulate the behavior of the two reference dimensions as a function of the position of the aquifer over time.

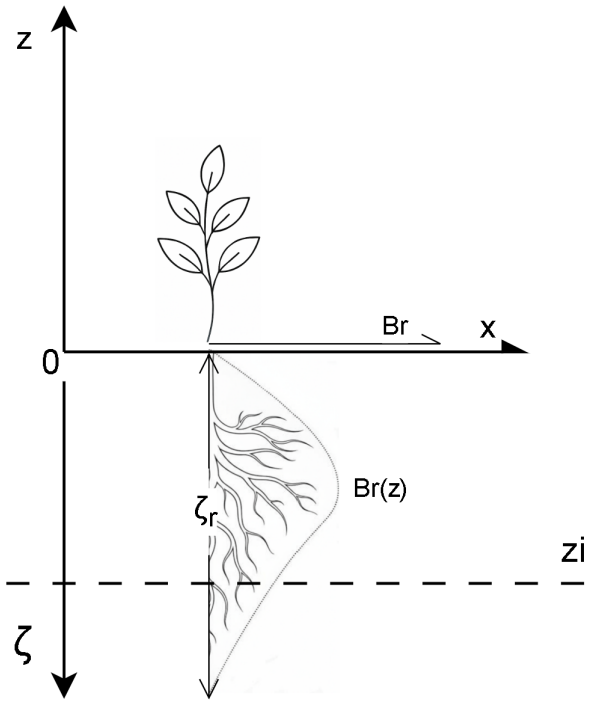

Figure 3.1: Single element of vegetation dimensions representation

Root Biomass

Root biomass values are adjusted according to various characteristics:

- Groundwater level z_i and capillary rise fringe L,
- Growth factor β [d^{-1}] and decay factor γ [d^{-1}],
- Time t of the temporal sequence of groundwater levels,
- Elevation z (distance from the bed), i.e., the portion of root considered,
- Carrying capacity $B_{r,\max}$, i.e., the maximum achievable biomass value.

All these variables contribute to describing the variations and fluctuations in root biomass values at various heights along the root depth reached over time.

The dynamics of the derivation are based on equations extrapolated from Tron et al. (2014) and are described by a piecewise differential function that describes the variation in biomass over time in two different cases.

$$\frac{dB_r(z)}{d\hat{t}} = \begin{cases} \tilde{f}_1\big(B_r(z)\big) = \beta(z)\left(B_{r,\max} - B_r(z)\right), & \text{if } z_i < z < z_i + L, \\ \tilde{f}_2\big(B_r(z)\big) = -\gamma B_r(z), & \text{if } z < z_i \ \vee \ z > z_i + L. \end{cases} \tag{3.1}$$

1. The first equation describes the dynamics of root biomass growth as a function of the position relative to the water table. The equation, which represents a

logistic-type growth tending toward the carrying capacity $B_{r,\max}$ and governed by the temporal growth factor β, is defined specifically for the interval between the water table height z_i and the zone called the capillary rise fringe. This fringe is a layer of height L [m] located above the water table, where soil moisture rises from the aquifer, creating ideal conditions for vegetation to locally develop.

2. The second equation instead describes the dynamics of root biomass decay as a function of the considered position. The equation, of exponential type and governed by the temporal decay factor γ (constant at any depth z), is defined outside the capillary rise fringe of the first equation. Therefore, it is valid both for depths z above the fringe and for those below it, representing two different phenomena. In the zone above the capillary rise fringe, the absence of soil moisture exposes roots to conditions of water stress. On the other hand, the same equation also applies to the zone below the water table, which, although saturated with water and thus meeting moisture requirements, lacks oxygen and results in anoxic conditions that are equally unfavorable for root growth.

Root Depth

As mentioned above, root depth ξ_r is the distance that roots travel through the soil during their growth process. It is modelled to simulate the tendency of phreatophytic plants to grow deeper through a taproot that grows vertically in order to reach the water table, even when it is deep. Its value is fundamental to establishing the presence of biomass and consequently the portion of soil to which the equations of root biomass growth and decay apply.

In contrast to previous approaches, the equation that determines this key variable is not based on academic research or mathematical models, but was hypothesised directly during the model's design.

While the root biomass equations were primarily based on Tron et al. (2014) with regard to root depth, when analyzing compatible models such as BASEveg, a different approach is used based on the use of the minimum groundwater level extrapolated from the time series and then applied to a law that predicts exponential growth of root depth with growth times independent of the position of the groundwater level over time but dependent only on the maximum depth value. The law is explained by the equation (2.9) seen above.

However, in order to follow a certain theoretical consistency that translates into a computational path without a priori assumptions about the variables involved (such as using a distribution of characteristic average biomass values from the outset or using a maximum groundwater depth value belonging to a time instant in the simulation), even for ξ_r the root growth trend is established instant by instant based on the boundary conditions available up to that time instant.

In particular, a value $\xi_{r,\max}$ is defined a priori as the "maximum attainable root depth" Unlike the formulation proposed by Caponi, Vetsch, and Siviglia (2020), this value does not depend on external hydraulic forcing but rather represents a physiological characteristic intrinsic to the species under consideration.

The equations used are as follows:

$$\zeta_r|_{\tilde{t}} = \begin{cases} \zeta_r|_{\tilde{t}-1} + k \cdot \Delta t, & \text{if } z_b - \zeta_r > z_i \ \wedge \ z_b - \zeta_r > z_b - \zeta_{r,\max} \ \wedge \ (z_b - \zeta_r) - z_i < h_{\min}, \\ \zeta_r|_{\tilde{t}-1}, & \text{if } z_b - \zeta_r \leq z_i \ \vee \ z_b - \zeta_r \leq z_b - \zeta_{r,\max}. \end{cases} \tag{3.2}$$

Where:

$$\begin{aligned} \tilde{t} &= \text{number of the actual iteration based on the timestep} \\ \Delta t &= \text{timestep} \\ k &= \text{root deepening rate [m/s]}, \\ z_b &= \text{bed elevation}, \\ \zeta_{r,\max} &= \text{maximum achievable root depth}, \\ h_{\min} &= \text{minimum root-relevant height}. \end{aligned}$$

1. The first equation defines the growth of root depth and thus the progression of roots. Depending on the time step between one groundwater level and the next, the roots deepen linearly by a factor k. This occurs only when the groundwater level is lower than the depth already reached by the roots, in order to describe the tendency of phreatophytic plant roots to grow deeper to reach the water table. The possibility of further deepening is clearly constrained by the maximum achievable depth value $\zeta_{r,\max}$.
   An additional condition included in the first equation is the one involving the term $h_{\min}$, which represents a minimum distance between the plant and the water table that must be respected for the root to grow.
   Although this condition does not have a precise physical meaning, it has been introduced to capture the difficulty of root deepening when the water table is considered too far away. Otherwise, the paradox would arise that, over time, a plant located very far from the water table (and thus realistically unable to grow, with root biomass equal to zero in the model) would continue to deepen until showing a behavior similar to plants positioned much closer to the water table. This feature is therefore essential to describe a more realistic distribution of vegetation, which is significantly reduced in areas farther from the water table.

2. The second equation instead defines the opposite behavior, in which part of the roots is already submerged by the groundwater table (i.e., the groundwater level is higher than the depth reached by the roots). In this case, the roots do not show a tendency to deepen further, as their water requirements are already satisfied. The same occurs when the maximum root depth $\zeta_{r,\max}$ has already been reached. In both situations, the root depth remains constant.

A peculiarity of vegetation in this model is the absence of mortality and regression dynamics, which would enrich the model and make it more suitable for describing the multitude of phenomena to which vegetation is subjected. These include hydromorphodynamic pressures from flow, as well as actual death due to drought or anoxia. As a result, at present, and somewhat counterintuitively, if a plant develops a certain root depth, although root biomass Br under unfavorable conditions could reach $Br = 0$ (the equivalent of being nonexistent), once favorable conditions reoccur, biomass growth resumes along the entire root length, since no regression of the value of ζ_r is allowed. This implies that a total $Br = 0$ does not by itself imply the death of the plant.

Although this model is clearly limited, its specific purpose is not to provide a tool capable of comprehensively describing the evolution of riparian vegetation and its interaction with the flow, but rather to investigate and improve the modeling aspect of root vegetation, seeking to place roots at the center of the modeling process.

3.3 Model implementation

The model was implemented as Python code that follows the following operational flow:

INPUT

Two .csv files are entered as input and are the only two input files in the model. The first contains numerical data relating to the topographical profile as the initial condition of the system, entered as the x-coordinate in the first column and the z-coordinate in the second. The second file contains the time series of the river's hydraulic gradient values (and, assuming high conductivity, also the groundwater level) in the second column, while the first column contains the associated time value.

The inputs, however, do not end here. Many of the values used by the system and defined a priori are in fact entered directly into the main code file `main.py`. These values are those required for the previously introduced equations that define root biomass B_r and root depth ξ_r, namely typical values related to the plant species and soil characteristics.

Typical plant species input values	
$B_{r,\max}$	Maximum root biomass per unit area $[-]$
$\xi_{r,\max}$	Maximum achievable root depth $[m]$
$\beta_{\max}$	Root growth factor $[d^{-1}]$
γ	Root decay factor $[d^{-1}]$
k	Root deepening velocity $[m/d]$
$h_{\min}$	Root interest height $[m]$
Typical soil input values	
ℓ	Capillary rise height $[m]$

Table 3.1: Typical input values for plant species and soil parameters.

By default, the model assumes that the initial conditions are set to $B_{r,0}(z) = 0$ and $\xi_{r,0} = 0$ (Bare soil). However, within the `main.py` section of the code, which defines the input files, it is possible to specify initial system conditions with a constant $B_{r,0}(z)$ along the entire $\xi_{r,0}$.

A fundamental part of the model is the use of the code "`generazione_livelli.m`," a Matlab file that allows the creation of stochastic series of values based on certain statistical values. Although these values do not specifically refer to hydrometric levels, they have growth and decline characteristics compatible with the variability of hydrological regimes. Through the correct choice of statistical variables, the time series of levels and, consequently, groundwater values are calculated.

The code is designed to be executed through a command in the "command palette" that contains the statistical values with which the time series must be constructed.

$$= \texttt{generazione\_livelli}(\mu,\, cv,\, \tau,\, tempo\_end\_gg)$$

Where:

$$\begin{aligned} \mu &= \text{desired mean level,} \\ cv = \tfrac{var}{\mu} &\quad \text{coefficient of variation,} \\ \tau &= \text{temporal correlation,} \\ tempo\_end\_gg &= \text{number of generated days.} \end{aligned}$$

Within the code, it is also possible to define the dt, i.e., the discretization of values for each day, which establishes the time step of the time series.
The choice of these values is decisive for the biomass results in the model. In fact, the variation of certain parameters essentially describes different hydraulic regimes, which, as will be seen later in the analysis of the model results, strongly influences the distribution and values of the final biomass.

MODEL

The code is structured as follows:

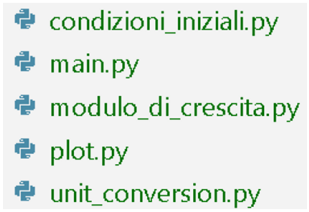

Figure 3.2: Files composing the python code

– "main.py" contains the code's supporting structure, which uses all the functions defined in the other files. Initially, there is a space dedicated to entering input data and inserting the two .csv files. Next, there is a section dedicated to reading the initial conditions and input files, extracting their values. This is followed by the most substantial phase of the model, which consists of modeling the actual plant dynamics over time as a function of groundwater levels. Once the simulation is complete, the data obtained can be used to produce outputs using the "plot.py" file.

– In "unit_conversion.py," conversions are performed to adapt the input data to the characteristics of the model. If the input data expressing length values are entered in meters, the resolution may not always be in meters but may differ depending on the resolution of the input profile points or on the user's choice. For this reason, the data is converted to adapt to the resolution of the two-dimensional matrix on which the root biomass and root depth values are calculated. As the resolution increases, so does the computational time.

– In "condizioni_iniziali.py", the input data are read and processed in order to set up the initial "Br" matrix and all the data required to start the actual computation. For example, through the functions reported below it is possible to: In the first case, read the values of the discharge time series and calculate the corresponding values of the capillary rise height, in the second case, create the biomass matrix, initialized either with values equal to 0 (if no specific initial conditions are provided) or with the values of $Br_0(z)$ and $\xi_{r,0}$ eventually specified as input.

```python
def leggi_quota_falda_e_risalita(file_path, altezza_risalita_capillare_0):

    # Leggi il file Excel
    dati = pandas.read_excel(file_path, skiprows=1)

    # Estrai gli istanti temporali e i valori della quota di falda
    istanti_temporali = dati.iloc[:, 0].to_numpy()  # Prima colonna: istanti temporali IN GG
    valori_falda = dati.iloc[:, 1].to_numpy()  # Seconda colonna: valori della quota di falda IN M

    # Calcola la quota di risalita capillare
    valori_risalita_capillare = valori_falda + (altezza_risalita_capillare_0)  # Converti in cm

    return istanti_temporali, valori_falda, valori_risalita_capillare

def crea_biomassa_iniziale(n_righe, n_colonne, profilo_topografico, profondita_massima, valore_biomassa, quota_topografica, profondita_iniziale):
    """
    Crea una matrice `Br` con valori iniziali di biomassa.
    La biomassa viene assegnata nelle celle comprese tra (indice_y, indice_z + 1) e (indice_y, indice_z_profondita).
    Tutte le altre celle rimangono a 0.
    """
    # Creazione della matrice per la biomassa radicale iniziale
    Br = np.zeros((n_righe, n_colonne))  # Matrice vuota per la biomassa

    # Creazione della quota di profondità massima per ogni punto del profilo topografico
    quota_profondita_massima = quota_topografica - profondita_massima

    # Assegna i valori di biomassa iniziale
    for y_val, z_val in profilo_topografico:
        indice_y = int(y_val)  # Coordinata y
        indice_z = int(z_val)  # Coordinata z
        #indice_z_profondita = indice_z + profondita_massima  # Calcola la profondità massima

        # Assegna il valore di biomassa nelle celle tra indice_z + 1 e indice_z_profondita
        for z in range(max(indice_z - profondita_iniziale, 0), indice_z):
            Br[z, indice_y] = valore_biomassa

    # Calcola la profondità radicale iniziale per ogni colonna `y`
    profondita_radicale = np.zeros(n_colonne)  # Inizializza la profondità radicale a zero
    for y in range(n_colonne):
        profondita_radicale[y] = profondita_iniziale
    quota_profondita_radicale_iniziale = quota_topografica - profondita_radicale

    return Br, profondita_radicale, quota_profondita_radicale_iniziale,  quota_profondita_massima
```

Figure 3.3: Code of "condizioni_iniziali.py"

– In "modulo_di_crescita.py", the actual vegetation process is implemented. Before computing the effect of the water level time series on vegetation, the value of $\beta(z)$ is processed. This parameter is not defined as constant but, according to the Tron model, starting from the input value $\beta_{\max}$, it decreases linearly until it reaches zero at the maximum root depth $\xi_{r,\max}$. This describes the decreasing ability of the plant element to produce biomass as it grows farther from the soil surface. This behavior is defined by the following function.

```python
def crea_beta(n_righe, n_colonne, quota_topografica, profondita_radicale_massima, passo_beta, Beta_max):

    # Inizializza Beta come una matrice di zeri
    Beta = np.zeros((n_righe, n_colonne))

    # Itera su ogni colonna per calcolare i valori di Beta
    for y in range(n_colonne):
        limite_superiore = int(quota_topografica[y])
        limite_inferiore = int(min(quota_topografica[y] - profondita_radicale_massima[y], 0))

        # Assegna valori decrescenti da Beta_max a passo_beta
        for z in range(limite_superiore, limite_inferiore, -1):
            Beta[z, y] = max(Beta_max - passo_beta * (limite_superiore - z), 0)

    return Beta
```

Figure 3.4: Code of "modulo_di_crescita.py" 1

Once the vector $\beta(z)$ has been initialized, all the prerequisites are set to begin the computation of root dynamics through the function `crescita_radicale`. This function stores two main arrays: "evoluzione_biomassa", which contains the matrices at each time step with the spatial values of local root biomass, and "evoluzione_profondità_radicale", where the positions correspond to the respective x-coordinates and the values represent the root depth ξ_r at time t for each x-coordinate, and consequently for each plant unit considered.
The computation is carried out at each time step. First, after initializing all the necessary matrices, the root depth values are updated. If the conditions satisfy those of Equation (3.2), the biomass value at coordinate x increases proportionally to the time step dt; otherwise, the value remains unchanged.

```
# Itera sugli istanti temporali
for t, giorno in enumerate(istanti_temporali):
    # Ottieni la quota di falda e la quota di risalita capillare per l'istante corrente
    quota_falda = int(valori_falda[t]*fattore_di_conversione_L)
    quota_risalita = int(valori_risalita_capillare[t]*fattore_di_conversione_L)

    # Aggiorna la profondità radicale per ogni colonna
    for y in range(n_colonne):
        if (quota_falda < quota_topografica[y] - profondita_radicale[y]) and ((quota_topografica[y] - profondita_radicale[y]) - quota_falda < z_min):
            # Calcola il nuovo valore di profondità radicale
            if t == 0:
                # differenza = istanti_temporali[t]
                differenza = istanti_temporali[t+1] - istanti_temporali[t]
                # differenza = 0.1
            else:
                differenza = istanti_temporali[t] - istanti_temporali[t-1]
            nuova_profondita = profondita_radicale[y] + (k_r * differenza)  # Incremento della profondità radicale (esempio: 0.5 unità)
            # Limita la profondità radicale in modo che non superi quota_profondita_massima
            if quota_topografica[y] - nuova_profondita < quota_profondita_massima[y]:
                profondita_radicale[y] = quota_topografica[y] - quota_profondita_massima[y]
            else:
                profondita_radicale[y] = nuova_profondita
```

Figure 3.5: Code of `"modulo_di_crescita.py"` 2

Then, still within the same "`for t`" loop, the update of root biomass B_r values takes place. For each cell (x, z), whose positional values correspond to the coordinates expressed in the units of spatial resolution, the value $B_r(t-1)$ is subjected to the equations (3.1), which determine its behavior as a function of groundwater levels.

The solution of the differential equations governing the evolution of biomass is implemented in the code through two approaches, which can be selected by the user: either analytically or numerically.

Analytic solution
The first method solves the differential equations by integrating in dt. The solution of the equations appears as follows:

$$B_r(z,t) = \begin{cases} B_{r,\max} - (B_{r,\max} - Br0(z,t)) \cdot e^{-\beta(z)\,\tau}, & \text{if } z_i < z < z_i + L, \\ Br0(z) \cdot e^{-\gamma\tau}, & \text{if } z < z_i \quad \vee \quad z > z_i + L. \end{cases} \tag{3.3}$$

Where:

$Br0(z,t)$	is the value of B_r at the moment when the cell at coordinates, (x,z) switches from one condition to another
$\tau = \sum dt$	represents the cumulative time elapsed since the transition be-. tween the two conditions

At each time iteration, the cell is updated based on the equation relating to the condition satisfied.

```
# Itera su ogni colonna per aggiornare la biomassa
for y in range(n_colonne):
    # Calcola i limiti della zona di crescita per la colonna corrente
    limite_inferiore = int(quota_topografica[y] - profondita_radicale[y])
    limite_superiore = quota_topografica[y]
    limite_radicale_massimo = quota_profondita_massima[y]

    # Aggiorna solo le celle comprese tra limite_inferiore e limite_superiore
    for z in range(max(limite_inferiore, limite_radicale_massimo, 0), limite_superiore):  # Escludi quota_topografica stessa

        # Aggiorna la matrice di controllo se la cella supera 0.1
        if Br[z, y] >= 0:
            raggiunto_minimo_1 = True
        if quota_falda - 1 < z <= quota_risalita - 1:
            if Flag[z,y] == 0:
                Br0[z,y] = Br[z,y]
                if t < len(istanti_temporali) - 1:
                    t_idx[z,y] = istanti_temporali[t+1] - istanti_temporali[t]
                else:
                    t_idx[z,y] = istanti_temporali[t] - istanti_temporali[t-1]
            if Flag[z,y] == 2:
                Br0[z,y] = Br[z,y]
                t_idx[z,y] = istanti_temporali[t] - istanti_temporali[t-1]

            # Crescita nella zona di risalita capillare
            Br[z, y] = Br_max - ( Br_max - Br0[z,y]) * math.e ** ( (- Beta[z, y]) * t_idx[z, y])

            if t < len(istanti_temporali) - 1:
                t_idx[z,y] += istanti_temporali[t+1] - istanti_temporali[t]
            Flag[z,y] = 1
        else:
            if Flag[z,y] == 0:
                Br0[z,y] = Br[z,y]
                if t < len(istanti_temporali) - 1:
                    t_idx[z,y] = istanti_temporali[t+1] - istanti_temporali[t]
                else:
                    t_idx[z,y] = istanti_temporali[t] - istanti_temporali[t-1]
            if Flag[z,y] == 1:
                Br0[z,y] = Br[z,y]
                t_idx[z,y] = istanti_temporali[t] - istanti_temporali[t-1]

            # Decrescita sopra e sotto la zona di risalita capillare
            Br[z, y] = Br0[z,y] * math.e ** ((- Gamma) * t_idx[z, y])

            if t < len(istanti_temporali) - 1:
                t_idx[z,y] += istanti_temporali[t+1] - istanti_temporali[t]
            Flag[z,y] = 2

        # Imposta Br[z, y] a 0.1 se è sceso sotto 0.1 dopo averlo raggiunto
        if raggiunto_minimo_1 and Br[z, y] <= 0:
            Br[z, y] = 0
```

Figure 3.6: Code of "modulo_di_crescita.py" 3 : Analitical solution

Numerical solution

It is also possible to solve the equations using the numerical method known as "Runge-Kutta," which solves the ordinary differential equation with a good degree of approximation.

```python
def runge_kutta_up(f, y0, Beta_2, t0, t_end, dt):
    t = t0
    y = y0
    Beta_3 = Beta_2

    while t < t_end:
        k1 = dt * f(t, y, Beta_3)
        k2 = dt * f(t + dt / 2, y + k1 / 2, Beta_3)
        k3 = dt * f(t + dt / 2, y + k2 / 2, Beta_3)
        k4 = dt * f(t + dt, y + k3, Beta_3)
        y += (k1 + 2 * k2 + 2 * k3 + k4) / 6
        t += dt

    return y
```

```python
def runge_kutta_down(f, y0, t0, t_end, dt):
    t = t0
    y = y0

    while t < t_end:
        k1 = dt * f(t, y)
        k2 = dt * f(t + dt / 2, y + k1 / 2)
        k3 = dt * f(t + dt / 2, y + k2 / 2)
        k4 = dt * f(t + dt, y + k3)
        y += (k1 + 2 * k2 + 2 * k3 + k4) / 6
        t += dt

    return y
```

Figure 3.7: Code of "modulo_di_crescita.py" 4: Numerical solution

```python
# Aggiorna solo le celle comprese tra limite_inferiore e limite_superiore
for z in range(limite_superiore, min(limite_inferiore, limite_radicale_massimo, n_righe)):

    # Aggiorna la matrice di controllo se la cella supera 0.1
    if Br[z, y] >= 0:
        raggiunto_minimo_1 = True

    if quota_risalita - 1 <= z < quota_falda - 1:
        # Crescita nella zona di risalita capillare
        Br[z, y] = runge_kutta_up(f1, Br[z, y], Beta[z, y], t_idx, t_idx + 1, 1)
    else:
        # Crescita sopra e sotto la zona di risalita capillare
        Br[z, y] = runge_kutta_down(f2, Br[z, y], t_idx, t_idx + 1, 1)

    # Imposta Br[z, y] a 0.1 se è sceso sotto 0.1 dopo averlo raggiunto
    if raggiunto_minimo_1 and Br[z, y] <= 0:
        Br[z, y] = 0
```

Figure 3.8: Code of "modulo_di_crescita.py" 5: Numerical solution

Once the values have been updated, the actual values of biomass and root depth are also updated for statistical purposes. In fact, for each time iteration, the mean and variance of each cell are calculated and are calculated on the same matrix, updating incrementally. This is to lighten the computational cost of the function, which can be burdensome for very large matrices.

```
    # Calcolo incrementale media/varianza
    n += 1
    delta = Br - mean
    mean += delta / n
    M2 += delta * (Br - mean)

    if giorno % gg_progressivi == 0 or t == len(istanti_temporali) - 1:
        evoluzione_biomassa.append(Br.copy())
        evoluzione_profondita_radicale.append(profondita_radicale.copy())

varianza = M2 / (n - 1) if n > 1 else np.zeros_like(mean)
```

Figure 3.9: Code of `"modulo_di_crescita.py"` 6: Statistical calculations

OUTPUT

The visualization of the results is possible through the file "plot.py", which allows the matrix Br to be displayed at a predetermined time and the profile given by the vector ξ_r with respect to the bed profile and the profile defined by the maximum root depth. The code also makes it possible to create short videos that are useful for showing the temporal succession of the values reached.

The execution of the code allows certain values to be saved in ".npz" format, such as average variance and certain B_r values at specific predefined times. Using a Python code called "analisi_statistica.py," it is also possible to perform additional analyses, such as those of the average root biomass value profiles, in order to establish an analysis based on the statistical characteristics of the input hydrological series.

Chapter 4

Model non-dimensionalisation

Before proceeding with a more detailed description of the model through the analysis of its results, a further modification is made to the code in order to non-dimensionalise and make models with different characteristics more comparable. This intervention will be useful in subsequent analyses.

4.1 non-dimensionalisation characteristics

The model is non-dimensionalized with respect to its temporal and spatial coordinates using the following reference values:

- The decay coefficient of root biomass, γ $[1/T]$, for the non-dimensionalization of temporal variables.
- The mean groundwater level, $\overline{h}$ $[L]$, for the non-dimensionalization of variables oriented along the vertical axis z.
- The horizontal distance between the riverbed and the intersection point between the bank and the mean hydraulic head (or mean groundwater level), expressed as $\overline{w}$ $[L]$, for the non-dimensionalization of variables oriented along the horizontal axis x.

In light of these choices, in order to apply this dimensionless approach, a very specific profile of the analysed section is required to define the third condition. The choice is an approximate profile of a generic, geometrically ideal river section. One common example that satisfies these conditions is the trapezoidal cross-section, where the horizontal portion corresponds to the riverbed and the sloping portion to the riverbank.

In this case, only the right half of the section is used to focus on the area of interest with regard to root growth phenomena. The central part of the river is excluded because it is assumed to be permanently submerged, so riparian vegetation cannot grow there.

Figure Figure 4.1 shows the type of section used.

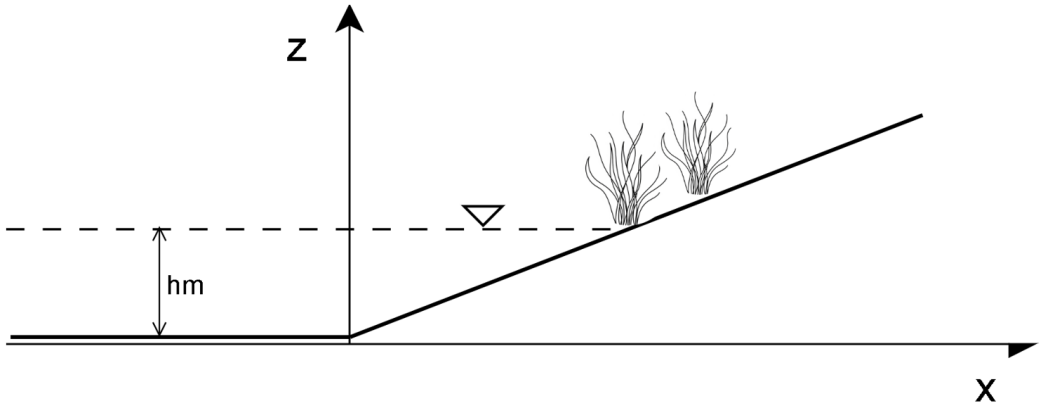

Figure 4.1: Semi-trapezoidal river section

4.2 Mathematical steps

Within the dimensionless process, dimensional values and coordinates are formally expressed with an asterisk (e.g. z^*), while dimensionless values are expressed normally.

The spatial reference coordinates are not only divided by the dimensionless reference value, but a translation also occurs (by subtracting the dimensionless factor in the numerator) as follows:

$$z = \frac{z^* - \overline{h^*}}{\overline{h^*}} \tag{4.1}$$

$$x = \frac{x^* - \overline{w^*}}{\overline{w^*}} \tag{4.2}$$

This approach makes it possible not only to standardize the final result with respect to the temporal average of the groundwater levels, but also to shift the origin of the axes from the point where the bottom meets the bank to the point of intersection of the bank with the average groundwater level.

The topographic profile of the bed, $\eta^*(x^*)$, is fixed and has a value for each x^* of the system. It is also adimensionalized according to the normalization and translation approach:

$$\eta(x) = \frac{\eta^*(x) - \overline{h^*}}{\overline{h^*}} \tag{4.3}$$

The rest of the typical values of the model are non-dimensionalised by simply dividing by the typical reference term without the need, for terms whose fundamental unit is length, to perform the translation within the reference system. The value of these terms is in fact independent of the position within the system.

$$\xi_{r,\max} = \frac{\xi^*_{r,\max}}{\overline{h^*}}, \quad h_{\min} = \frac{h^*_{\min}}{\overline{h^*}}, \quad \ell = \frac{\ell^*}{\overline{h^*}} \tag{4.4}$$

The steps for dimensionless conversion of all equations and typical conditions of the model are indicated below:

Equation for the growth/Decrease of Root biomass

The first equation analyzed is the one governing the dynamics of B_r, defined by equation (3.1). It is not non-dimensionalized in terms of time or length, but only by dividing the equation by its maximum attainable value (or carrying capacity) $B_{r,\max}$ [g/dm^2]. In this way, the semi-logistic equation will not tend toward the maximum value itself, but instead toward the dimensionless value of 1.

The term describing biomass growth is analyzed.

$$\begin{gathered}
\frac{dB_r^*}{dt} = \beta(z^*)\left(B_{r,\max}^* - B_r^*\right) \quad \Rightarrow \quad \textit{divided by } B_{r,\max}^* \quad \Rightarrow \\
\frac{B_r^*}{B_{r,\max}^*} = \varphi \quad \Rightarrow \\
\frac{dB_r^*}{dt \cdot B_{r,\max}^*} = \frac{\beta(z^*)\left(B_{r,\max}^* - B_r^*\right)}{B_{r,\max}^*} \quad \Rightarrow \\
\frac{d\varphi}{dt} = \beta(z^*)(1-\varphi)
\end{gathered} \tag{4.5}$$

At this point, the root biomass values are normalized, and their values range between 0 (absence of biomass) and 1 (maximum attainable biomass).

The next non-dimensionalization is applied to the growth and decay factors. The decay factor γ is chosen as the reference parameter for the non-dimensionalization of all temporal variables of the system. In particular, both β and γ are non-dimensionalized following the same approach. As a result, we obtain:

$$\frac{\beta}{\gamma} = \theta\ [-] \tag{4.6}$$

$$\frac{\gamma}{\gamma} = 1 \tag{4.7}$$

At this point, θ becomes the only term used to define the dynamics of vegetation growth and decay. This provides the advantage of not having to use two distinct terms within the model, but rather relying on a single parameter that describes both growth and decay tendencies.

The resulting growth equation is as follows:

$$\frac{d\varphi}{dt} = \theta(z^*)(1-\varphi) \tag{4.8}$$

While γ is a constant value, β is still a function of the dimensional variable z^*, varying with its vertical position.

In particular, β is defined so that it reaches its maximum value $\beta_{\max}$ at z^* corresponding to the bed profile $\eta^*(x)$, and decreases linearly from the bed profile down to the depth z^* of the maximum root depth $\xi_{r,\max}$, such that:

$$z^*_{\text{end}} = \eta^* - \xi^*_{r,\max} \tag{4.9}$$

In order to calculate β and, consequently, all the equations that govern the values of root biomass B_r, a local reference system is introduced to describe the depth ξ^* with respect to the bed profile. This system is opposite to the fixed reference system (as z^* increases, ξ^* decreases, and vice versa) and originates at the profile η for each coordinate x^* of the system.

The equation describing this behavior of β is the following:

$$\beta(z^*) = \beta(\xi^*) = \beta_{\max}\left(1 - \frac{\xi^*_r}{\xi^*_{r,\max}}\right) \tag{4.10}$$

where $\quad \xi^*_r = \eta^*(x^*) - z^*$

Considering:

$$z = \frac{z^* - \overline{h}^*}{\overline{h}^*} \qquad\qquad \eta = \frac{\eta^* - \overline{h}^*}{\overline{h}^*} \tag{4.11}$$

$$\xi^*_r = \eta\,\overline{h}^* + \overline{h}^* - z\,\overline{h}^* - \overline{h}^* = (\eta - z)\,\overline{h}^* \;\Rightarrow$$

$$\frac{\xi^*_r}{\overline{h}^*} = \frac{(\eta - z)\,\overline{h}^*}{\overline{h}^*} \;\Rightarrow \tag{4.12}$$

$$\xi_r = \eta - z$$

Substituting into the main equation:

$$\beta(\eta^*) = \beta_{\max}\left(1 - \frac{(\eta - z)\,\overline{h}^*}{\xi^*_{r,\max}}\right) =$$

$$= \beta_{\max}\left(1 - \frac{\xi_r \cdot \overline{h}^*}{\xi^*_{r,\max}}\right) \;\Rightarrow\; \xi_{r,\max} = \frac{\xi^*_{r,\max}}{\overline{h}^*} \;\Rightarrow \tag{4.13}$$

$$\beta(\xi) = \beta_{\max}\left(1 - \frac{\xi_r}{\xi_{r,\max}}\right)$$

After non-dimensionalizing the spatial variables, the temporal aspect is considered by non-dimensionalizing the growth factor, $\beta/\gamma = \theta$, and consequently its maximum value $\beta_{\max}$, such that:

$$\theta(\xi) = \theta_{\max}\left(1 - \frac{\xi_r}{\xi_{r,\max}}\right) \tag{4.14}$$

Consequently, the main equation will be:

$$\frac{d\varphi}{dt} = \theta(\xi)\,(1-\varphi) \tag{4.15}$$

Just as the equation is subject to dimensionless transformation, so too are its conditions:

$$\begin{gathered} z_i^* < z^* < z_i^* + \ell^* \quad \Rightarrow \\ z_i \cdot \bar{h}^* + \bar{h}^* < z \cdot \bar{h}^* + \bar{h}^* < z_i \cdot \bar{h}^* + \bar{h}^* + \ell \cdot \bar{h}^* \quad \Rightarrow \\ z_i < z < z_i + \ell \end{gathered} \tag{4.16}$$

It is now analyzed the term describing biomass decline using the same approach used for the equation determining growth dynamics:

$$\begin{gathered} \frac{dBr^*}{dt} = -\gamma \cdot Br^* \quad \Rightarrow \quad \textit{divided by } Br^*_{max} \quad \Rightarrow \\ \frac{Br^*}{Br^*_{max}} = \varphi \quad \Rightarrow \\ \frac{\frac{dBr^*}{dt}}{Br^*_{max}} = \frac{-\gamma \cdot Br^*}{Br^*_{max}} \quad \Rightarrow \\ \frac{d\varphi}{dt} = -\gamma \cdot \varphi \end{gathered} \tag{4.17}$$

By Non-dimensionlized scaling the time scale, we obtain:

$$\frac{d\varphi}{dt} = -\varphi \tag{4.18}$$

Its conditions become:

$$\begin{gathered} z_i^* < z^* \ \wedge \ z^* > z_i^* + \ell^* \quad \Rightarrow \\ z \cdot \overline{h^*} + \overline{h^*} < z_i \cdot \overline{h^*} + \overline{h^*} \quad \wedge \quad z \cdot \overline{h^*} + \overline{h^*} > z_i \cdot \overline{h^*} + \overline{h^*} + \ell \cdot \overline{h^*} \quad \Rightarrow \\ z < z_i \ \wedge \ z > z_i + \ell \end{gathered} \tag{4.19}$$

The result of the dimensionless equation system is as follows:

$$\frac{d\varphi}{dt} = \begin{cases} \theta(\xi)(1-\varphi), & \text{if } z_i < z < z_i + \ell, \\ -\varphi, & \text{if } z < z_i \ \wedge \ z > z_i + \ell. \end{cases} \tag{4.20}$$

Equation for the growth of root depth
The second set of equations discussed (eq. (3.2)) governs the dynamics of root depth evolution, i.e., the value that, starting from the bottom profile, establishes the vertical extent of soil involved in root growth dynamics, as well as the actual root depth reached at time t.

In analyzing the first of the two equations, we first non-dimensionalize the root depth value ξ_r^* (so that, with the spatial scaling already introduced, $\xi_r = \eta - z$).

$$\begin{gathered}\frac{d\xi_r^*(t)}{dt} = \xi_r^*(t-1) + k^* \cdot \Delta t \quad \Rightarrow \quad \textit{divided by } \overline{h}^* \quad \Rightarrow \\ \frac{\xi_r^*}{\overline{h}^*} = \xi_r \quad \Rightarrow \\ \frac{d\xi_r^*(t)}{dt \cdot \overline{h}^*} = \frac{\xi_r^*(t-1)}{\overline{h}^*} + \frac{k^* \cdot \Delta t}{\overline{h}^*} = \\ \frac{d\xi_r(t)}{dt} = \xi_r(t-1) + \frac{k^* \cdot \Delta t}{\overline{h}^*}\end{gathered} \tag{4.21}$$

At the same time, the radical deepening velocity k^* [m/s] is dimensionless by dividing it by the average water table level and the decay factor in order to act on the time dependence:

$$\frac{k^*}{\overline{h}^* \cdot \gamma^*} = k \quad \Rightarrow \quad \frac{k^*}{\overline{h}^*} = k \cdot \gamma^* \tag{4.22}$$

Consequently, substituting within the equation results in:

$$\frac{d\xi_r(t)}{dt} = \xi_r(t-1) + k \cdot \gamma^* \cdot \Delta t \tag{4.23}$$

The equation is defined for the following conditions, which are in turn dimensionless.

$$\begin{gathered}z_b^* - \xi_r^* > z_i^* \quad \wedge \quad z_b^* - \xi_r^* > z_b^* - \xi_{r,\max}^* \quad \wedge \quad (z_b^* - \xi_r^*) - z_i^* < h_{\min}^* \quad \Rightarrow \\ z_b \cdot \bar{h}^* + \bar{h}^* - \xi_r \cdot \bar{h}^* > z_i \cdot \bar{h}^* + \bar{h}^* \quad \wedge \quad z_b \cdot \bar{h}^* + \bar{h}^* - \xi_r \cdot \bar{h}^* > z_b \cdot \bar{h}^* + \bar{h}^* - \xi_{r,\max} \cdot \bar{h}^* \quad \wedge \\ (z_b \cdot \bar{h}^* + \bar{h}^* - \xi_r \cdot \bar{h}^*) - z_i \cdot \bar{h}^* - \bar{h}^* < h_{\min} \cdot \bar{h}^* \quad \Rightarrow \\ z_b + 1 - \xi_r > z_i + 1 \quad \wedge \quad z_b + 1 - \xi_r > z_b + 1 \quad \wedge \quad z_b + 1 - \xi_r - z_i - 1 < h_{\min} \\ z_b - \xi_r > z_i \quad \wedge \quad z_b - \xi_r > z_b \quad \wedge \quad z_b - \xi_r - z_i < h_{\min}\end{gathered} \tag{4.24}$$

The second equation is very similar but slightly simpler, since it lacks the incremental term $k^* \cdot \Delta t$. The equation under analysis states that, under certain conditions, the root depth value remains unchanged over time.

$$\frac{d\xi_r^*(t)}{dt} = \xi_r^*(t-1) \implies \frac{d\xi_r^*(t)}{dt \cdot h^*} = \frac{\xi_r^*(t-1)}{h^*} \implies \cdots \implies \frac{d\xi_r(t)}{dt} = \xi_r(t-1) \tag{4.25}$$

And its conditions similarly:

$$Z_b^* - \xi_r^* \leq Z_i^* \quad \wedge \quad Z_b^* - \xi_r^* \leq Z_b^* - \xi_{r,max}^* \implies \cdots \implies$$
$$Z_b - \xi_r \leq Z_i \quad \wedge \quad Z_b - \xi_r \leq Z_b$$

The result of the dimensionless equation system is as follows:

$$\frac{d\xi_r(t)}{dt} = \begin{cases} \xi_r(t-1) + k \cdot \gamma^* \cdot \Delta t & \text{if } z_b - \xi_r > z_i \ \wedge \ z_b - \xi_r > z_b \ \wedge \ z_b - \xi_r - z_i < h_{\min} \\ \xi_r(t-1) & \text{if } z_b - \xi_r \leq z_i \ \wedge \ z_b - \xi_r \leq z_b \end{cases} \tag{4.26}$$

Throughout this series of equations and dimensionless calculations, the time values considered (t) have always been assumed to be without units of measurement [-]. This is because the dimensionless approach is applied directly to the time series instants during the generation of the time series itself using the hydraulic level generation tool introduced above.

Normalization is achieved by acting on the input values entered directly into the code, which are: = `mu, cv, tau, tempo_end_gg, dt`

In particular, the last three parameters, *tau*, *tempo_end_gg*, and *dt*, are temporal values $[T]$ and are adimensionalized using the reference value γ $[1/T]$.

As a result, the resulting input command is:

$$= generazione\_livelli(mu, cv, tau \cdot \gamma, tempo\_end\_gg \cdot \gamma); \quad dt \cdot \gamma$$

By applying the mathematical simplifications indicated, the model is now dimensionless and applicable to case studies with different hydrological and topographical characteristics.

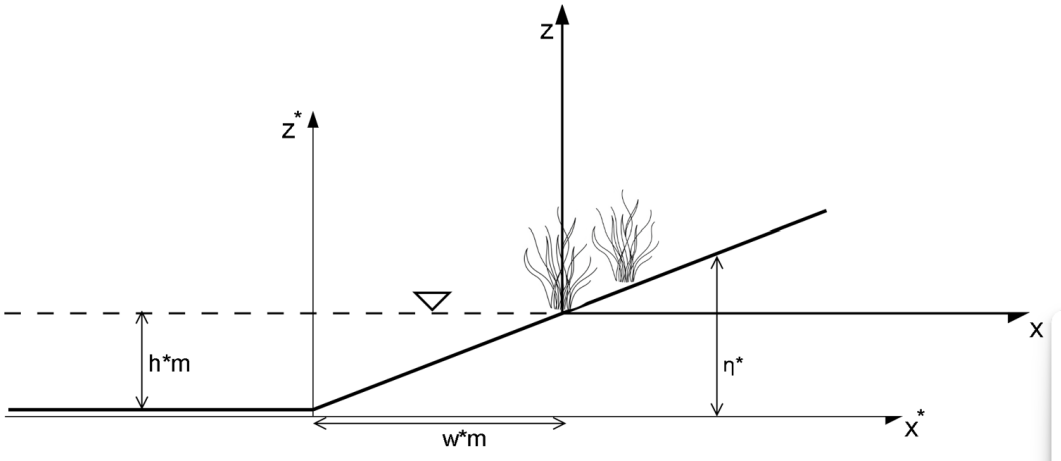

Figure 4.2: Inertial systems of river section

Chapter 5

Simulations

The discussion now proceeds to the application phase of the model produced, in which a series of simulations of different conditions and characteristics are carried out in order to test its potential and accuracy in reproducing root distribution.

5.1 Methods and objectives

The planned approach is to carry out a series of simulations using different system characteristics and boundary conditions in order to study and compare the behavior of the system under all the different conditions.

This approach has two main functions. First, by comparing the different results with previous reference studies regarding the characteristics of riparian plant species, we can verify the consistency of our results and qualitatively assess the quality of the chosen modeling. Furthermore, by trying to vary the factors that make up the system as much as possible, it is possible to determine the influence that the internal and external characteristics of the system have on the final results.

The factors subject to variation tend to be typical characteristics of the plant, the soil, or the hydrological regime to which the riverbed and vegetation are subject.

The peculiar characteristics of the plant can essentially be summarized in its tendency to grow and decrease depending on the hydraulic forcing. In fact, since the model does not currently have modules that describe its interaction with hydrodynamics and morphodynamics (for example, in flood events), events such as scouring removal, on which the distribution of root biomass would have a certain influence, are not considered, nor are the related characteristic variables. Furthermore, since only root biomass is described at present, which is nevertheless intended to be the key element in a more complete future ecological model, there are still no elements or relationships linking the amount of 'above_ground' biomass to 'below_ground' biomass, nor are there any allometric laws defining its spatial dimensions. The only characteristics currently influencing vegetation dynamics are the growth factor $\beta(z)$, which depends on β_{max}, and the decay factor γ, and consequently, in our dimensionless model, the unified growth/decay factor $\theta(z)$, which depends on θ_{max}. Two

additional plant-specific traits introduced in the model and relevant to the obtained results are the maximum root depth $\xi_{r,\max}$ and the root deepening rate k. Their values are clearly fundamental in determining the spatial limits and the temporal dynamics of root development and, although k may become less critical in long-term analyses, they are the determining parameters for establishing the root depth ξ_r of each specimen. In the simulations, these values are assumed to be constant in order to focus the analysis on an ideal plant species typical of the context of interest.

Soil characteristics can certainly have some influence on vegetation proliferation. Soil porosity is in fact a key factor in determining groundwater propagation in the soil and key physical phenomena such as capillary rise. In some less porous soils, such as clay soils, the latency of lateral propagation of groundwater levels can be considerable and can therefore have a decisive effect on the timing and lateral extent of plant growth (which depends primarily on the position of the water table). The typical effect of low porosity is therefore a marked difference between the water table levels near the basin and those further away from the riverbed, especially when the variation in hydraulic head is considerable. As already mentioned, low-porosity soil also leads to an amplification of the capillary rise phenomenon, which increases as the depth decreases. Capillary rise that we know to be absolutely decisive in the variation of growth and decay dynamics.

However, our model is currently designed to describe the dynamics of phreatophytes in gravel-bed rivers, whose porosity and lateral conductivity are much higher than those of clay soil rivers. For this reason, we approximate the height of the water table to a constant value equal to the hydraulic head of the river (condition of high lateral conductivity) and assume a single capillary rise value for that type of soil, effectively rendering the assumption of porosity as a determining value useless and, more generally, the characteristics of the soil are resolved solely by identifying the value l of capillary rise, which does not vary during our simulations.

Most of the variations in the simulations performed occur by modifying the parameters of the generated hydrological regime. Through the level generation code, we have said that it is possible to insert multiple temporal and spatial statistical values that significantly influence the magnitude of the generated values. By reproducing different hydrological regimes, it will be possible to identify the direct influence on the development of root biomass.

These values are modified mainly by manipulating the values previously entered.

$$= \texttt{generazione\_livelli}(\mu,\, cv,\, \tau,\, tempo\_end\_gg)$$

The input parameters can be summarized as follows:

- μ, which represents the mean groundwater level, is kept constant during the simulations to simplify the parameterization. Different μ values would not only result in different and less comparable values of cv, but any variation of μ would also be nullified by the effect of the adimensionalization, whose purpose is precisely to make flows with different characteristics comparable.

- cv (coefficient of variation) is defined as σ/μ and represents the average amplitude of the oscillations of the generated hydrological values. A higher cv implies that the water table reaches higher/lower values more often, and it will be less likely to remain at specific values. By varying this factor, it is possible to represent more dynamic or more static hydrological regimes.

- τ is the temporal correlation of the generated series, and specifies the dependency (in days) of a generated value on the previous ones. The larger τ is, the stronger the dependency of a value on its predecessors, and consequently the harder it is to observe sudden fluctuations: floods and variations alternate more gradually.

- *tempo_end_gg* simply indicates the total number of generated days, which in these simulations is kept constant in order to obtain stationary and statistically valid results.

- Finally, dt can also influence the results. This effect does not arise because different values would necessarily lead to different system responses, but because an excessively large dt (and thus a too coarse temporal resolution) can negatively affect the results by altering the description of the natural succession of events.

By experimenting with various applications and varying the individual values each time, it is possible to make a more informed comparison between the various cases and associate each "cause" with a relative "effect."

5.2 Datas and initial conditions

A total of five long-term simulations are proposed, in which the key variables that are manipulated are: the growth/decay coefficient θ, the coefficient of variation of the levels cv, and the temporal correlation τ.

In particular, two different case studies are implemented, which differ in the values of β and γ and in their ratio θ, referred to as "Case A" and "Case B".

- The first choice is based on one of the approaches previously implemented by Tron et al. (2014) to describe root biomass dynamics. In particular, comparable values of β and γ are assumed, with β decreasing linearly from β_{max} to 0. In this case, γ (the dominant value for adimensionalization) is set to $\gamma = 0.01\ d^{-1}$, and β_{max} is taken as twice the decay coefficient, $\beta_{max} = \gamma = 0.01\ d^{-1}$. Consequently, the adimensionalized term will be $\theta_{max} = 1$. This assumption may appear counterintuitive, since extrapolating the growth and decay times obtained from the corresponding equations shows that the t_{95} decay time from $B_r^{max} = 1$ to $B_r = 0.05$ is $t_{95} = 300\ d$, while the t_{95} growth time from $B_r = 0$ to $B_r = 0.95$ (in the zone subject to β_{max}) is $t_{95} = 85\ d$. It is evident that the decay time, which reflects the pressure caused by the water table submerging the roots, is longer than the growth time of the roots themselves. This

would imply that a plant exposed to anoxia or drought degrades more slowly than it grows, which is paradoxical. Nevertheless, it is still interesting to analyze a case study in which growth and decay times are broadly comparable, in order to observe in the results of the temporal variations of root biomass values. It must be remembered, however, that the modeling framework also represents an approximation of many biological and non-biological phenomena, which would be impractical to describe otherwise. For this reason, in the root biomass decay equation and in its coefficient, additional processes may be included depending on the user's objectives. For instance, if the model aims to represent only the effects of anoxia and drought on root biomass, the decay time will likely be higher than if we were to also include other flood-related effects not represented in this model, such as hydro-morphodynamic stresses.

– In this case, β and γ are chosen in light of the previous considerations regarding the expected imbalance between decay and growth times, favoring a likely tendency of plants to grow more slowly than they decay under hydrological stress conditions. For this reason, γ is set to $\gamma = 0.1\ d^{-1}$ ($t_{95} = 30\ d$), while β_{max} is chosen based on a growth time of $t_{95} = 200\ d$, resulting in $\beta_{max} = 0.072\ d^{-1}$.

A further distinction made through the simulations consists in the variation of the coefficient of variation cv. It (with reference to a constant average level) is assumed to be:

- $cv = 0.2$
- $cv = 0.4$

By alternating the two values, it is possible to simulate and observe the effects of a more variable and less variable hydrological regime.

The temporal correlation coefficient is also varied, assuming more drastic and more gradual variability by inserting three different values.

- $\tau = 10\ d$
- $\tau = 20\ d$
- $\tau = 40\ d$

Finally, the additional simulation values concerning the biological environment, soil characteristics, and other characteristics of the hydrological regime are all assumed to be constant during the simulations.

- μ (mean groundwater level) $= 4$
- $t_{\text{simulazione}} = 50$ years
- $dt = 0.1$

- ℓ (capillary rise height) $= 1\,m$
- $\xi_{r,\max}$ (maximum root depth) $= 6\,m$
- k (root deepening velocity) $= 0.025\,m/d$
- $h_{\min}$ (root interest zone) $= 4\,m$

The data relating to each simulation with attached dimensionless values are presented below. For each simulation, the time series requiring the previously introduced parameters are consequently generated and presented.

Simulation 1

Table 5.1: Simulation 1

γ (decay factor)	$\frac{1}{10}d^{-1} = 0.1\,d^{-1}$	
$\beta_{\max}$ (growth factor)	$0.0072\,d^{-1}$ $(t_{95} = 180)$	$\theta = \frac{\beta_{\max}}{\gamma} = 0.072\,[-]$
k (root deepening rate)	$0.025\,\mathrm{m/d}$	$\frac{k}{\gamma \cdot \xi_{i,m}} = 0.000125\,[-]$
$\xi_{r,\max}$ (maximum root depth)	$6\,\mathrm{m}$	$0.3\,[-]$
L (capillary rise height)	$1\,\mathrm{m}$	$0.05\,[-]$
$h_{\min}$ (minimum root interest depth)	$4\,\mathrm{m}$	$0.2\,[-]$
$B_{r,\max}$ (maximum root biomass)	$1\,[-]$	$1\,[-]$

$$= generazione\_livelli(4, 0.2, 20 \cdot \gamma, 50 \cdot 365 \cdot \gamma); \qquad dt = 0.1 \cdot \gamma$$

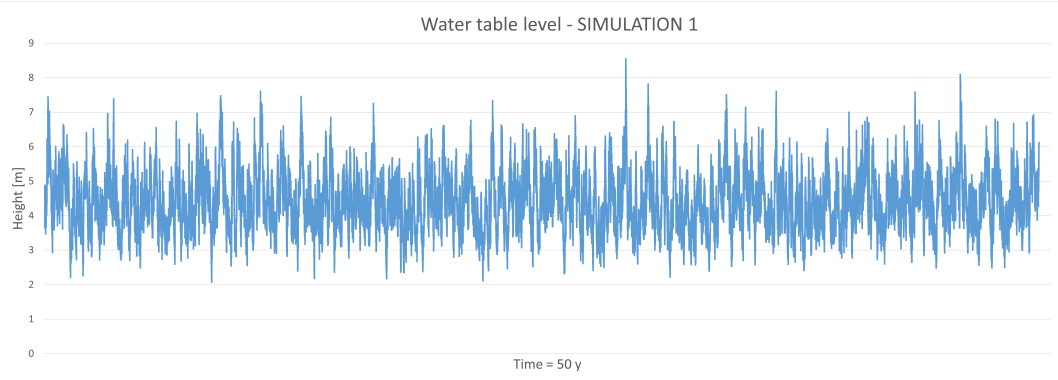

Figure 5.1: GW time series simulation 1

Simulation 2

Table 5.2: Simulation 2

γ (decay factor)	0.01 d^{-1}	
$\beta_{\max}$ (growth factor)	0.01 d^{-1}	$\theta = \beta_{\max}/\gamma = 1$ [−]
k (root depth growth rate)	0.025 m/d	$k/(\gamma \cdot z_{i,m}) = 0.000125$ [−]
$\xi_{r,\max}$ (maximum root depth)	6 m	0.3 [−]
L (capillary rise height)	1 m	0.05 [−]
$h_{\min}$ (minimum root interest depth)	4 m	0.2 [−]
$B_{r,\max}$ (maximum root biomass)	1 [−]	1 [−]

$$= generazione\_livelli(4, 0.2, 20 \cdot \gamma, 50 \cdot 365 \cdot \gamma); \qquad dt = 0.1 \cdot \gamma$$

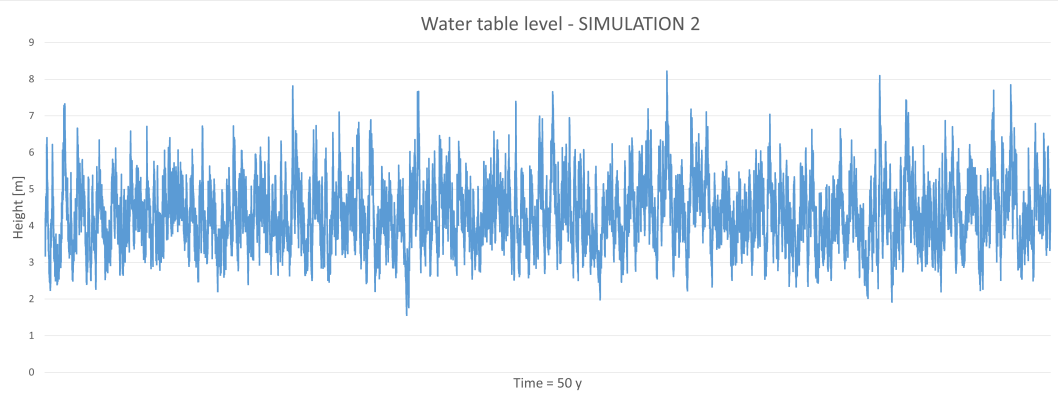

Figure 5.2: GW time series simulation 2

Simulation 3

Table 5.3: Simulation 3

γ (decay factor)	$\frac{1}{10} d^{-1} = 0.1\, d^{-1}$	
$\beta_{\max}$ (growth factor)	0.0072 d^{-1} ($t_{95} = 180$)	$\theta = \frac{\beta_{\max}}{\gamma} = 0.072$ [−]
k (root deepening rate)	0.025 m/d	$\frac{k}{\gamma \cdot \xi_{i,m}} = 0.000125$ [−]
$\xi_{r,\max}$ (maximum root depth)	6 m	0.3 [−]
L (capillary rise height)	1 m	0.05 [−]
$h_{\min}$ (minimum root interest depth)	4 m	0.2 [−]
$B_{r,\max}$ (maximum root biomass)	1 [−]	1 [−]

$$= generazione\_livelli(4, 0.4, 20 \cdot \gamma, 50 \cdot 365 \cdot \gamma); \qquad dt = 0.1 \cdot \gamma$$

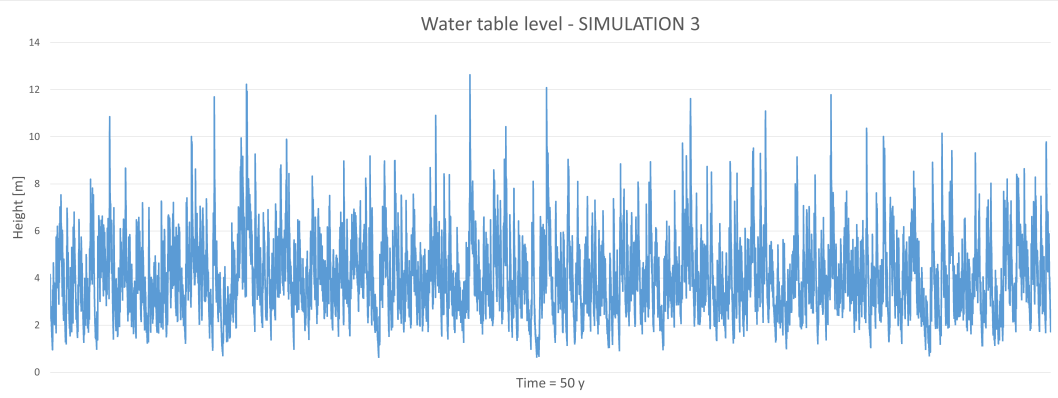

Figure 5.3: GW time series simulation 3

Simulation 4

Table 5.4: Simulation 4

γ (decay factor)	$\frac{1}{10}d^{-1} = 0.1\,d^{-1}$	
$\beta_{\max}$ (growth factor)	$0.0072\,d^{-1}$ $(t_{95} = 180)$	$\theta = \frac{\beta_{\max}}{\gamma} = 0.072\,[-]$
k (root deepening rate)	$0.025\,\mathrm{m/d}$	$\frac{k}{\gamma \cdot \xi_{i,m}} = 0.000125\,[-]$
$\xi_{r,\max}$ (maximum root depth)	$6\,\mathrm{m}$	$0.3\,[-]$
L (capillary rise height)	$1\,\mathrm{m}$	$0.05\,[-]$
$h_{\min}$ (minimum root interest depth)	$4\,\mathrm{m}$	$0.2\,[-]$
$B_{r,\max}$ (maximum root biomass)	$1\,[-]$	$1\,[-]$

$$= generazione\_livelli(4, 0.2, 10 \cdot \gamma, 50 \cdot 365 \cdot \gamma); \qquad dt = 0.1 \cdot \gamma$$

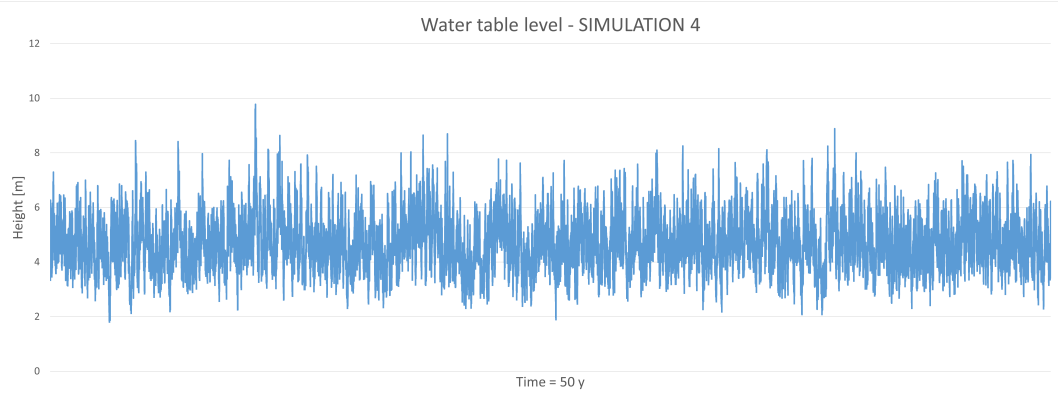

Figure 5.4: GW time series simulation 4

Simulation 5

Table 5.5: Simulation 5

γ (decay factor)	$\frac{1}{10}d^{-1} = 0.1\,d^{-1}$	
$\beta_{\max}$ (growth factor)	$0.0072\,d^{-1}$ $(t_{95} = 180)$	$\theta = \frac{\beta_{\max}}{\gamma} = 0.072\,[-]$
k (root deepening rate)	$0.025\,\mathrm{m/d}$	$\frac{k}{\gamma \cdot \xi_{i,m}} = 0.000125\,[-]$
$\xi_{r,\max}$ (maximum root depth)	$6\,\mathrm{m}$	$0.3\,[-]$
L (capillary rise height)	$1\,\mathrm{m}$	$0.05\,[-]$
$h_{\min}$ (minimum root interest depth)	$4\,\mathrm{m}$	$0.2\,[-]$
$B_{r,\max}$ (maximum root biomass)	$1\,[-]$	$1\,[-]$

$$= generazione\_livelli(4, 0.2, 40 \cdot \gamma, 50 \cdot 365 \cdot \gamma); \qquad dt = 0.1 \cdot \gamma$$

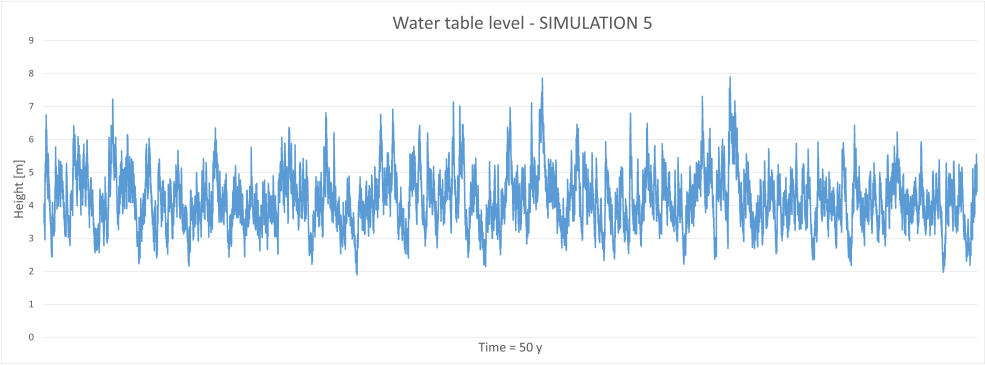

Figure 5.5: GW time series simulation 5

As previously mentioned, the section in question reproduces the right side of an almost trapezoidal section with a horizontal bottom and an oblique side, which is represented as follows:

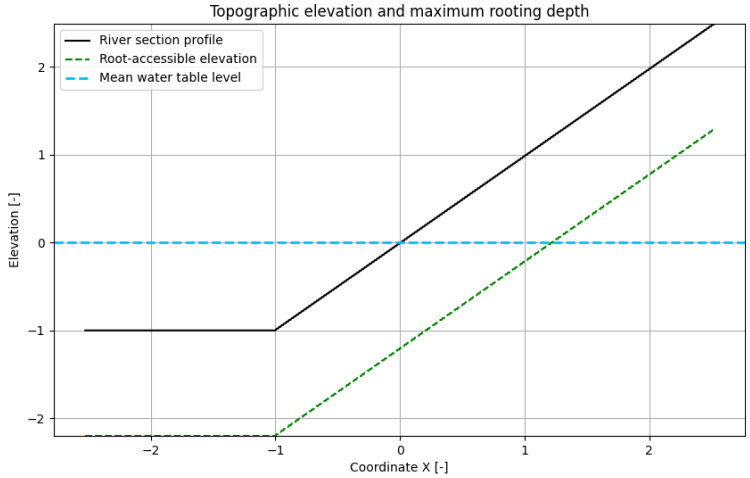

Figure 5.6: Dimensionless profile, maximum root growth and average Gw level

5.3 Results

By inserting the required conditions into the dedicated fields within the `main.py` file of the root development code (either in numerical form or as the path to the file containing the corresponding data, such as the time series information or the analyzed profile), and executing the run, the code computes the variables B_r and ξ along the defined time series. The results are then processed by the `analisi_statistica.py` file, producing the following outputs.

5.3.1 Simulation 1

The first simulated case is the reference case, in which all the "intermediate" values within the simulation range are assumed:

$\theta = 0.072$ (difference between β and γ larger and more realistic), $cv = 0.2$, $\tau = 20\,d$.

The results are shown below:

The first result shown in Figure 5.7 represents the average biomass values recorded throughout the entire simulation period for each cell of the matrix. The mean values were updated incrementally at each time step starting from the values of $Br(t)$. The "cloud" of positive values, which reach up to 0.08 (always considering 1 as $Br_{\max}$), is logically distributed around the zero elevation (corresponding to the mean temporal groundwater level), and the farther away one moves, the smaller the values become.

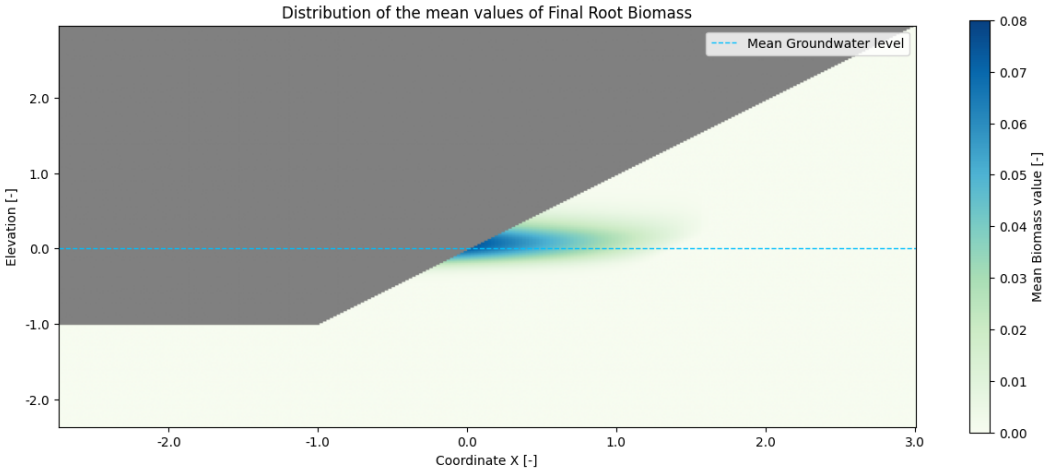

Figure 5.7: Mean Br Value of Simulation 1

The next plot represents the variance σ of the final values, whose distribution appears slightly less homogeneous but still follows the logic of the Root Biomass equations, and exhibits peak values reaching up to $\sigma = 0.04$.
The variance, just like the mean, was obtained incrementally at each time step.

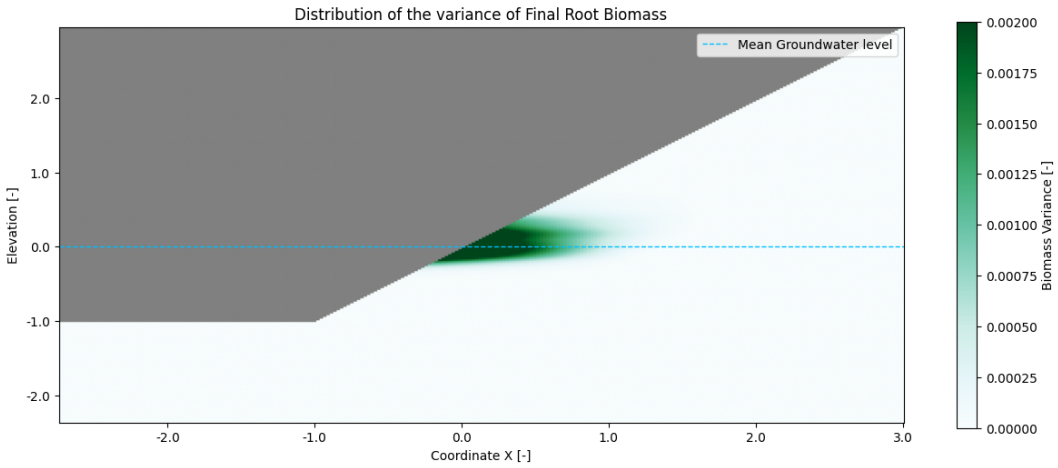

Figure 5.8: Br Variance of Simulation 1

The following plot shows the root depth reached with respect to the profile and the maximum attainable depth values. The values of ξ_r are updated at each time step and, since this is a long-term simulation, the main changes in root depth occur at the beginning of the simulation, when the roots are still very young and shallow and thus have considerable growth potential.
In the long term, the roots undergo only sporadic and slight variations, and the results are similar across all simulations. However, by focusing on the lateral extent of the reached depths, it is possible to associate them with the characteristics of the hydrological regime.

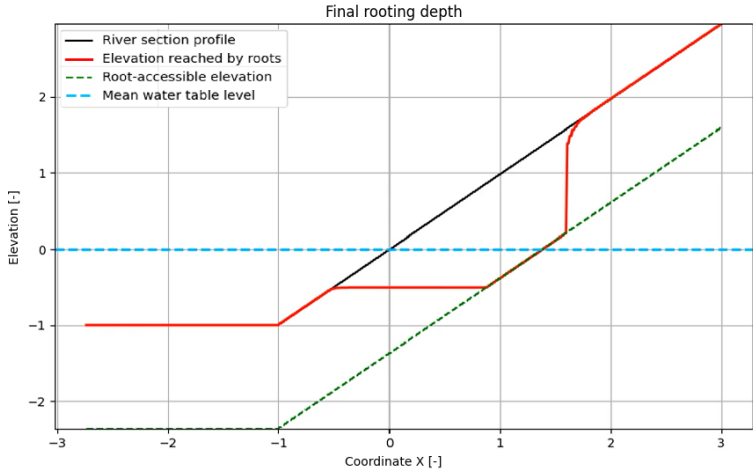

Figure 5.9: Br Reached root depth at the end of simulation 1

Figure 5.10 shows the same plot of the mean biomass values presented in Figure 5.7, with the positions of some specimens highlighted according to the obtained mean Br values. In particular, the red dashed line represents the point (with respect to its x-coordinate) where the total mean root biomass is greatest.

The $\overline{Br}_{\text{tot}}$ is defined as the sum of the values of the cells belonging to the root system of a given specimen:

$$\overline{Br}_{\text{tot}} = \sum_{i}^{z} \overline{Br}_i \tag{5.1}$$

That is, from the sum of the $\overline{Br}_z$ values sharing the same x-coordinate.

The red dashed line represents the x-position where vegetation shows the highest $\overline{Br}$. It is interesting to note how, according to expectations, the maximum $\overline{Br}$ corresponds to a point on the bed profile located above the mean river level. This result is consistent both logically and with the expected position of the capillary rise height above the groundwater table.
The orange dashed line corresponds to the position where the value of $\overline{Br}$ is 50% of the maximum value, while the yellow dashed line corresponds to 10% of the maximum value. It is interesting to observe that, despite the symmetry of the growth and decay law (particularly regarding the behavior under anoxic conditions and absence of moisture), there is a certain asymmetry in the horizontal distance between the highlighted lines, and thus a distribution of the "cloud" that is more concentrated downstream and more dispersed upstream.

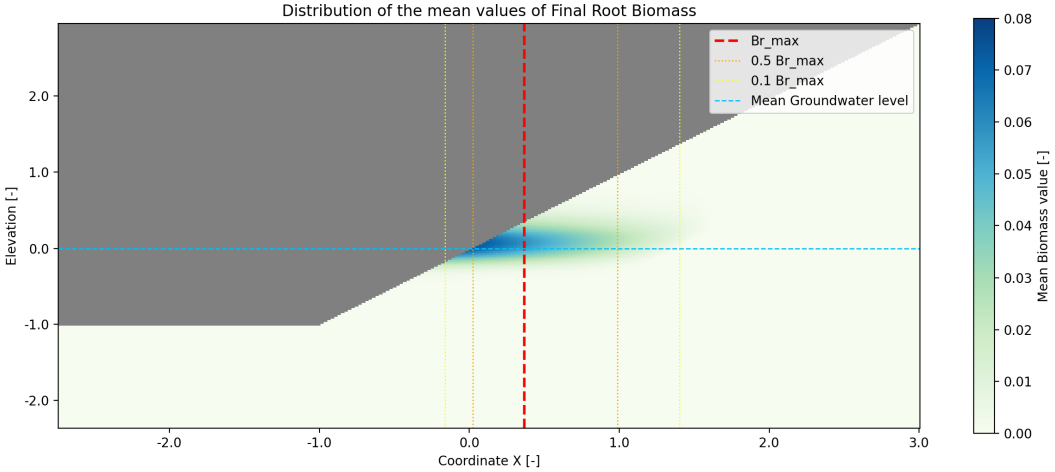

Figure 5.10: Mean Br Value of Simulation 1 with position of: Br_{max}, $0.5Br_{max}$, $0.1Br_{max}$

Figure 5.11,shows the profiles of the $\overline{Br}$ values along the corresponding z-axis for each vegetation element.

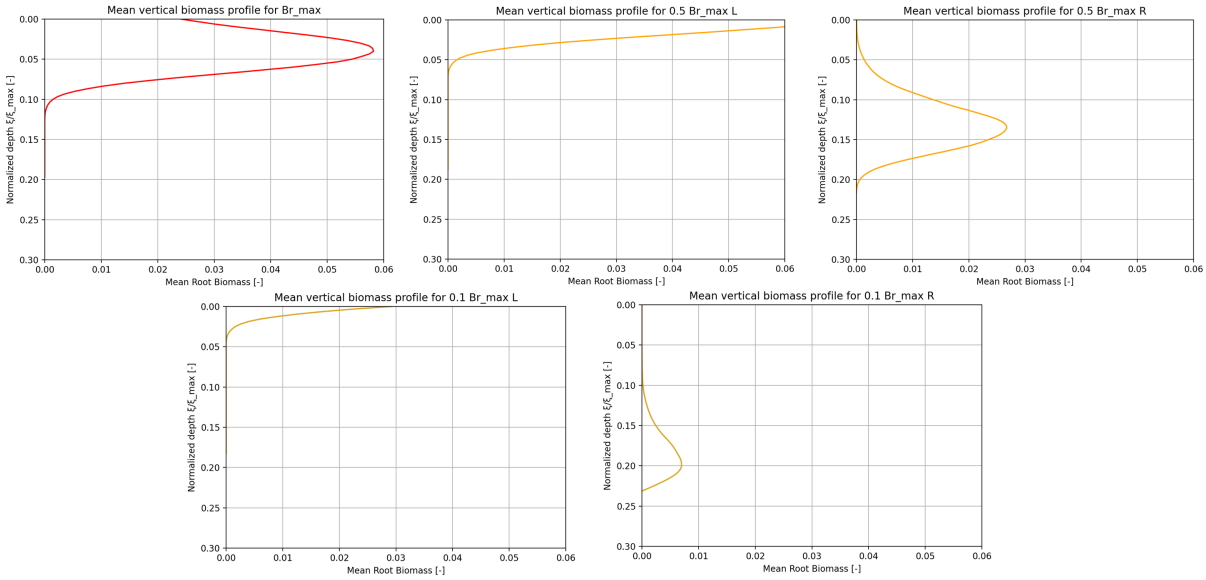

Figure 5.11: Profile distribution corresponding to: Br_{max}, $0.5Br_{max}$, $0.1Br_{max}$

5.3.2 Simulation 2

The following case differs from the previous one in the values of β and γ, and consequently of θ. In this case, Case B was applied, that is, a vegetation type with more homogeneous growth and decay tendencies and a resulting value of $\theta_{\max} = 1$, in order to analyze a completely different type of vegetation and a very different response to the external forcing.
Figure 5.12 shows the mean root biomass values $\overline{Br}$, which are significantly higher than in the previous case, reaching up to 0.4.

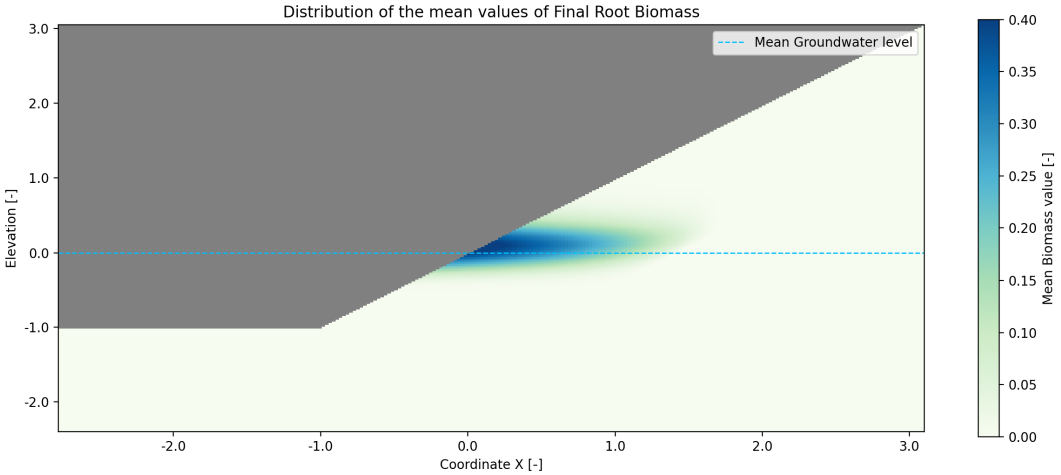

Figure 5.12: Mean Br Value of Simulation 2

The next plot represents the variance in the distribution of biomass averages. Referring to the same scale of variance as in simulation 1, the values are much higher than the previous ones, to the extent that they are not comparable. For this

reason, a second graph of the variance is shown in figure 5.13, with a scale adapted to its peak values (σ= 0.0016)

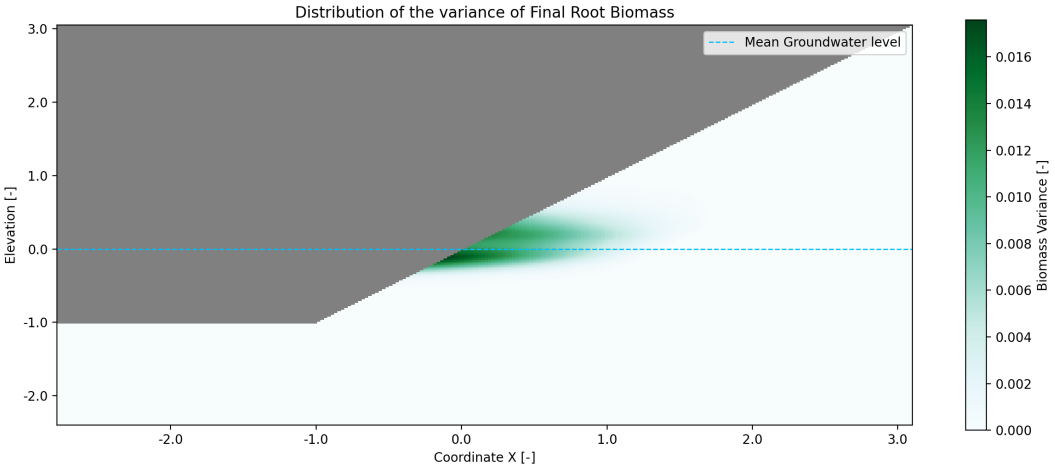

Figure 5.13: *Br* Variance of Simulation 2

The graph below shows the final root depths at the end of the simulation with a duration of $t = 50$ years.

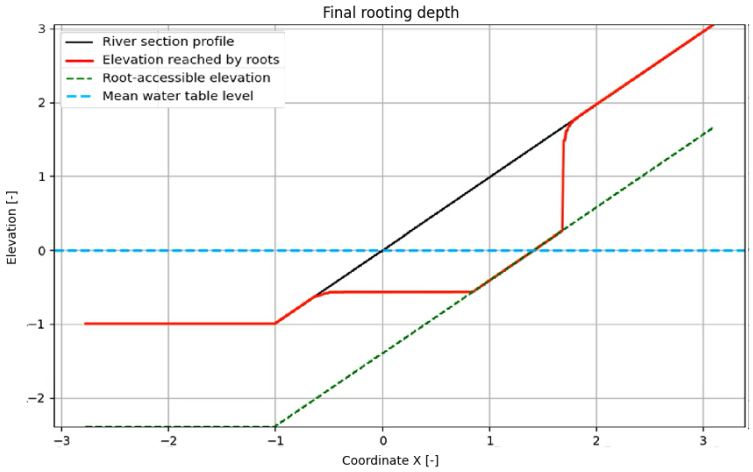

Figure 5.14: *Br* Reached root depth at the end of simulation 2

Figure 5.15 shows the plot of the mean root biomass $\overline{Br}$, with the positions highlighted of the element with maximum root biomass $\overline{Br}_{\max}$, as well as those with values $0.5\,\overline{Br}_{\max}$ and $0.1\,\overline{Br}_{\max}$.

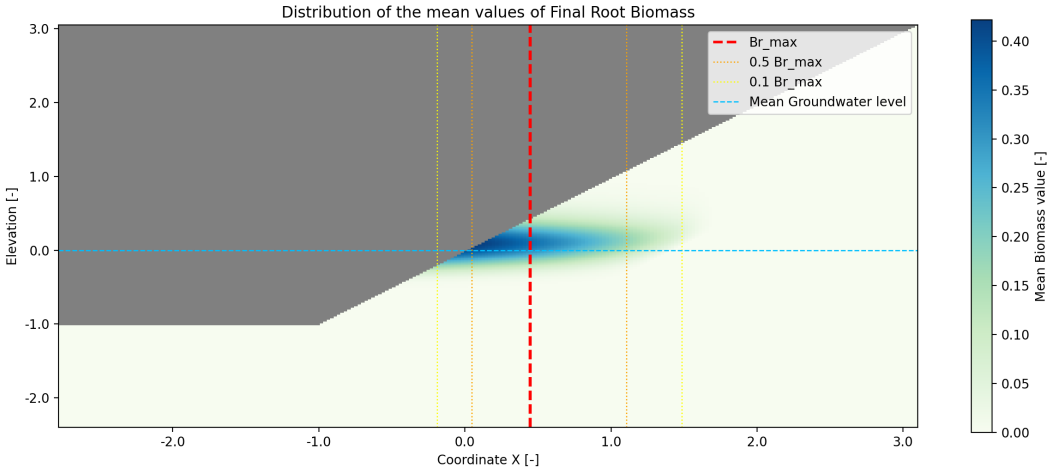

Figure 5.15: Mean Br Value of Simulation 2 with position of: Br_{max}, $0.5Br_{max}$, $0.1Br_{max}$

5.3.3 Simulation 3

The following case differs from the previous ones in that it has a different value for the characteristics that define the hydrological regime. While in the previous cases the time series was always generated with a $cv = 0.2$, in this case a $cv = 0.4$ was assumed, which implies a regime with twice the variability. All other characteristics are consistent with simulation 1.

Figure 5.16 shows the mean root biomass values $\overline{Br}$, which reach up to 0.03.

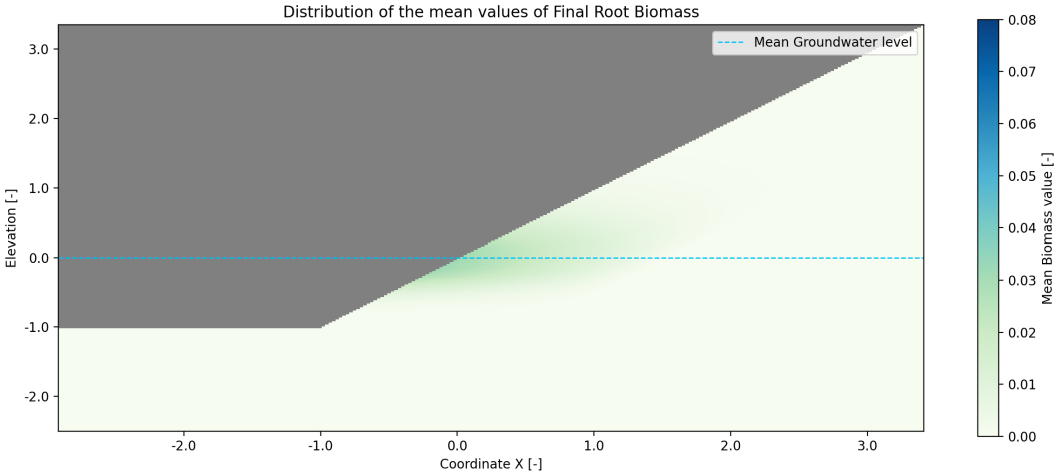

Figure 5.16: Mean Br Value of Simulation 3

The next plot in Figure 5.17 represents the variance σ of the distribution of the mean biomass. The values, which follow a spatial distribution similar to that of the means, reach peak values of $\sigma = 0.0012$.

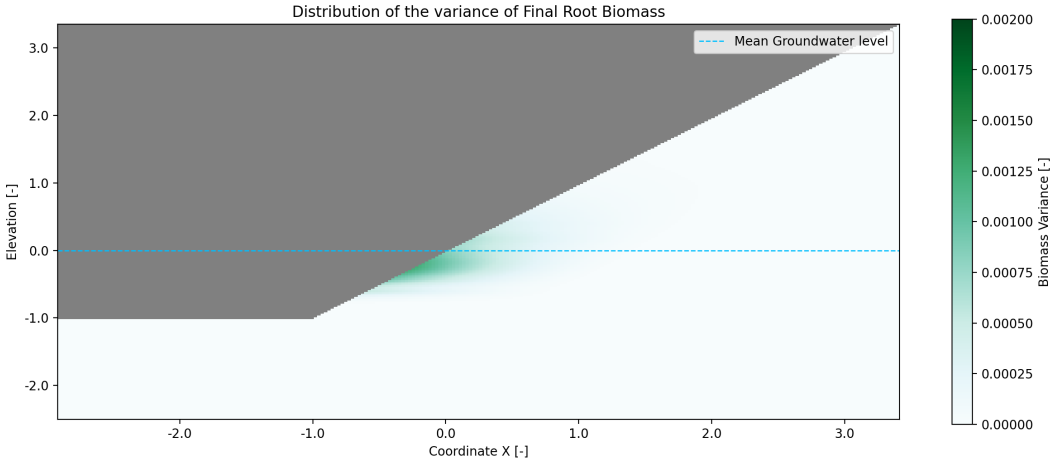

Figure 5.17: *Br* Variance of Simulation 3

The graph below shows the final root depth at the end of the simulation.

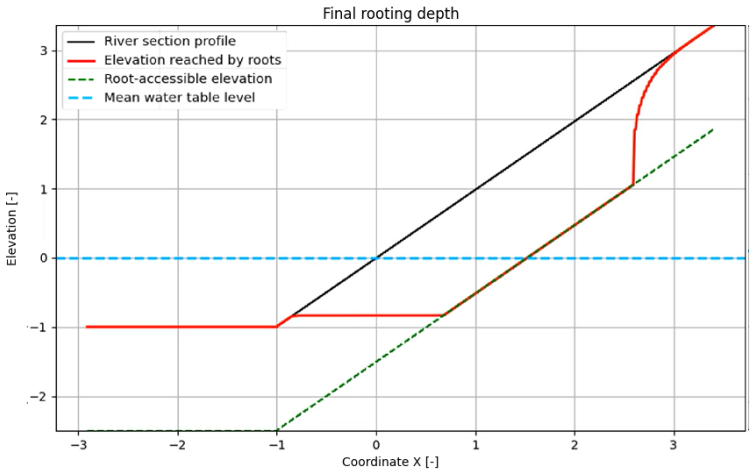

Figure 5.18: *Br* Reached root depth at the end of simulation 3

Figure 5.18 shows the plot of the mean root biomass $\overline{Br}$, with the highlighted positions of the element with maximum root biomass $\overline{Br}_{\max}$, as well as those with values $0.5\,\overline{Br}_{\max}$ and $0.1\,\overline{Br}_{\max}$.

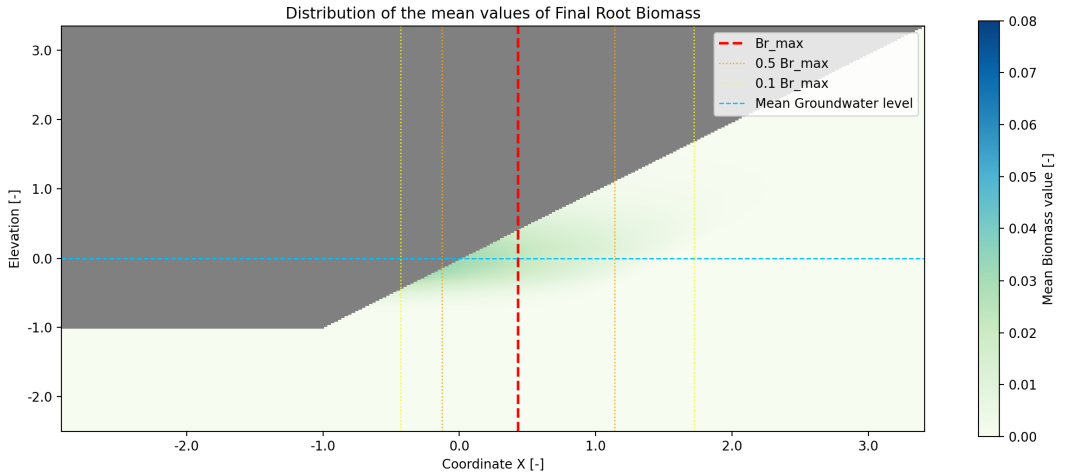

Figure 5.19: Mean Br Value of Simulation 3 with position of: Br_{max}, $0.5Br_{max}$, $0.1Br_{max}$

5.3.4 Simulation 4

The following case differs from the previous ones in that it has a different value of in the characteristics that define the hydrological regime. While in the previous cases the time series was always generated with a $ct = 20$ *days*, in this case a $ct = 10$ *days* was assumed, which implies a regime with a higher frequency of variation. All other characteristics are consistent with simulation 1.

Figure 5.20 shows the mean root biomass values $\overline{Br}$, which reach up to 0.05.

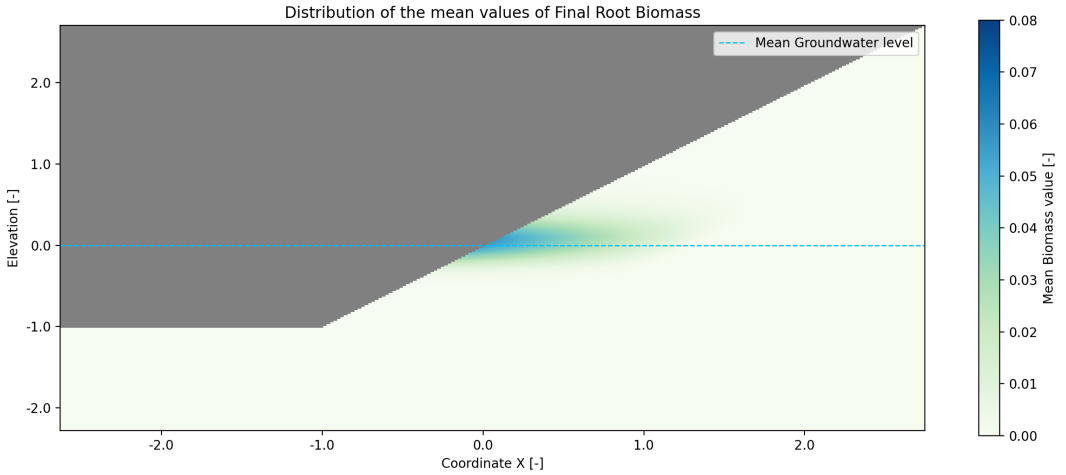

Figure 5.20: Mean Br Value of Simulation 4

The next plot in Figure 5.21 represents the variance σ of the distribution of the mean biomass, with values up to $\sigma = 0.0016$.

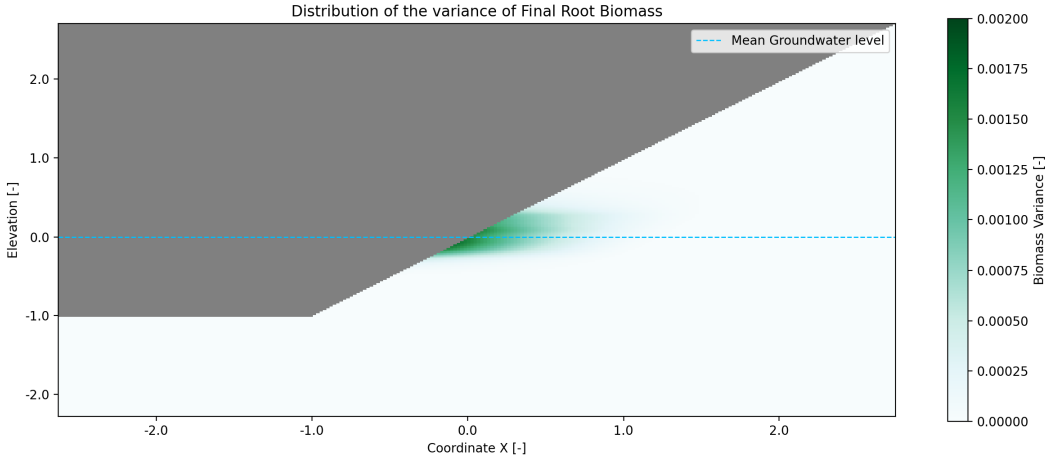

Figure 5.21: Br Variance of Simulation 4

The graph below shows the final root depth at the end of the simulation.

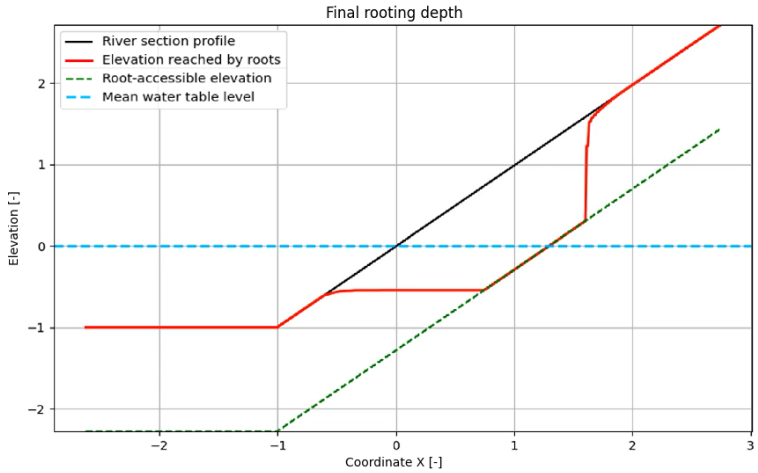

Figure 5.22: Br Reached root depth at the end of simulation 4

Figure 5.23 shows the plot of the mean root biomass $\overline{Br}$, with the highlighted positions of the element with maximum root biomass $\overline{Br}_{\max}$, as well as those with values $0.5\,\overline{Br}_{\max}$ and $0.1\,\overline{Br}_{\max}$.

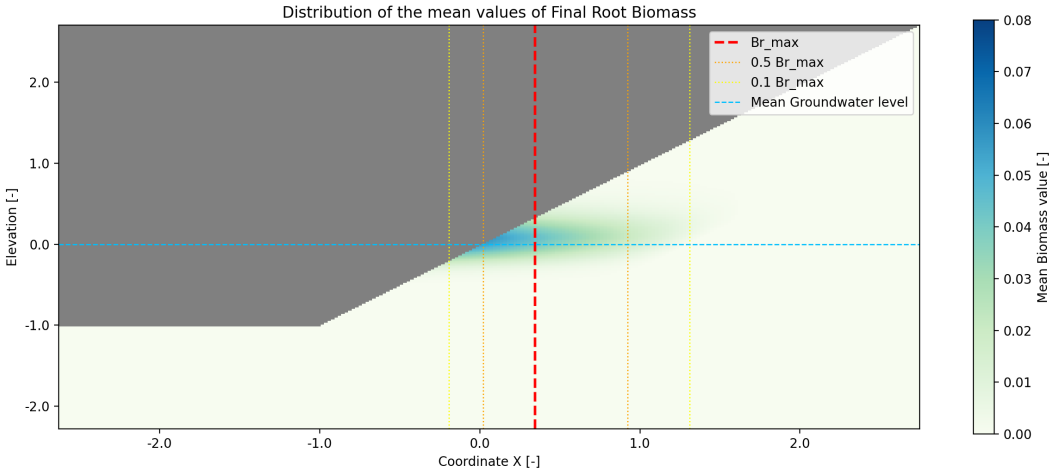

Figure 5.23: Mean Br Value of Simulation 4 with position of: Br_{max}, $0.5Br_{max}$, $0.1Br_{max}$

5.3.5 Simulation 5

The following case differs from the previous ones as it presents a different c_t value among the characteristics defining the hydrological regime. While in the previous cases the time series was always generated with $c_t = 20$ days, In this case $c_t = 40$ days was assumed, implying a regime with a lower frequency of variation. All other characteristics are instead consistent with Simulation 1

Figure 5.24 shows the mean root biomass values $\overline{Br}$, which reach up to 0.1.

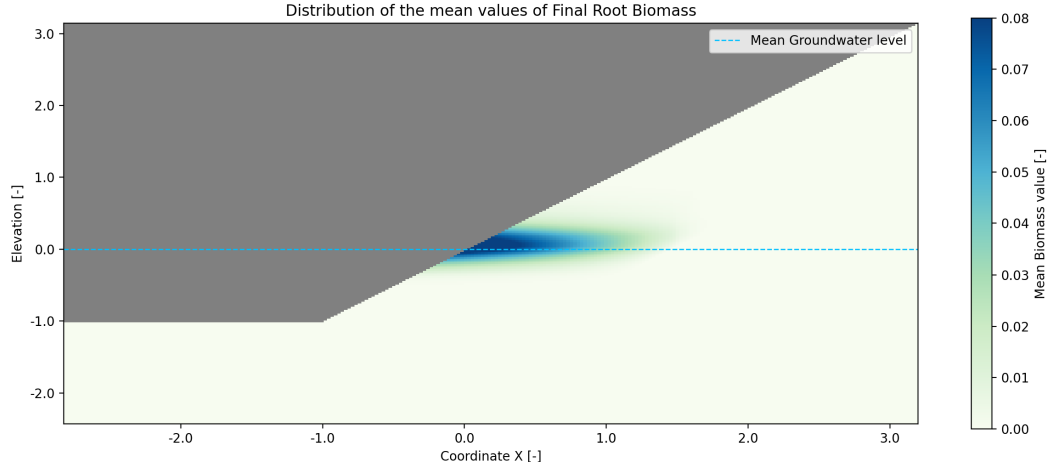

Figure 5.24: Mean Br Value of Simulation 5

The next plot in Figure 5.25 represents the variance σ of the distribution of the mean biomass, with values up to $\sigma = 0.008$.

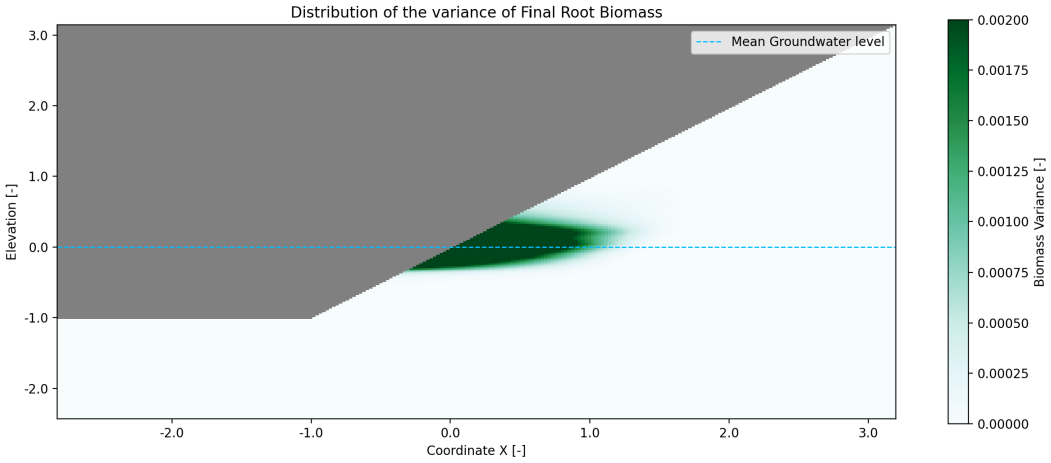

Figure 5.25: Br Variance of Simulation 5

The graph below shows the final root depth at the end of the simulation.

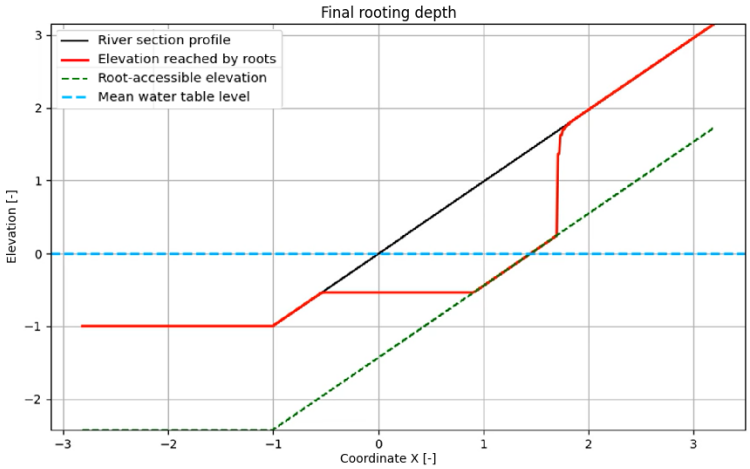

Figure 5.26: Br Reached root depth at the end of simulation 6

Figure 5.27 shows the plot of the mean root biomass $\overline{Br}$, with the highlighted positions of the element with maximum root biomass $\overline{Br}_{\max}$, as well as those with values $0.5\,\overline{Br}_{\max}$ and $0.1\,\overline{Br}_{\max}$.

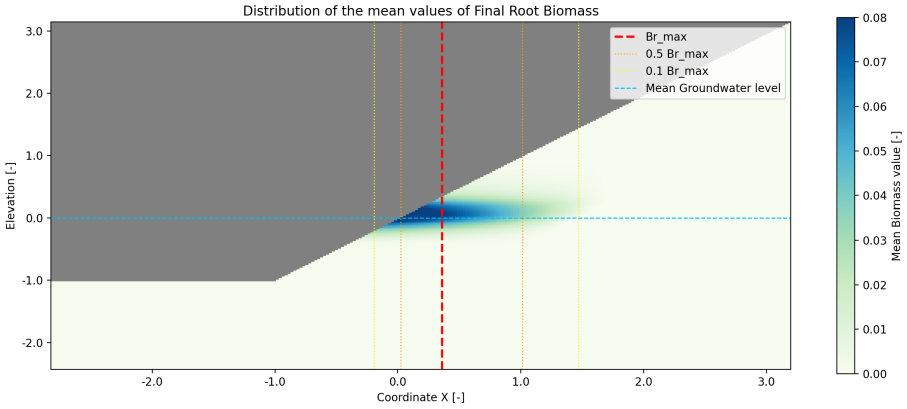

Figure 5.27: Mean Br Value of Simulation 5 with position of: Br_{max}, $0.5Br_{max}$, $0.1Br_{max}$

5.4 Analysis and comparison

Although the previously presented outputs mainly focus on statistical values extrapolated from the mean and variance, the actual results of the model consist in the calculation of root depth values ξ_r (already shown in the outputs above), which are nonetheless functional to the computation of the core variable of the model: the amount of root biomass at different depths, $Br(z)$.

This is because the modeling approach described here is designed to be embedded within a broader framework of vegetation modeling and flow interaction, in which Br would constitute a fundamental unit of the modeling process. This applies both in the case where Br is used to evaluate resistance criteria of vegetation against flow-induced stresses—by comparing the distribution of root biomass with the depth of scouring caused by morphodynamic changes—and in the case where root biomass is the central element of the modeling itself, being directly or indirectly linked through a relationship to the above-ground biomass. In such a case, Br would in itself represent a key term to quantify the physical presence of vegetation and, consequently, the disturbance it would impose on the flow by increasing shear stress and, more generally, by altering hydrodynamic characteristics.

To achieve this, the use of Br values must not be restricted to their statistical descriptors but must be obtained at each time step, since flow characteristics vary at every Δt. This, in fact, represents the main output of the simulation.

In order to evaluate and appreciate more concretely the results of the simulation and the succession of Br stages in response to the evolution of the aquifer, part of the simulations performed previously are now presented, on time scales suitable for visualizing the response of vegetation to changes in boundary conditions.

Below is represented a section of simulation 1 of 300 days in which it is possible to appreciate the evolution of root biomass and root depth over time.

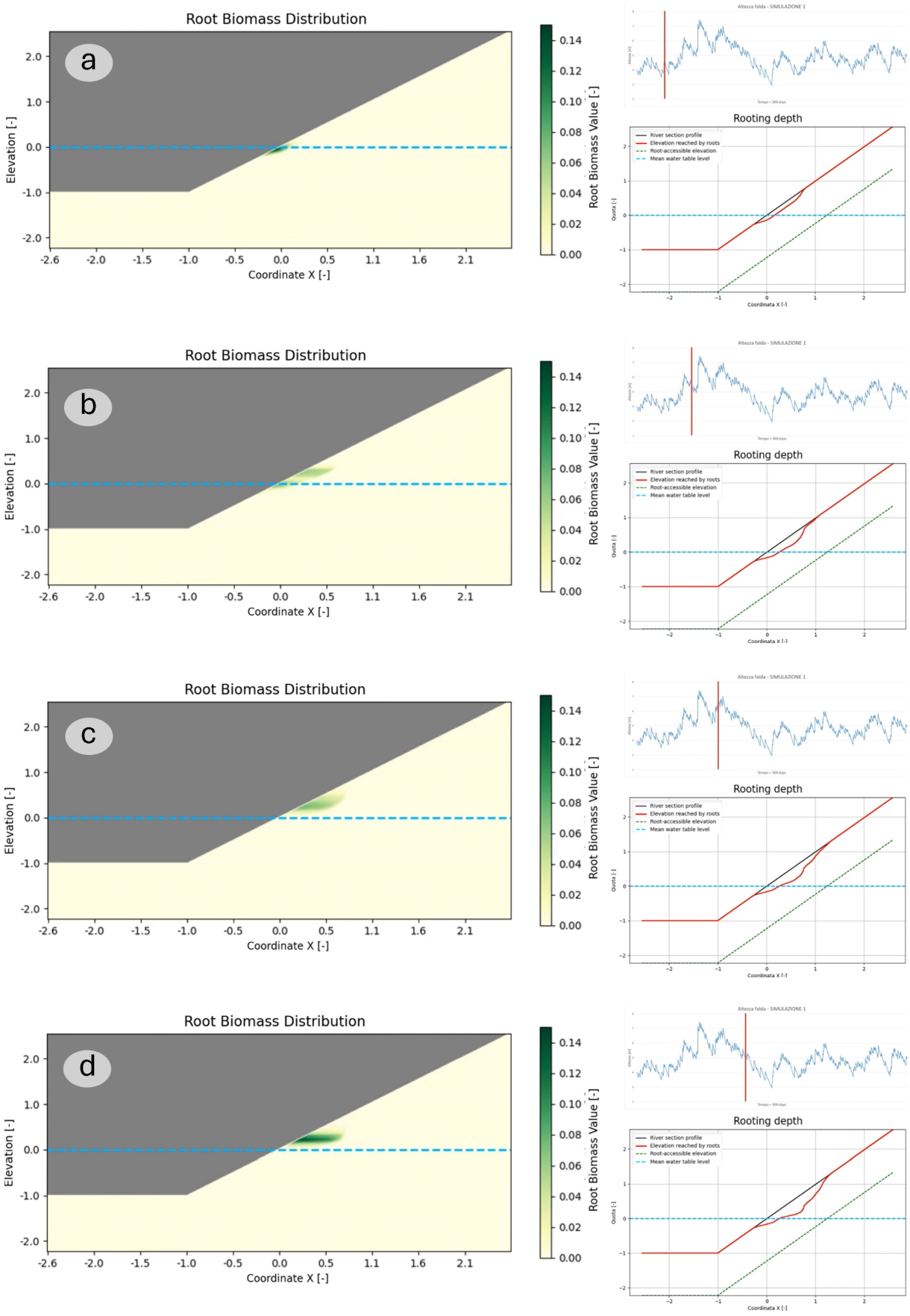
Root Biomass Distribution
a
b
c
d
Elevation [-]
Coordinate X [-]
Root Biomass Value [-]
Rooting depth
River section profile
Elevation reached by roots
Root-accessible elevation
Mean water table level
Coordinata X [-]

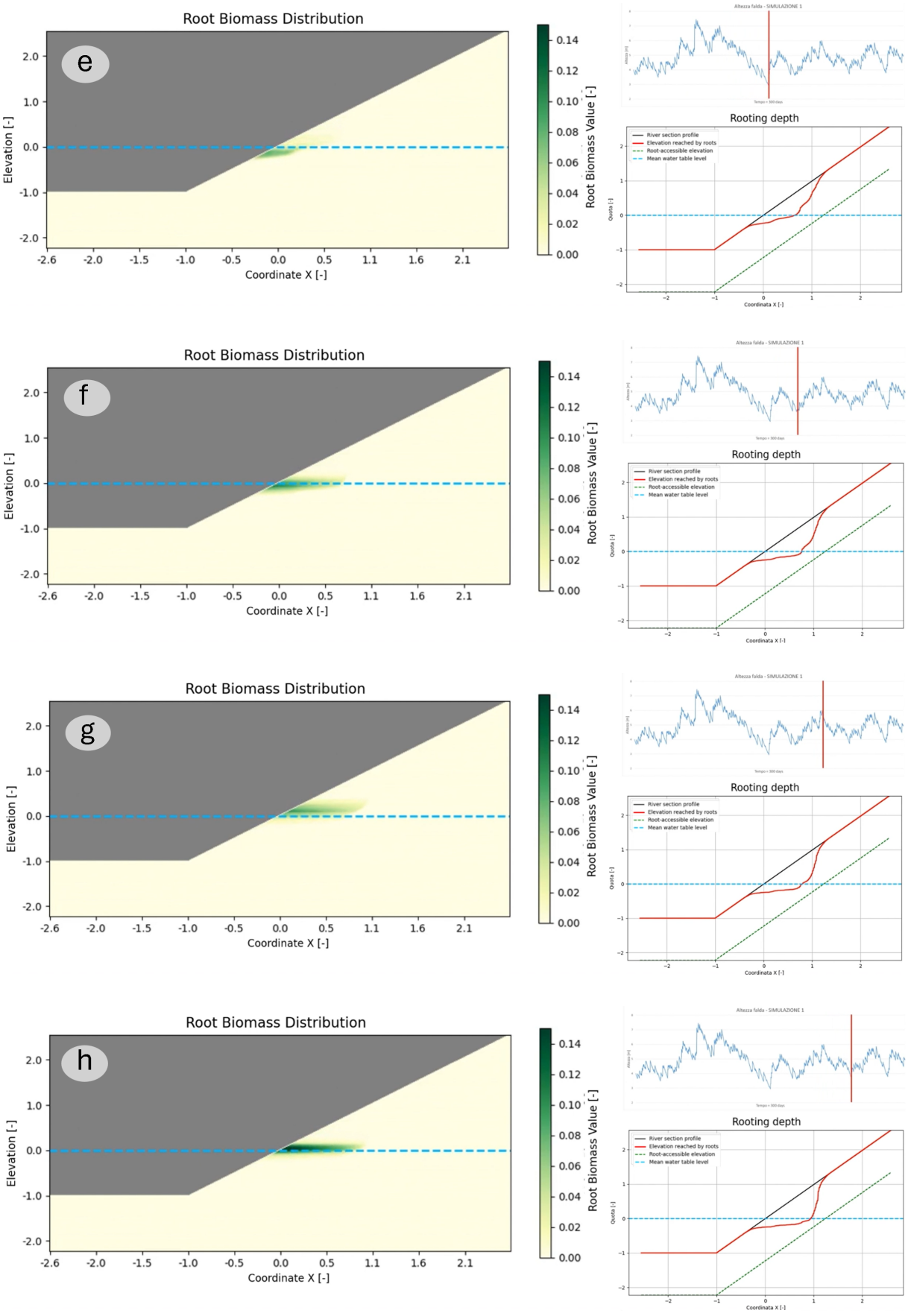
Root Biomass Distribution
e
Elevation [-]
Coordinate X [-]
Root Biomass Value [-]
Rooting depth
River section profile
Elevation reached by roots
Root-accessible elevation
Mean water table level
Root Biomass Distribution
f
Elevation [-]
Coordinate X [-]
Root Biomass Value [-]
Rooting depth
River section profile
Elevation reached by roots
Root-accessible elevation
Mean water table level
Root Biomass Distribution
g
Elevation [-]
Coordinate X [-]
Root Biomass Value [-]
Rooting depth
River section profile
Elevation reached by roots
Root-accessible elevation
Mean water table level
Root Biomass Distribution
h
Elevation [-]
Coordinate X [-]
Root Biomass Value [-]
Rooting depth
River section profile
Elevation reached by roots
Root-accessible elevation
Mean water table level

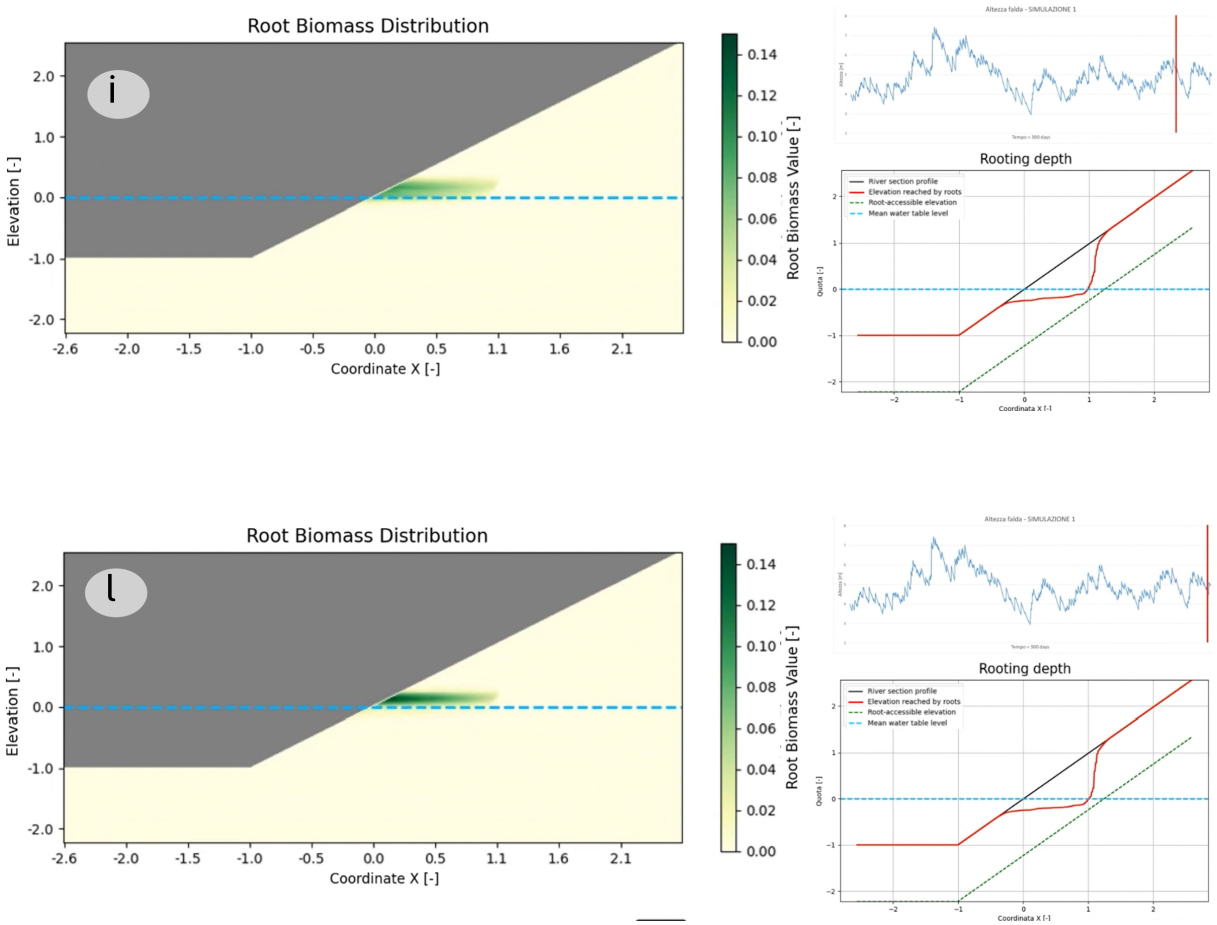

Figure 5.28: Root Biomass evolution in the considered section along 300 days with a $timestep = 30$ $days$ of simulation 1 ($\beta_{max}/\gamma = 0.072$)

In this sequence of images, one snapshot is shown every 30 days, and by referring to the position of the red line on the time series (its temporal position), each variation in groundwater levels can be associated with a corresponding variation in the values and distribution of Br and in the values of ξ_r.
The simulation starts at $t = 0$, from Bare Soil conditions $\xi_{r,t=0}(x) = 0$, in order to better highlight the variations in ξ_r. This is because, considering the chosen values of k and the characteristics of the hydrological regime, the most significant part of root depth evolution occurs within the first 1–2 years. Conversely, although under these conditions root biomass Br appears less distinguishable, it is still possible to infer the way vegetation responds to hydrological disturbances.

As can be easily inferred, ξ_r—which increases only for points above the water table and not too far from it—shows a central zone in which the roots deepen much faster than at elevations around or below 0 and around 1. This behavior is consistent with the pdf of the generated time series, which follows a Gaussian-like trend as shown in Figure 5.29. Since there is only one peak, coinciding with the mean, and considering the limits imposed by the "root interest zone" $h_{\min}$, the roots grow predominantly in the zone above these limits, as is clearly evident in the figure.

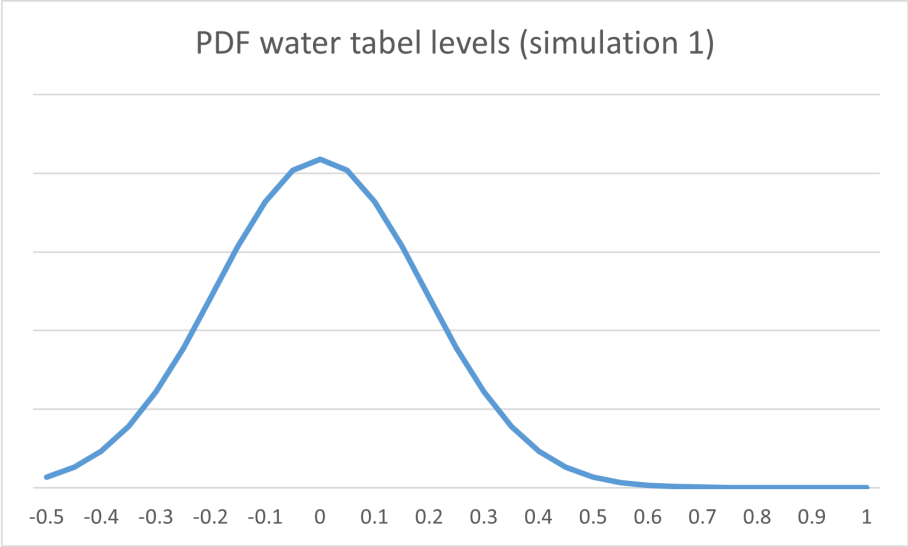

Figure 5.29: PDF of water level for simulation 1 time series

It should be noted that, in general, the distribution of Br values closely follows the fluctuations in the water table. For example, in figure c, i.e., 90 days after the start of the simulation, we see the first real "flood" period in which the levels temporarily stabilize at values that are significantly higher than the previous average, a transition that already occurs in case b, where the values are, however, lower.

It is clear, for example, when comparing case a with case b, that the values appear to be completely independent of each other and that the vegetation residues belonging to the period when the oscillations were stable at lower values have almost completely disappeared. This occurs essentially for two reasons: first of all, the height of the capillary rise (L=1m) is small when compared to the difference in height found in the variation of the water table and, above all, to the variation in height of the side bank, which is designed to be oblique in order to emulate an idealized case. By assuming higher capillary rise values, for example, or profile values that are more "proportionate" to the physics of the soil and more realistic, the differences would be much less pronounced. Another factor that should not be underestimated is the γ decay factor which, in an attempt to more faithfully emulate phenomena of anoxia and absence of moisture, has very high values and very rapid decay times in simulation 1. This, considering the small portion in which the growth process (L) occurs compared to the magnitude of the oscillations, creates a large variability of values and a low time dependence.

Persistence and consistency in groundwater values (without significant variability) can be observed in an increase in biomass values (higher values and more pronounced color). Conversely, if conditions have changed recently, although the area affected by significant values may appear similar, the values would be lower.

The situation is instead very different for ξ_r, which is a cumulative value over time and does not involve decay phenomena. It is easy to observe that, while the central part keeps deepening further and further, the extremes—being evidently shallower

(thinner)—advance only when rarer events occur (both in excess and in deficit), as in cases b, c, and e.

When analyzing the evolution of root biomass and its distribution, it is useful to consider simulation 2. This simulation assumes the same hydrological conditions as input but with different (and unique among the simulations performed) vegetation characteristics. In fact, simulation 2 assumes a greater balance between growth and decay factors, assuming $\beta = \gamma = 0.01$.

This balance between the two factors, which keeps the growth factor similar to that in case A and the decay factor 10 times smaller, has a strong impact on the variation and distribution of biomass values.

A more detailed analysis can be seen in figure5.30.

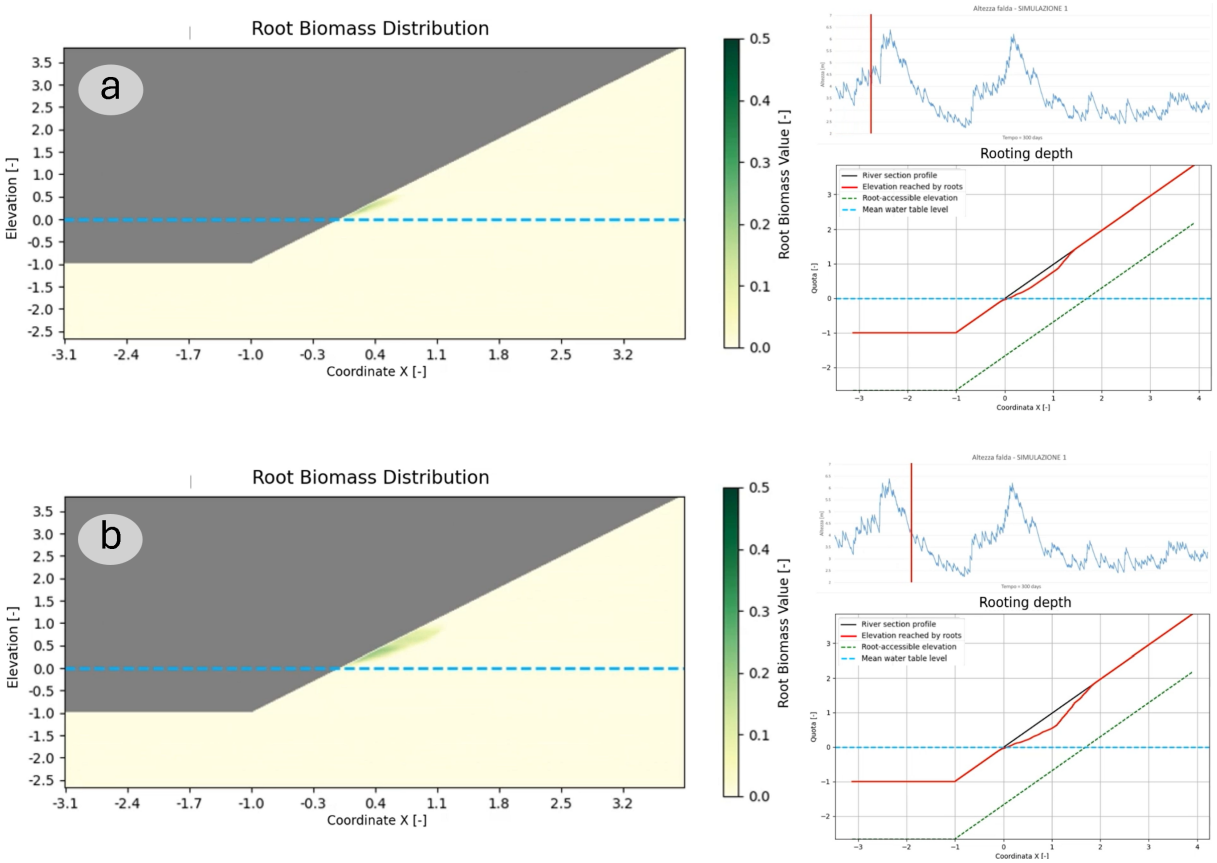

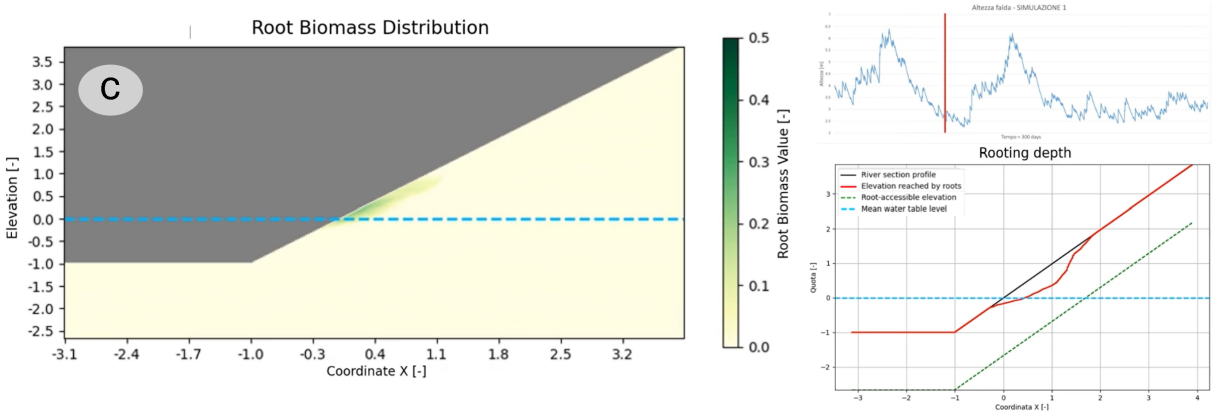
Root Biomass Distribution
c
Elevation [-]
Coordinate X [-]
Root Biomass Value [-]
Rooting depth
River section profile
Elevation reached by roots
Root-accessible elevation
Mean water table level
Coordinata X [-]

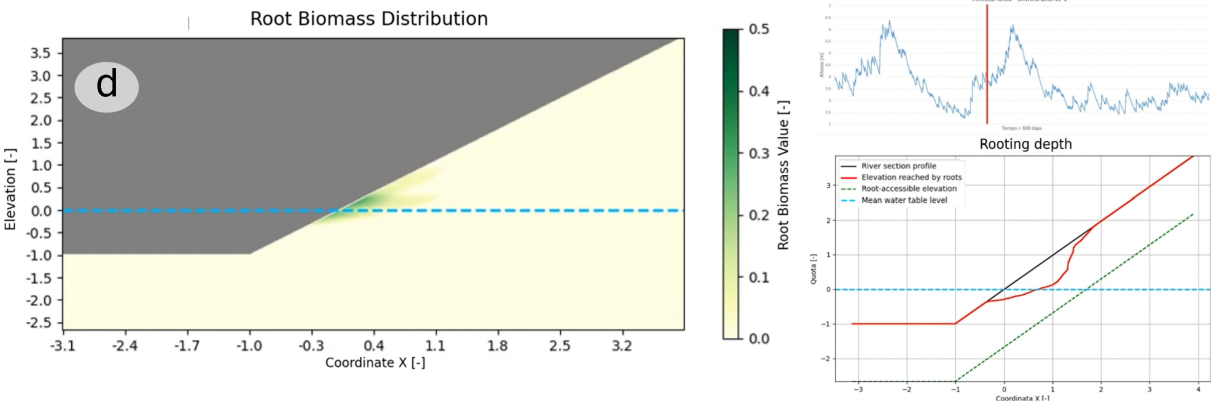
Root Biomass Distribution
d
Elevation [-]
Coordinate X [-]
Root Biomass Value [-]
Rooting depth
River section profile
Elevation reached by roots
Root-accessible elevation
Mean water table level
Coordinata X [-]

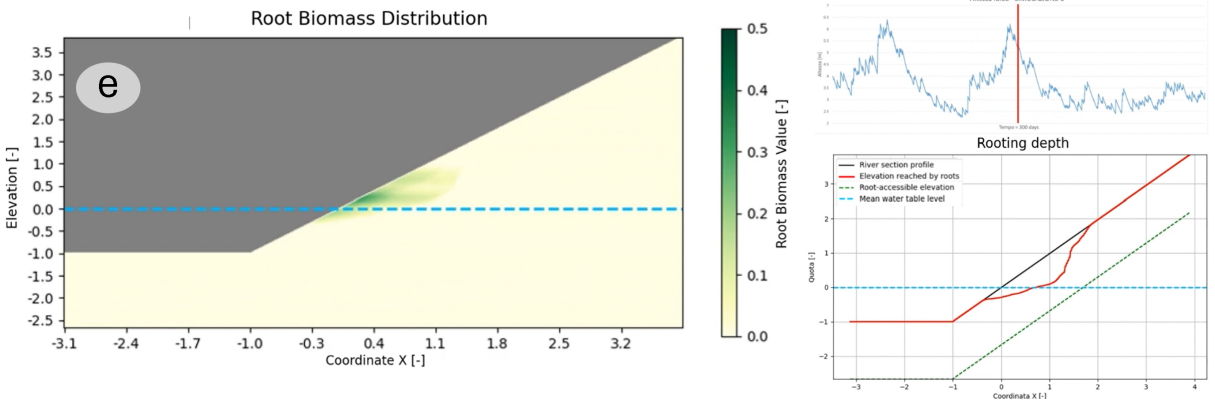
Root Biomass Distribution
e
Elevation [-]
Coordinate X [-]
Root Biomass Value [-]
Rooting depth
River section profile
Elevation reached by roots
Root-accessible elevation
Mean water table level
Coordinata X [-]

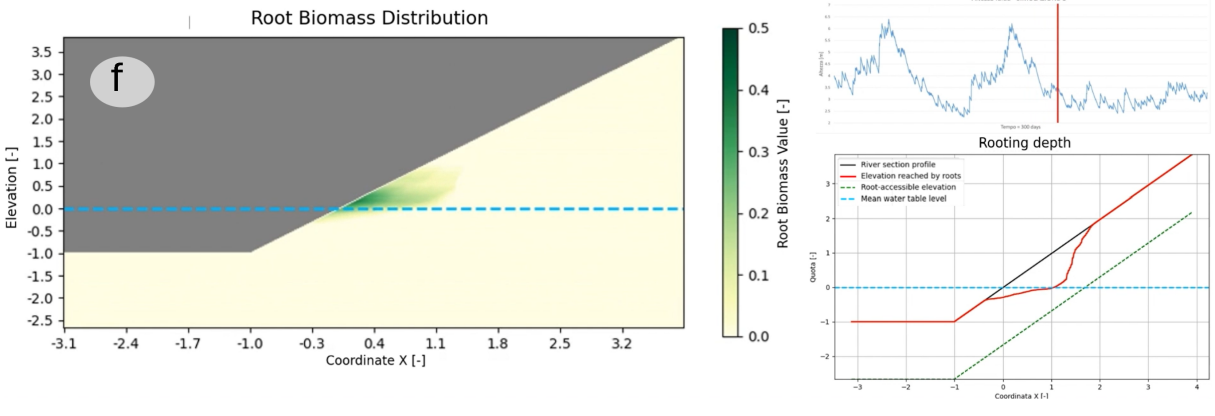
Root Biomass Distribution
f
Elevation [-]
Coordinate X [-]
Root Biomass Value [-]
Rooting depth
River section profile
Elevation reached by roots
Root-accessible elevation
Mean water table level
Coordinata X [-]

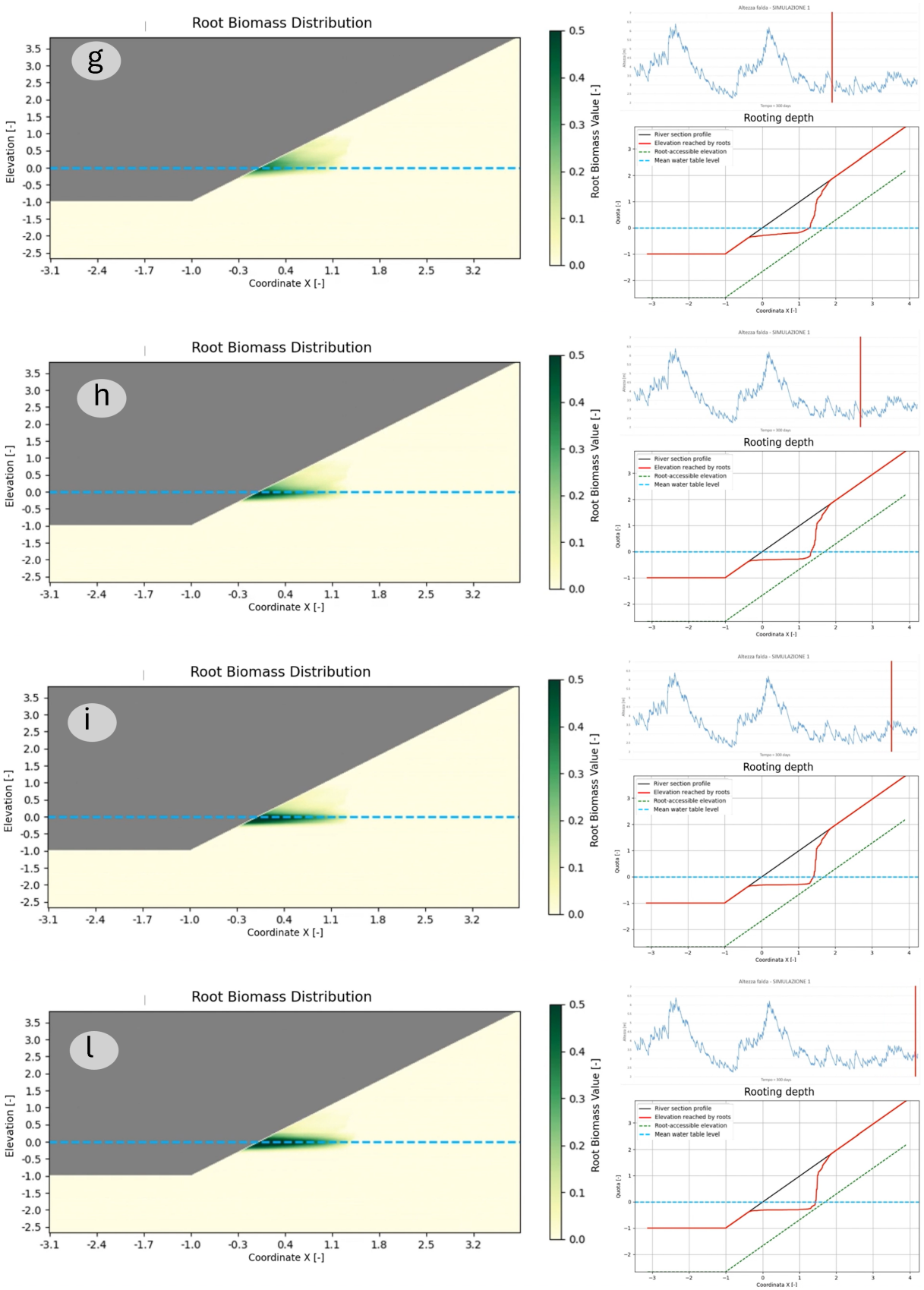

Figure 5.30: Root Biomass evolution in the considered section along 300 days with a $timestep = 30days$ of simulation 2 ($\beta_{max}/\gamma = 1$)

The distinctive feature of these results compared to those of case 1 or cases 2, 3, and 4 is the persistence of biomass values over time in areas of decline, as the values are lower in absolute terms and no longer higher than those of β, and consequently the presence of these values persists and is more evident over time. This results in a more widespread distribution at different levels and more similar and correlated over time. This particular feature can be identified above all in periods when there are significant variations in the water table.

These characteristics are particularly visible in figure 5.30 in images d, e, f, and g, for example. In these images, there is a gradual but marked increase and decrease in groundwater levels, with a consequent increase in the distribution area of significant root biomass values.

In images g, h, i, and l, we can see how, following stabilization of the water table levels, the distribution of values is increasingly concentrated around the typical average value for the period, resulting in a trend more similar to that of root biomass in simulation 1.

Another interesting analysis can be performed by examining the distribution of the mean Br value along the x-axis. As can be seen in Figure 5.31, the shape of the distribution changes based on the distance from the mean water level. Figure 5.31 shows a more detailed progression of the mean values along the x-axis.

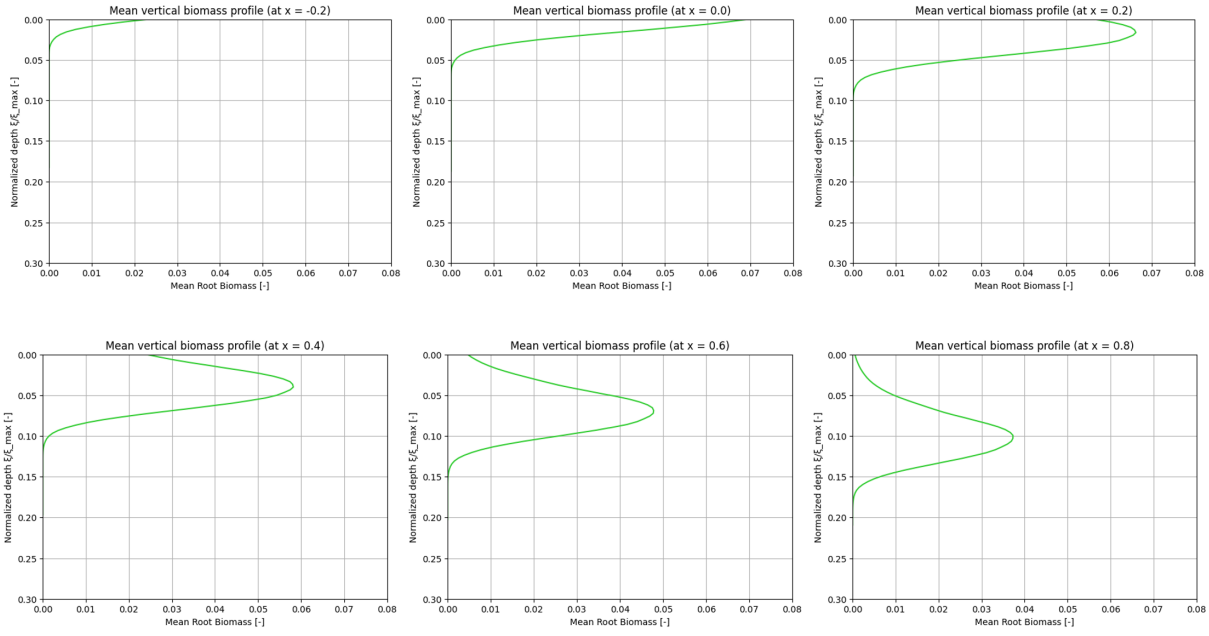

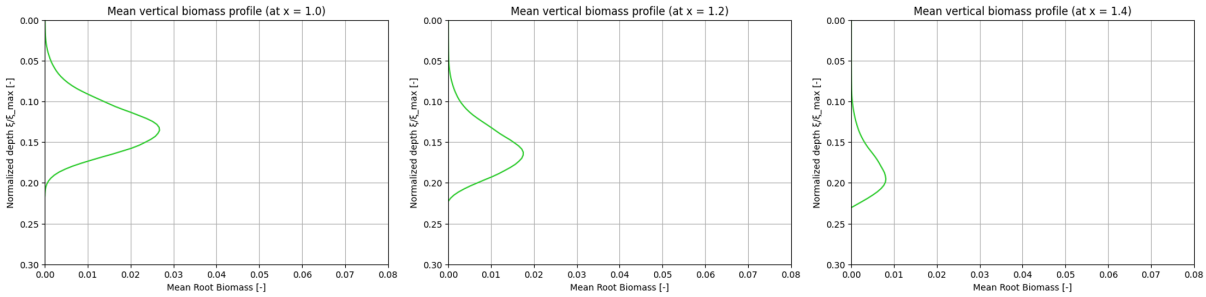

Figure 5.31: Mean Root Biomass profiles at different distances in the x-axis

It is clear that as the x-coordinate increases, and consequently as we move towards the shore, the distribution of average biomass along the z-axis starting from the point on the section varies considerably, both in terms of values and shape.

By observing its variation, it can be seen that the shape of the distribution changes substantially. Starting from negative values and increasing, the distribution of $\overline{Br}$ initially shows a logarithmic-like shape, with a peak corresponding to the point coinciding with the profile of the section. It then changes around $x = 0.1$, where the peak no longer coincides with the profile but begins to have a relative position with respect to the profile (expressed as the normalized depth $\xi_r/\xi_{r,\max}$), which increases as x increases. From that point onward, the shape changes and becomes more comparable to an asymmetric parabola.

The variability of the $\overline{Br}$ distributions and the point at which the peak no longer coincides with the profile elevation are mainly effects due to the characteristics of the hydrological regime.

As previously emphasized, the descriptive characteristics of vegetation that affect the evolution of root biomass are minor compared to the characteristics that describe the hydrological regime, which, as the only external forcing factor in the system, has a significant influence on the final result.

For this reason, four of the five simulations differ only in terms of hydrological characteristics, while only two of them differ in terms of plant characteristics.

By analyzing again the plot of the mean root biomass values ($\overline{Br}$), further distinctive details can be observed. Referring to Simulation 1, for example, Figure 5.10 shows the same plot already presented in Figure 5.7 but with the positions of some selected vegetation specimens highlighted. In particular, the positions and profiles of the specimen with the greatest Br_{tot} are shown, together with those having values equal to $0.5\,\overline{Br}_{\text{tot,max}}$ and $0.1\,\overline{Br}_{\text{tot,max}}$.

For each simulation, the element with value $\overline{Br}_{\text{tot,max}}$ is unique, while for both $0.5\,\overline{Br}_{\text{tot,max}}$ and $0.1\,\overline{Br}_{\text{tot,max}}$ there are two specimens, one located upstream and the other downstream of the position of $\overline{Br}_{\text{tot,max}}$.

The distance between the represented lines reveals two interesting insights: the first is the asymmetry between the downstream zone (to the left of the maximum value) and the upstream zone (to the right of the maximum value). Based on the distance between the dashed lines that identify the previously mentioned values, it can be observed that the lines in the left-hand side zone are closer together compared to those on the right-hand side. This indicates that the distribution of root biomass values is generally asymmetric, showing a wider and less concentrated spread for the specimens located upstream of the position of $\overline{Br}_{\text{tot,max}}$, while it is more concentrated for the values downstream of the position of $\overline{Br}_{\text{tot,max}}$, which may even refer to positional elevations on the topography lower than the mean groundwater table elevation of the input regime.

It can also be observed that, for Simulation 1 (and also for the subsequent ones), the position of the plant with $\overline{Br}_{\text{tot,max}}$ is always located at an elevation slightly higher than $\overline{z}_i$, as could be expected, considering the modeling approach used and the dependence on capillary rise L, which is located above the groundwater level. This predictable result can indeed be observed for all the other simulations as well.

The positions of the plants with total root biomass values of $0.5\,\overline{Br}_{\text{tot,max}}$ and $0.1\,\overline{Br}_{\text{tot,max}}$ constitute two excellent visual indicators that provide information about the spread of $\overline{Br}$ values greater than 0. When analyzed together with the $\overline{Br}$ values themselves, they help to understand how vegetation responds to the input hydrological regime.

Below is a comparison between simulations 1, 3, 4, and 5, referring to the graphs containing the average Br values and the positions of the plants indicated above (details of which are shown in figure 5.32).

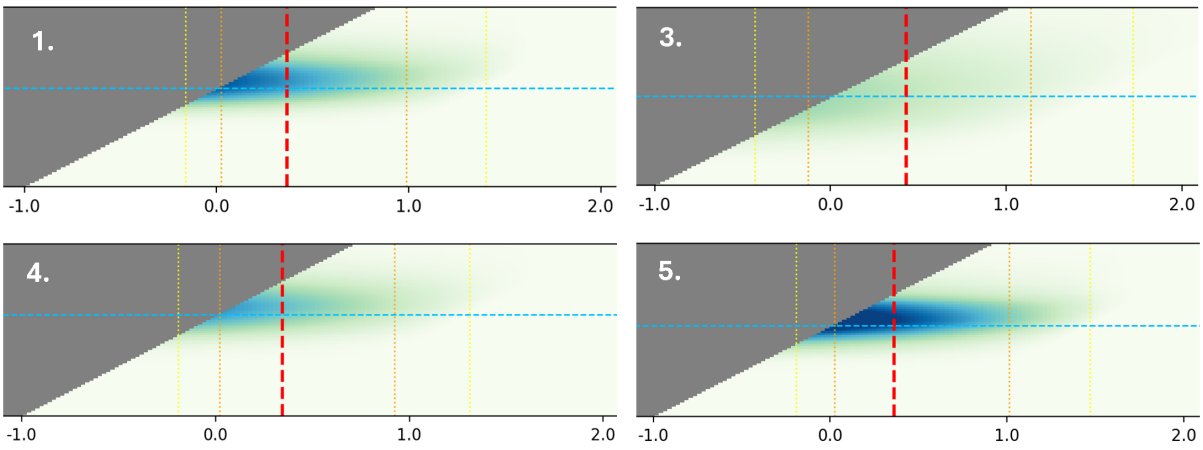

Figure 5.32: Comparision between Mean Root Biomass for simulations 1, 3, 4, 5

At first glance, it can be seen that simulation 1 differs from simulation 3 in terms of a particular characteristic of the hydrological regime: the coefficient of variation cv, which is equal to 0.2 in the first case and 0.4 in the second.

There are essentially two differences. Considering the greater variability of the values in simulation 3, the "cloud of values," as shown by the vertical dotted lines, is wider, and samples further from the average groundwater value have higher $\overline{Br}$ values than those in simulation 1, where they are either lower or not present at all.

Simulations 4 and 5 reveal another aspect of the hydrological regime, namely its frequency of variation. Compared to simulation 1, they have the same cv, i.e. the same range of variability, but a different coefficient of temporal variation ct, which translates into the frequency with which high and above-average levels alternate with lower and below-average levels. In simulation 1 $ct = 20$, in simulation 4 $ct = 10$, the values alternate more quickly, while in simulation 5 $ct = 40$, the values alternate more slowly.

It can be observed that, firstly, with reference to the extent of the area in which values of $\overline{Br} \gg 0$ are present, it remains overall unchanged between cases 1, 4, and 5, unlike the evidently larger extent observed in case 3.
Referring to the dashed lines, it can be noted that downstream the respective positions in cases 1, 4, and 5 remain almost unchanged, while upstream they differ slightly (extending somewhat more in case 5 and slightly less in case 1).

These differences can be seen by comparing the root depth graphs shown in figure5.33, where it is clear that the roots extend laterally deeper in the case of simulation 3.

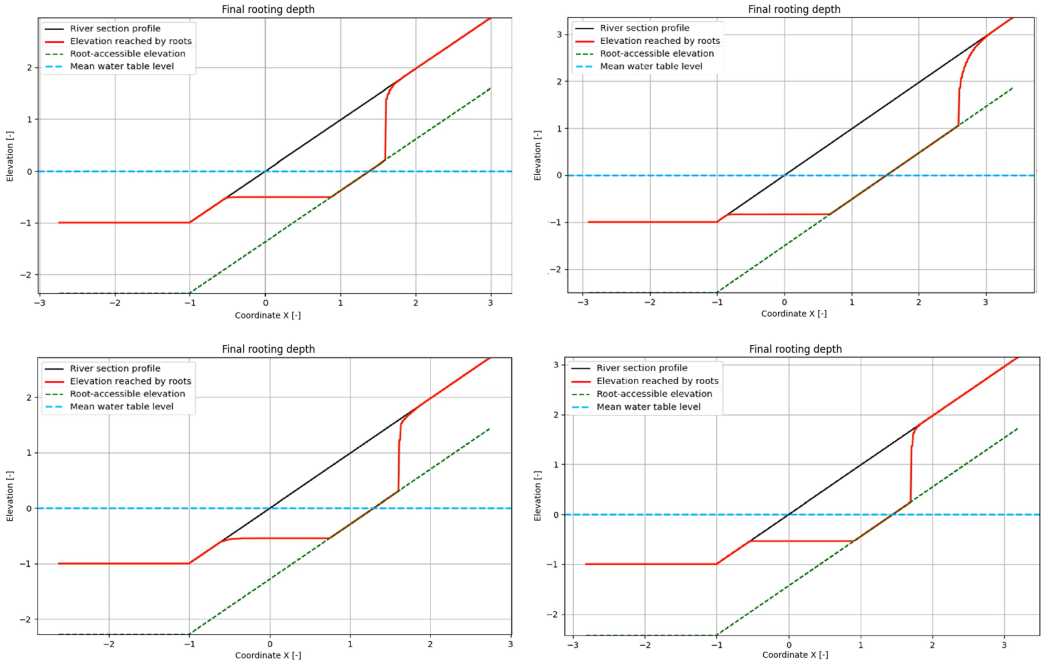

Figure 5.33: Comparision between final root depth for simulations 1, 3, 4, 5

However, the substantial difference can be understood by observing the actual average values. In fact, although the hypothesis theorized for case 3 no longer applies, in which the cause of the lower average values was attributed to a higher range

of variability, which would have led each cell to spend time in the optimal growth state, another factor comes into play. Although in this case the total time during which each cell is subject to optimal conditions is the same in all three cases, what changes is the consecutive time during which the cells are subject to growth and decay conditions. In particular, with regard to growth conditions, the logistic function that describes them predicts growth that increases as the consecutive time during which the cell is subjected to these conditions increases.

It can therefore be concluded that root biomass is closely dependent on the following factors:

- From the vegetation characteristics represented by the growth and decay factors β and γ, which drastically influence the values with respect to the carrying capacity but do not significantly affect the spatial distribution.
- From the *cv* characteristic of the hydrological regime, which particularly influences the spatial extent and range of elevations relative to the average river level where the profile has significant vegetation values, but which also has a certain influence on root biomass values.
- From the characteristic *ct* of the hydrological regime, which has a small influence on the spatial distribution of vegetation, but which has a much greater effect on the root biomass values obtained.

Chapter 6

Conclusions

The analysis performed represents a clear improvement on current, more common approaches to modelling riparian vegetation. Although rarely used, the focus on describing plant dynamics based on the root system is very innovative, as it attempts to describe plant development in a way that is closer to the plant's biological reality. This behaviour is commonly addressed through a numerical approach that aims to find numerical factors or equations that describe the evolution of the plant and its reaction to certain external behaviours as coherently as possible, without generally indicating or specifying their extent.

The model in question (based on Tron's model) focuses on development dynamics (positive or negative) through a physical description of behaviour. It places the interaction between the water table and the root system at the centre of the modelling. This interaction varies continuously depending on the river's hydraulic pull and consequently describes values in absolute and local terms at various heights along the roots' vertical extension. While this approach has previously only been studied in theory to extrapolate an equation describing the average profile over a given time series, the code produced during this research turns these principles into a model that varies over time, allowing variation in values and proportions at various root heights (profiles) at any given moment.

This type of modelling was chosen because there is ample evidence showing that, from a biological point of view, the water table height is the element that most influences plant dynamics, and that the roots are the part of a plant that primarily comes into contact with, and reacts to, the water table and its variations. The development of the above-ground section of the plant depends on this.

The resulting model correctly responds to variations in the external forcing 'groundwater level', and statistical investigations are conducted to more closely associate the characteristics of the hydrological regime with the evolution of the vegetation itself. Furthermore, unlike the 'prescriptive' approach on which the theory is based, the 'dynamic' approach allows for more varied results and describes a much wider range of situations and cases than hydromorphodynamic computation, which can contribute to a more accurate description of vegetation's role in the computational

process.

However, the current level of implementation is still in its infancy and only addresses the management of root biomass reaction and evolution processes in relation to the water table. This is expressed and regulated by growth and decay factors that are typical of the plant species in question, and it could potentially include other phenomena related to biomass evolution. For example, a different decay factor could be chosen. Nevertheless, this approach is inconvenient as it would prevent the model from describing the process in a more consistent phenological manner.

Future steps therefore involve enriching the modelling by including a description of all the physical and biological phenomena necessary for a comprehensive description of plant behaviour in a river environment, with the aim of more accurately enriching the hydromorphodynamic computation.

Firstly, a relationship must be established between root biomass and surface biomass, for example through allometric laws. Root biomass itself does not significantly influence the interaction process with water flow and sediments, except in cases of vegetation damage through scouring, where it becomes a fundamental element in describing the phenomenon. Therefore, the model must be enriched with an actual description of surface biomass and its influence on flow. Furthermore, the current description of the growth and decline of plant biomass involves two processes: growth in favourable conditions and decline due to a lack of moisture and anoxia. To these, the effect of flow on vegetation through scouring and burial processes must be added, as these drastically accelerate the decay of vegetation.

From a practical point of view, many of these processes are already present in BASEMENT software and its BASEveg module. As this software is closely aligned with the theoretical principles of the produced model, it is a good starting point for implementing the improvements resulting from this research in the description of root vegetation. This can be achieved by enriching the description of surface vegetation to make it less autonomous and more dependent on the root system itself.

References

Anderson, B. G., I. D. Rutherfurd, and A. W. Western (2006). "An analysis of the influence of riparian vegetation on the propagation of flood waves". In: *Environmental Modelling & Software* 21.9, pp. 1290–1296. DOI: 10.1016/j.envsoft.2005.04.027.

Asaeda, Takashi, Leelananda Rajapakse, et al. (2000). "Structural development of Phragmites australis: ramet density, biomass and morphology". In: *Aquatic Botany* 67.3, pp. 263–278. DOI: 10.1016/S0304-3770(00)00092-4.

Asaeda, Takashi, Md Harun Rashid, and Jonas Schoelynck (2020). "Tissue Hydrogen Peroxide Concentration Can Explain the Invasiveness of Aquatic Macrophytes: A Modeling Perspective". In: *Frontiers in Environmental Science* 8. Frontiers vol. 8 (2020); pubblicato online il 29 Jan 2021, p. 516301. DOI: 10.3389/fenvs.2020.516301.

Asaeda, Takashi and Md. H. Rashid (2014). "Modeling the influence of sediment grain size and composition on herbaceous vegetation in a lowland river floodplain". In: *Ecohydrology* 7.5, pp. 1295–1309. DOI: 10.1002/eco.1458.

Asaeda, Takashi, Md. H. Rashid, and R. Abu Bakar (2015). "Dynamic Modelling of Soil Nitrogen Budget and Vegetation Colonization in Sediment Bars of a Regulated River". In: *River Research and Applications* 31.4, pp. 470–484. DOI: 10.1002/rra.2802.

Baniya, Mahendra B. et al. (2020). "Mechanism of Riparian Vegetation Growth and Sediment Transport Interaction in Floodplain: A Dynamic Riparian Vegetation Model (DRIPVEM) Approach". In: *Water* 12.1, p. 77. DOI: 10.3390/w12010077.

Baptist, M. J. et al. (2007). "On Inducing Equations for Vegetation Resistance". In: *Journal of Hydraulic Research* 45.4, pp. 435–450. DOI: 10.1080/00221686.2007.9521778.

Barenblatt, Grigory Isaakovich (1996). *Scaling, Self-similarity, and Intermediate Asymptotics*. Cambridge: Cambridge University Press.

Benjankar, R., E.M. Yager, D. Tonina, G. Egger, and C. Plank (2014). "An efficient model for simulating riparian vegetation dynamics in gravel-bed rivers". In: *Environmental Modelling & Software* 53, pp. 98–110. DOI: 10.1016/j.envsoft.2013.11.002.

Benjankar, R., E.M. Yager, D. Tonina, G. Egger, C. Plank, and C. Segura (2011). "A spatially explicit riparian vegetation model for gravel-bed rivers". In: *River Research and Applications* 27.7, pp. 772–783. DOI: 10.1002/rra.1384.

Brückner, Muriel Z. M. et al. (2019). "Salt Marsh Establishment and Eco-Engineering Effects in Dynamic Estuaries Determined by Species Growth and Mortality".

In: *Journal of Geophysical Research: Earth Surface* 124.12, pp. 2962–2986. DOI: 10.1029/2019JF005092.

Camporeale, Carlo and Luca Ridolfi (2006). "Riparian vegetation distribution induced by river flow variability: A stochastic approach". In: *Water Resources Research* 42.10, W10415. DOI: 10.1029/2006WR004933.

— (2010). "Significance of riverbank vegetation dynamics on meandering river morphodynamics". In: *Water Resources Research* 46.9. DOI: 10.1029/2009WR008173.

Caponi, Francesco and Annunziato Siviglia (2018). "Numerical modeling of plant root controls on gravel bed river morphodynamics". In: *Geophysical Research Letters* 45.17, pp. 9013–9023. DOI: 10.1029/2018GL078696.

Caponi, Francesco, David F. Vetsch, and Annunziato Siviglia (2020). "A model study of the combined effect of above and below ground plant traits on the ecomorphodynamics of gravel bars". In: *Scientific Reports* 10.1, p. 17062. DOI: 10.1038/s41598-020-74106-9.

Caponi, Francesco, David F. Vetsch, and Davide Vanzo (2023). "BASEveg: A python package to model riparian vegetation dynamics coupled with river morphodynamics". In: *SoftwareX* 22, p. 101361. DOI: 10.1016/j.softx.2023.101361.

Corenblit, D., A. C. W. Baas, et al. (2011). "Feedbacks between geomorphology and biota controlling Earth surface processes and landforms: A review of foundation concepts and current understandings". In: *Earth-Science Reviews* 106.3–4, pp. 307–331. DOI: 10.1016/j.earscirev.2011.03.002.

Corenblit, D., E. Tabacchi, et al. (2007). "Reciprocal interactions and adjustments between fluvial landforms and vegetation dynamics in river corridors: A review of complementary approaches". In: *Earth-Science Reviews* 84.1–2, pp. 56–86. DOI: 10.1016/j.earscirev.2007.05.004.

Corenblit, Dov et al. (2015). "Considering river structure and stability in the light of evolution: Feedbacks between riparian vegetation and hydrogeomorphology". In: *Earth Surface Processes and Landforms* 40.2, pp. 189–207. DOI: 10.1002/esp.3643.

De Saint-Venant, Adhémar Jean Claude Barré (1871). "Théorie du mouvement non permanent des eaux, avec application aux crues des rivières et à l'introduction des marées dans leurs lits". French. In: *Comptes Rendus Hebdomadaires des Séances de l'Académie des Sciences* 73, pp. 147–154, 237–240.

Deltares (2025). *Delft3D Flexible Mesh User Manual*. Version 2025. Dynamic Vegetation Module. URL: https://www.deltares.nl/en/software/delft3d-flexible-mesh-suite/ (visited on 06/03/2025).

Edmaier, K., P. Burlando, and P. Perona (2011). "Mechanisms of vegetation uprooting by flow in alluvial non-cohesive sediment". In: *Hydrology and Earth System Sciences* 15, pp. 1615–1627. DOI: 10.5194/hess-15-1615-2011.

Egger, G. et al. (2011). "Riparian vegetation model for long-term predictions of vegetation patterns in floodplains". In: *Ecohydrology* 4.6, pp. 722–732. DOI: 10.1002/eco.170.

— (2013). "Assessing the impact of flow regime changes on riparian vegetation: A multi-scale modeling approach". In: *Ecohydrology* 6.4, pp. 512–527. DOI: 10.1002/eco.1294.

Engelund, Frank (1966). "Hydraulic Resistance of Alluvial Streams". In: *Journal of the Hydraulics Division* 92.HY2, pp. 315–326. DOI: 10.1061/JYCEAJ.0001417.

Exner, Felix Maria (1925). "Über die Wechselwirkung zwischen Wasser und Geschiebe in Flüssen". In: *Sitzungsberichte der Akademie der Wissenschaften in Wien, Mathematisch-Naturwissenschaftliche Klasse, Abteilung IIa* 134, pp. 165–203.

García-Arias, A. et al. (2013). "Implementing a dynamic riparian vegetation model in three European river systems". In: *Ecohydrology* 6.4, pp. 635–644. DOI: 10.1002/eco.1331.

García-Arias, Alicia and Félix Francés (2015). "A distributed rainfall–runoff model for flood analysis in Mediterranean basins based on reducing effective parameters through expert knowledge (RVDM)". In: *Journal of Hydrology* 524, pp. 233–251. DOI: 10.1016/j.jhydrol.2015.02.040.

Gurnell, A. M., W. Bertoldi, and D. Corenblit (2012). "Changing river channels: The roles of hydrological processes, plants and pioneer fluvial landforms". In: *Earth-Science Reviews* 111.1-2, pp. 129–141. DOI: 10.1016/j.earscirev.2011.11.005.

Gurnell, Angela M. (2014). "Plants as river system engineers". In: *Earth Surface Processes and Landforms* 39.1, pp. 4–25. DOI: 10.1002/esp.3397.

— (2016). "Hydrogeomorphological significance of vegetation in river corridors". In: *Earth Surface Processes and Landforms* 41.1, pp. 7–22. DOI: 10.1002/esp.3851.

Huthoff, Freek, Dionysius C. M. Augustijn, and Suzanne J. M. H. Hulscher (2007). "Analytical solution of the depth-averaged flow velocity in case of submerged rigid cylindrical vegetation". In: *Water Resources Research* 43, W06413. DOI: 10.1029/2006WR005625.

Järvelä, Juha (2004). "Determination of flow resistance caused by non-submerged woody vegetation". In: *International Journal of River Basin Management* 2.1, pp. 61–70. DOI: 10.1080/15715124.2004.9635222.

Karrenberg, Sophie, Peter J. Edwards, and Johannes Kollmann (2002). "The life history of Salicaceae living in the active zone of floodplains". In: *Freshwater Biology* 47.4, pp. 733–748. DOI: 10.1046/j.1365-2427.2002.00894.x.

Kleinhans, Maarten G. et al. (2018). "Living landscapes: Muddy and vegetated floodplain effects on fluvial pattern in an incised river". In: *Earth Surface Processes and Landforms* 43.14, pp. 2948–2963. DOI: 10.1002/esp.4437.

Kouwen, Nicholas and Ruh-Ming Li (1980). "Biomechanics of vegetative channel linings". In: *Journal of the Hydraulics Division* 106.HY6, pp. 1085–1103. DOI: 10.1061/JYCEAJ.0005444.

Li, X. X. et al. (2022). "Morphodynamic impact of vegetation pattern on vegetated channels using two-dimensional modelling". In: *Advances in Water Resources* 167, p. 104313. DOI: 10.1016/j.advwatres.2022.104313.

Mahoney, John M. and Stewart B. Rood (1998). "Streamflow requirements for cottonwood seedling recruitment—An integrative model". In: *Wetlands* 18.4, pp. 634–645. DOI: 10.1007/BF03161678.

Manning, Robert (1891). "On the Flow of Water in Open Channels and Pipes". In: *Transactions of the Institution of Civil Engineers of Ireland* 20, pp. 161–207.

Naiman, Robert J. and Henri Décamps (1997). "The Ecology of Interfaces: Riparian Zones". In: *Annual Review of Ecology and Systematics* 28, pp. 621–658. DOI: 10.1146/annurev.ecolsys.28.1.621.

Naumburg, Elke et al. (2005). "Phreatophytic vegetation and groundwater fluctuations: a review of current research and application of ecosystem response modeling with an emphasis on Great Basin vegetation". In: *Environmental Management* 35.6, pp. 726–740. DOI: 10.1007/s00267-004-0194-7.

Nepf, Heidi M. (2012). "Hydrodynamics of vegetated channels". In: *Journal of Hydraulic Research* 50.3, pp. 262–279. DOI: 10.1080/00221686.2012.696559.

Palmer, Margaret A. and Albert Ruhi (2019). "Linkages between flow regime, biota, and ecosystem processes: Implications for river restoration". In: *Science* 365.6459, eaaw2087. DOI: 10.1126/science.aaw2087.

Pollen-Bankhead, Natalie and Andrew Simon (2010). "Hydraulic erosion of cohesive riverbanks". In: *Geomorphology* 116.1-2, pp. 393–409. DOI: 10.1016/j.geomorph.2009.11.003.

Shields, Albert (1936). "Anwendung der Ähnlichkeitsmechanik und der Turbulenzforschung auf die Geschiebebewegung". PhD thesis. Berlin: Technische Hochschule Berlin.

Solari, L. et al. (May 22, 2015). "Advances on modelling riparian vegetation–hydromorphology interactions". In: *River Research and Applications*. Online first; assegnato poi a River Research and Applications 32(2):164–178 (2016). DOI: 10.1002/rra.2910.

Stella, John C. et al. (2013). "Riparian vegetation research in Mediterranean-climate regions: Common patterns, ecological processes, and considerations for management". In: *Hydrobiologia* 719.1, pp. 291–315. DOI: 10.1007/s10750-012-1373-9.

Tal, M. and C. Paola (2007). "Dynamic links of river vegetation and morphology". In: *Geology* 35.4, pp. 347–350. DOI: 10.1130/G23260A.1.

Tron, Stefania, Francesco Laio, and Luca Ridolfi (2014). "Effect of water table fluctuations on phreatophytic root distribution". In: *Journal of Theoretical Biology* 360, pp. 102–108. DOI: 10.1016/j.jtbi.2014.06.035.

Van Oorschot, M. M. P. et al. (2015). "Willow vegetation dynamics and braided river morphodynamics". In: *Earth Surface Processes and Landforms* 40.3, pp. 341–355. DOI: 10.1002/esp.3645.

Van Oorschot, Maartje M. P. (2017). "Modelling the influence of vegetation on river morphodynamics". Doctoral dissertation. PhD thesis. Delft University of Technology. URL: https://repository.tudelft.nl/islandora/object/uuid%3A09d70cf2-8916-4bc1-8278-244859e00ee4.

Van Splunder, Irene et al. (1995). "Establishment of alluvial forest species in floodplains: The role of dispersal timing, germination characteristics and water level fluctuations". In: *Acta Botanica Neerlandica* 44.3, pp. 269–278. DOI: 10.1111/j.1438-8677.1995.tb00712.x.

Vanzo, Davide et al. (2021). "BASEMENT: An open-source framework for environmental flow and sediment transport simulations". In: *SoftwareX* 16, p. 100870. DOI: 10.1016/j.softx.2021.100870.

Vargas-Luna, A., A. Crosato, and W. S. J. Uijttewaal (2014). "A review of the effects of riparian vegetation on fluvial morphodynamics and sediment transport". In:

Knowledge and Management of Aquatic Ecosystems 413.01, p. 01. DOI: 10.1051/kmae/2013086.

Wang, Yun et al. (2018). "Modeling riparian vegetation succession along regulated rivers using HEC-RAS RVSM". In: *Ecological Modelling* 381, pp. 47–61. DOI: 10.1016/j.ecolmodel.2018.04.003.

Zencich, S. J. et al. (2002). "Influence of groundwater depth on the seasonal sources of water accessed by Banksia tree species on a shallow, sandy coastal aquifer". In: *Oecologia* 131, pp. 8–19. DOI: 10.1007/s00442001-0855-7.

Zeng, F. et al. (2006). "Water and nutrient dynamics in surface roots and soils are not modified by short-term flooding of phreatophytic plants in a hyperarid environment". In: *Functional Plant Biology* 33.3, pp. 224–235. DOI: 10.1071/FP05265.

Zhang, Zhongqiang et al. (2019). *HEC-RAS Riparian Vegetation Simulation Module (RVSM)*. Tech. rep. Technical Reference Manual. US Army Corps of Engineers, Hydrologic Engineering Center. URL: https://www.hec.usace.army.mil/software/hec-ras/documentation/HEC-RAS-Riparian-Vegetation-Simulation-Module-RVSM.pdf.